DOCTORAL DISSERTATION SERIES

Publication No.: 19, 678

AUTHOR: David Rudolph Bach, Ph. D., 1956

University of Michigan

TITLE: AN INVESTIGATION OF THE LOW-LYING LEVELS IN O^{18}

University Microfilms, Ann Arbor, Michigan

AN INVESTIGATION OF THE LOW-LYING LEVELS IN O^{18}

by
David R. Bach

A dissertation submitted in partial fulfillment
of the requirements for the degree of
Doctor of Philosophy in the
University of Michigan
1955

Doctoral Committee:

Assistant Professor Paul V. C. Hough, Chairman
Associate Professor Kenneth M. Case
Assistant Professor W. Wayne Meinke
Associate Professor William C. Parkinson
Associate Professor Marcellus L. Wiedenbeck

AN INVESTIGATION OF THE LOW-LYING LEVELS IN O^{18}

by David R. Bach

The characteristics of the excited states of O^{18} are of interest because the nucleus consists of a two nucleon system outside the doubly magic O^{16} core. Predictions can be made of the spins, parities, and excitation energies of the excited states by application of nuclear spectroscopic techniques. Comparison with experimental measurements can be expected to restrict the types of nucleon-nucleon interaction potentials by which the system can be described.

LiOH targets enriched in O^{17} and O^{18} were made by forming the hydroxide from thin layers of evaporated lithium using enriched water made by explosion of oxygen with hydrogen. These targets were bombarded with 7.8 Mev deuterons produced by the University of Michigan cyclotron. Proton and deuteron spectra were obtained at several scattering angles by means of nuclear plates placed in the image plane of a double focusing magnetic analyzer.

The installation, shimming, and resolution of focusing and analyzing magnets used in conjunction with the cyclotron are discussed. Measurement of an unknown Q value for a nuclear reaction with an accuracy of $\pm$ 0.010 Mev is described.

The first excited state of O^{18} at an excitation energy of 1.986 Mev was observed by the reactions $O^{17}(d,p)O_1^{18}$ and $O18(d,d')O_1^{18}$ in agreement with observations made by Ahnlund and Holmgren et al. There is no evidence on the deuteron or proton spectrum for a

level reported by the latter at an excitation energy of 2.445 Mev. A previously unreported level was observed at an excitation energy of 3.550 Mev by the reaction $O^{17}(d,p)O_2^{18}$ at the scattering angles 49.7° and 58.5° and by the reaction $O^{18}(d,d')O_2^{18}$ at 49.7° and 68.5°.

The positive results of this experiment combined with the work of Ahnlund demonstrate the existence of excited states in O^{18} at the excitation energies 1.986 ± 0.014 Mev and 3.550 ± 0.010 Mev. These are the only strong levels in the excitation region from 0 to 3.55 Mev.

Tensor force interaction energies in the jj coupling limit were calculated for the configurations $(d_{5/2})^2$, $(d_{5/2}d_{3/2})$, $(d_{5/2}s_{1/2})$, and $(d_{3/2}s_{1/2})$. Comparison of the theoretical and experimental level schemes demonstrates the failure of the pure jj coupling approximation. The calculation of Elliott and Flowers, which includes configuration interaction in intermediate coupling, is in better agreement with experiment but indicates that further theoretical investigation is necessary.

ACKNOWLEDGMENTS

I am especially indebted to Dr. Hough, the chairman of my committee, for his constant enthusiasm, encouragement, and wealth of ideas which were essential for the solution of the problem. The help of Dr. Parkinson in the installation of the analyzing magnet and associated equipment is greatly appreciated.

Association with Roger W. Hockney during all except the final phases of the investigation provided stimulating discussion and valuable assistance. Dr. Igal Talmi was most helpful in giving an introduction to the details of the nuclear spectroscopic calculations. Cecil R. Lubitz provided a valuable check on these calculations.

The construction, shimming, and installation of the focusing and analyzing magnets required the cooperation of the entire cyclotron group. Colleagues who joined in this program were William J. Childs and Roger Grismore. With apologies for not pointing out their individual efforts, the technical staff consisted of James C. Cline, Ralph D. Pittman, Harvey M. Nye, Robert H. White, and Melvin G. Whybra.

Thanks are due to Olexa M. Bilaniuk for assistance in taking the data and to Quin McLoughlin for his careful reading of many of the plates.

I am most grateful to my wife, for her patience and understanding during the course of this work. Our two small daughters have provided sparks of encouragement in times of discouragement.

Financial assistance for the investigation was provided by the United States Atomic Energy Commission under Contract No. AT(11-1)-275.

TABLE OF CONTENTS

CHAPTER		Page
I.	INTRODUCTION	1
II.	APPARATUS	5
	Over-All System	5
	Focusing Magnet	5
	Analyzing Magnet	11
	Particle Detectors	14
III.	EXPERIMENTAL PROCEDURE	17
	Preliminary Investigation	17
	Resolution	17
	Analyzing magnet dispersion	25
	Background reduction	28
	Target Preparation	29
	Collection of Data	34
	Data Analysis	35
	Target thickness	35
	Variation of scattering angle with image plane position	37
	Reaction kinematics	38

CHAPTER Page

Determination of deuteron energy and scattering angle 40

Determination of an unknown Q 47

Probable errors in the measurements 47

Reduction of errors 50

IV. EXPERIMENTAL RESULTS 52

Spectra 52

Relative Intensities 63

V. THEORY 65

Nuclear Spectroscopic Calculations 65

Tensor Interaction Energies 71

Central Interaction Energies 74

Radial Integrals 77

Theoretical Spectra 77

VI. CONCLUSIONS 81

Experimental Conclusions 81

Theoretical Conclusions 82

Future Work 84

APPENDIX I. THE TRANSFORMATIONS $\psi^{m_1}_{n_1 l_1}(\vec{r}_1)\psi^{m_2}_{n_2 l_2}(\vec{r}_2) \rightarrow \psi^{M}_{NL}(\vec{R})\psi^{m}_{n\lambda}(\vec{r})$ 86

APPENDIX II. SLATER PARAMETERS IN TERMS OF TALMI RADIAL INTEGRALS 93

Page

APPENDIX III. NUMERICAL VALUES FOR THE I_1 USED FOR $\sqrt{s} = 0.499 \times 10^{13}$ 94

LIST OF REFERENCES 95

LIST OF TABLES

TABLE		Page
I.	Results of Q Measurements on the Second Excited State of O^{18}	62
II.	Relative Intensities	64
III.	The Diagonal T = 1 Tensor Force Matrix Elements $(j_1 j_2 m_{j_1} m_{j_2} \mid S_{12} \mid j_1 j_2 m_{j_1} m_{j_2})$	91

LIST OF ILLUSTRATIONS

FIGURE		Page
1.	Over-all system	6
2.	Schematic diagram of stretched wire apparatus	8
3.	Stretched wire data before and after correction	9
4.	Analyzing magnet	12
5.	Monitor, target, and exit slit	15
6.	Beam path through major components showing position of slits	18
7.	Paths of polonium alpha particles in analyzing magnet	20
8.	Data showing stability of system	21
9.	Elastic scattered deuterons from an Au target	23
10.	90° protons from the reaction $Al^{27}(d,p)Al^{28}$	24
11.	Analyzing magnet dispersion curve	27
12.	Explosion and hydroxidation chambers	32
13.	Target structure and $C^{12}(d,p)C^{13}$ peaks	36
14.	Rate of energy loss of protons in LiOH	44
15.	High energy deuteron spectrum	53
16.	50° deuteron spectrum	54
17.	70° deuteron spectrum	55

FIGURE Page

18. 50° proton spectrum 56

19. 70° proton spectrum 57

20. 90° proton spectrum 58

21. 60° spectrum 59

22. 30° proton spectrum 60

23. The matrix $(j_1 j_2 JT|V|j_3 j_4 JT)$ for T = 1 69

24. Central force level diagram of O^{18} 78

25. Central + tensor force level diagram of O^{18} 79

CHAPTER I

INTRODUCTION

The fundamental problem of nuclear physics is the understanding of the forces that exist between nucleons. Study of these forces is best accomplished by the examination of simple systems of nucleons due to the complexity of many body problems in quantum mechanics. The two-body problem has been studied by the interpretation of the experimental information derived from nucleon-nucleon scattering and the properties of the deuteron.

Spins and parities of the ground states of nuclei have been described in considerable detail by means of the nuclear shell model. The model seems to break down, however, in attempts to predict the measured magnetic moments, quadrupole moments, and characteristics of excited states of nuclei. Modification of the original shell model by including the effects of nucleon-nucleon interaction is a more realistic approach to the problem.

Nuclei which may be considered, in first approximation, two-body systems are especially amenable to theoretical interpretation and therefore are of prime importance. The nuclei O^{18} and F^{18} are of this type since they consist of two nucleons outside the doubly magic O^{16} core. O^{18} is the simpler nucleus since the Pauli principle places a greater restriction on the number of admissible states. The wave functions of the low-lying even parity states are expected to be made up of wave functions of 1d and 2s nucleons. The lower odd parity states require core excitation, or a removal of a 1p nucleon from the core in combination with 1d and 2s nucleons.

A determination of the spins and parities of the excited states of O^{18} can be expected to restrict the types of potentials by which the nucleus may be described.

Determination of the O^{18} energy levels and the spins and parities of these levels requires one of two types of nuclear reactions. The first type of reaction utilizes standard bombarding particles (e.g., deuterons, protons, alpha particles) and requires enriched isotopic targets. The second type makes use of more inconvenient bombarding particles (e.g., tritons, neutrons) and abundant isotopic targets.

Excited states of O^{18} can be observed by the deuteron stripping reaction $O^{17}(d,p)O^{18}$ and by inelastic scattering of deuterons on O^{18}. Both of these reactions require targets enriched in O^{17} and O^{18} as the natural abundance of O^{17} is 0.037 percent and that of O^{18} is 0.204 percent. Through the courtesy of Professor A. O. C. Nier at the University of Minnesota, enriched oxygen gas containing 1 percent O^{17} and 45 percent O^{18} has been made available. The inelastic deuteron reaction is useful in searching for excited states because of the greater enrichment in O^{18}. The angular distributions of the stripping reactions are more difficult experimentally because of the small amount of O^{17} but lead to more definite interpretation than the inelastic deuteron angular distributions. The stripping reactions give unambiguously the parity of the final nuclear states and place limits on the J values. The relative intensities of the stripping reactions leading to O^{18} can possibly measure the spins of some of the excited states.

O^{18} is of additional interest due to the small number of experimental data that have been obtained up to this time. At the beginning of this investigation, no search for excited states had been made, mainly because of the rarity of appropriate target nuclei in nature.

The problem of transforming a small amount of enriched gas into a usable cyclotron target through several chemical operations can be considered one of the major difficulties of the investigation (see page 29).

Any search for excited states in O^{18} requires that reaction product energies be measurable to 50 Kev or less, since the target of necessity contains oxygen isotopes of masses 16, 17, and 18 a.m.u. The change of reaction product energy with scattering angle is a positive method of assigning nuclear mass. Since the mass must be known to less than one mass unit, this resolution is necessary.

A long-range program entailing installation of focusing and analyzing magnets to be used with the University of Michigan cyclotron was accelerated by the interest in the O^{18} problem. The resolution available with this system is shown to be greater by an order of magnitude than that obtainable by range methods. Measurement of an unknown Q value for a nuclear reaction with an accuracy of ±0.010 Mev is described.

Results of nuclear spectroscopic calculations in the jj coupling limit for probable low-lying configurations in O^{18} are given. Since the tensor force has been proved necessary for the explanation of the quadrupole moment of the deuteron, it seems likely that the tensor force should be included for the description of the forces between nucleons in the nucleus. The tendency has been to neglect tensor forces because of the tedious calculations which are involved. Certain tensor force interaction energies are given which have not been reported previously.

This investigation cannot be considered a complete experimental and theoretical examination of the O^{18} nucleus. The experiment, in conjunction with others, has demonstrated the existence of only two strong levels in the region of excitation in O^{18} from 0 to 3.55 Mev.

The nuclear spectroscopic calculations are of an approximate nature and demonstrate the failure of the pure jj coupling scheme. It is felt, however, that both the experiment and the theory presented are a foundation for future work on the O^{18} problem.

CHAPTER II

APPARATUS

Over-All System

The source of bombarding particles is the University of Michigan forty-two inch cyclotron which produces a beam of 7.8 Mev deuterons (Figure 1). The external beam of the cyclotron is deflected and focused on the center of a scattering chamber by means of a fifty degree wedge magnet. Reaction particles are then detected in the focal plane of a ninety degree double focusing magnetic spectrometer. This magnet is capable of measuring reaction particles at reaction angles which are continuously variable from -7° to 112°.

Focusing Magnet

The focusing magnet is used to produce a beam of fairly monoenergetic deuterons from the external cyclotron beam. Extensive semiempirical shimming was required to make the magnet usable because of the deviations from the predicted behavior caused by large fringe field effects. Virtually no freedom was allowed in the positioning of the focusing magnet because of the small amount of space available in the cyclotron room. It was necessary to keep the image point of the focusing magnet as close as possible to the exit side of the water shielding wall in order to allow space for the analyzing magnet image circle in the analyzing room. The image circle was required

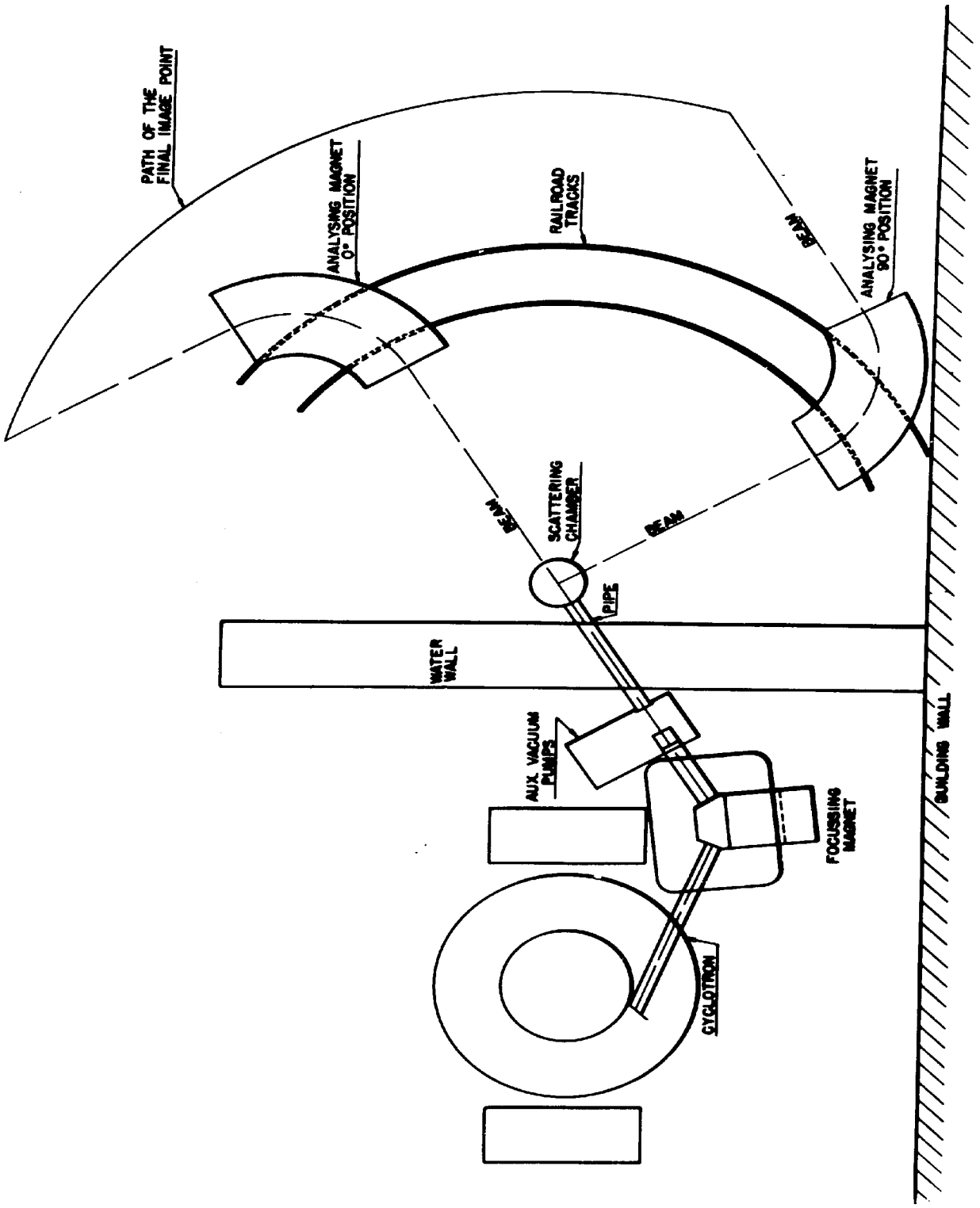


Figure 1. Over-all system.

to be less than 472 cm. because of interference caused by two building support columns.

The focal properties of the focusing magnet were determined by the stretched wire method. Measurements are made of the path described by a flexible current-carrying wire in the magnetic field. It can be shown that

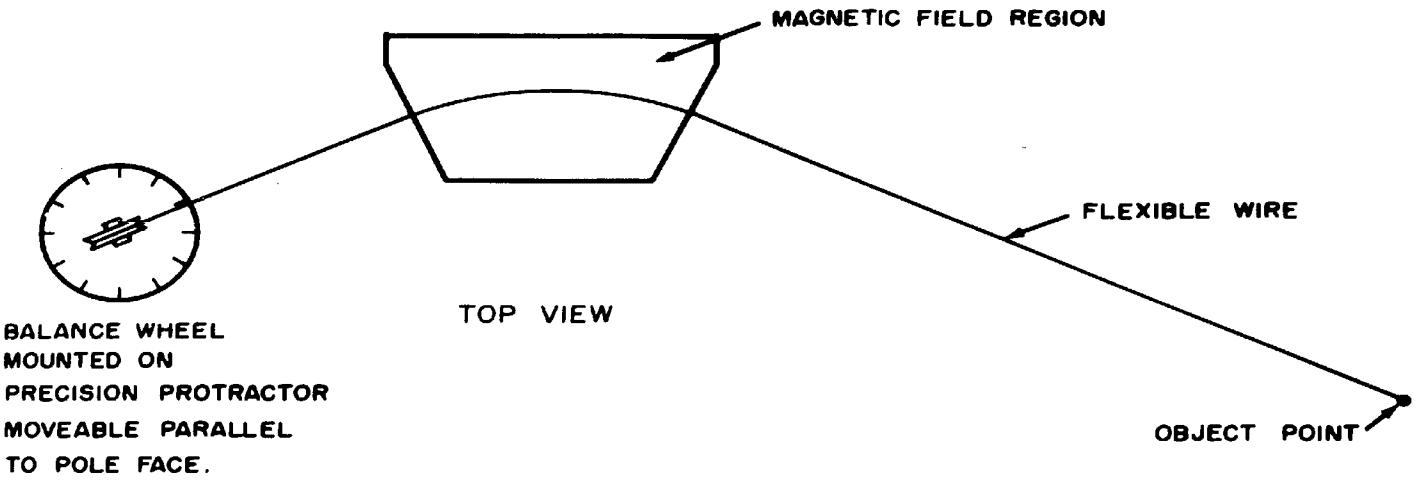
$$\frac{T}{I} = H\rho = \frac{mv}{e}$$

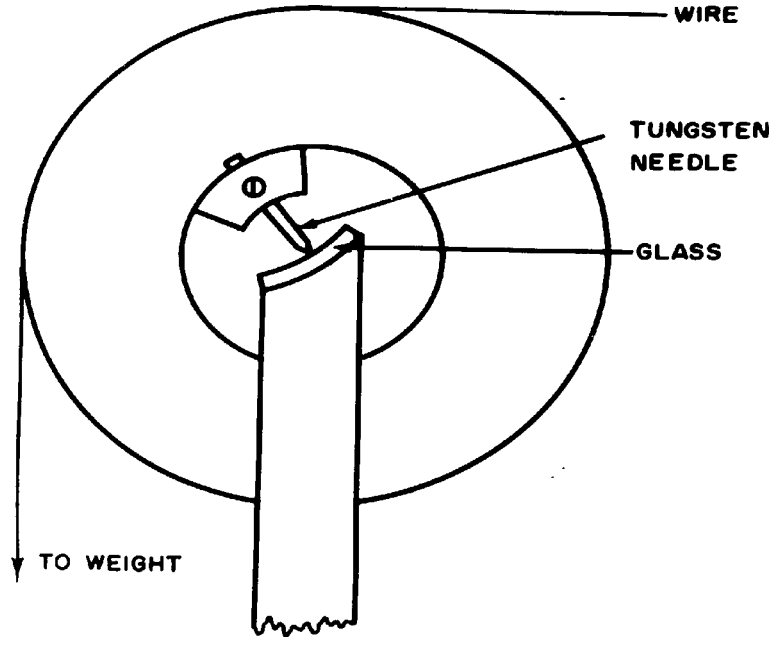
where H is the magnetic field intensity in Gauss, ρ is the radius of curvature described by the wire in cm., T is the tension in dynes in the wire, I is the direct current in abamperes passing through the wire, m is the mass of the particle in grams, v is the velocity in cm/sec, and e is the charge in e.m.u. A massless wire is assumed.

One end of the wire is supported by a flexible joint at the object point of the magnet. The wire then extends through the gap of the magnet, is passed over a balance wheel, and supports a weight which produces the desired tension (Figure 2). The balance wheel is placed as close to the exit of the magnet as possible. Measurements are made of the radial position of the wire in the magnet and the direction of the wire at the balance wheel.

This arrangement enables the path of a "particle" to be measured in detail at various radial positions. A plot (Figure 3) is made of wire direction at the balance wheel against radial position and the deviations from the direction required for perfect focus are noted. Iron is added or subtracted at the pole face at the radial positions where more or less bending is required.

Good current regulation for both the magnet and stretched wire current is necessary for such a measurement. It was found that reliable data could not be obtained without reducing the friction in the balance wheel to an absolute minimum. This was accomplished





DETAIL SIDE VIEW OF
BALANCE WHEEL.

SCHEMATIC DIAGRAM
OF STRETCHED WIRE
APPARATUS.
NOT TO SCALE.

Figure 2

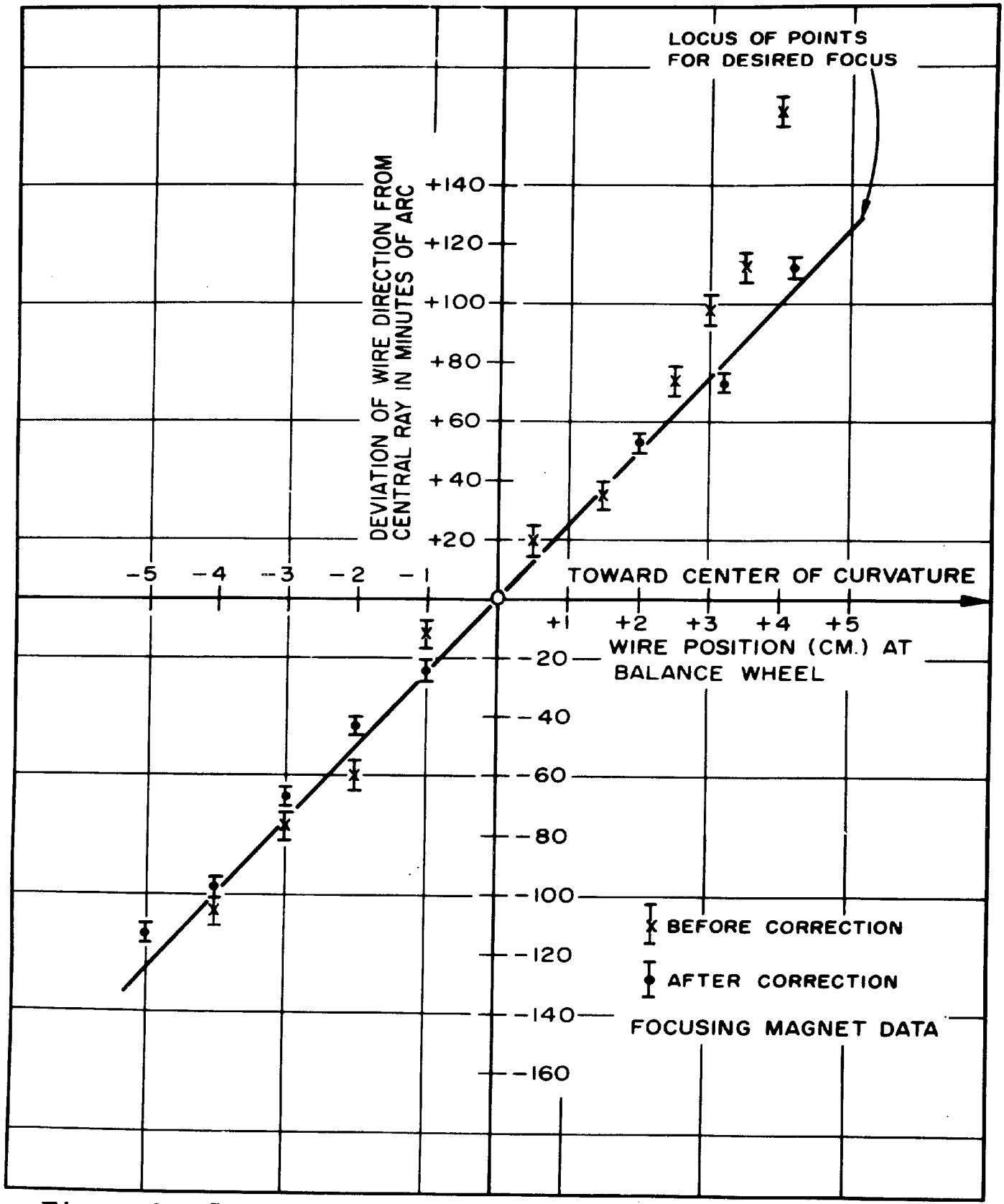


Figure 3. Stretched wire data before and after correction.

by mounting the wheel on two tungsten needle points which rested on glass surfaces. Determination of wire direction with an accuracy of ± 3 minutes of arc was possible.

The focusing magnet was found to be radially defocusing by preliminary stretched wire measurements. New pole tips were machined in order to obtain radial focusing and final measurements indicate that the n, or falloff parameter of the magnetic field intensity, is about 0.2. A statement can be made concerning the degree of correction to the magnetic field obtainable by the stretched wire method. The spread in energy at one point in the image plane from a heterogeneous point source is shown to be ± 18 Kev for 7.8 Mev deuterons. This is a measure of the accuracy of the stretched wire measurement and does not necessarily represent the quality of focus finally attained.

The dispersion of the focusing magnet was measured with the stretched wire by observing the change in direction of the wire at the balance wheel when a small change in wire current (particle momentum) was made. Relevant data on the focusing magnet are as follows:

Object to pole face distance	171 cm.
Image to pole face distance	228 cm.
Central radius of curvature	45 cm.
Angle of bend including fringe field	55°
Useful aperture at center of magnet	14 cm.
Dispersion (at image for 7.8 Mev deuterons)	6.5 Kev/mm
Average gap	5.7 cm.
Average flux density to focus 7.8 Mev deuterons	9,000 Gauss
$n = \frac{1}{B}\frac{dB}{dr}$	0.2

Analyzing Magnet

The 90° double focusing analyzing magnet was constructed from sections of the University of Michigan synchrotron magnet (Figure 4). The only iron change made in each of the sections was the addition of new pole tips machined to produce the required n, or fall-off parameter, of the magnetic field. The basis (1, 2) for the choice of n can be seen most easily by considering the first order relation between the total angle of bend Φ , n, and the distance t from the pole faces to the object and image positions for an equal arm magnet:

$$t = \frac{\cot \sqrt{1-n}\,\Phi + \csc \sqrt{1-n}\,\Phi}{\sqrt{1-n}}$$

For the case in question, Φ is fixed at 90° and t is limited by the requirement that the image circle be kept below 472 cm. Calculations showed that n = 0.45 leads to an object distance t of 208 cm. which leaves a distance of about eighteen inches outside the image circle for counting equipment.

The analyzing magnet required far less shimming than the focusing magnet because of the relatively small effect of the fringe field. However, some iron was added along the entire length of the pole tips on the inner and outer radii of the gap region in order to enlarge the useful aperture. The defocusing effects predicted by the second order calculation (1, 2) are probably partially removed by the empirical shimming.

Object and image points of the magnet were measured with the stretched wire and the magnet placed in position relative to the scattering chamber according to these data. The stretched wire data indicate that the spread in energy at one point in the image plane

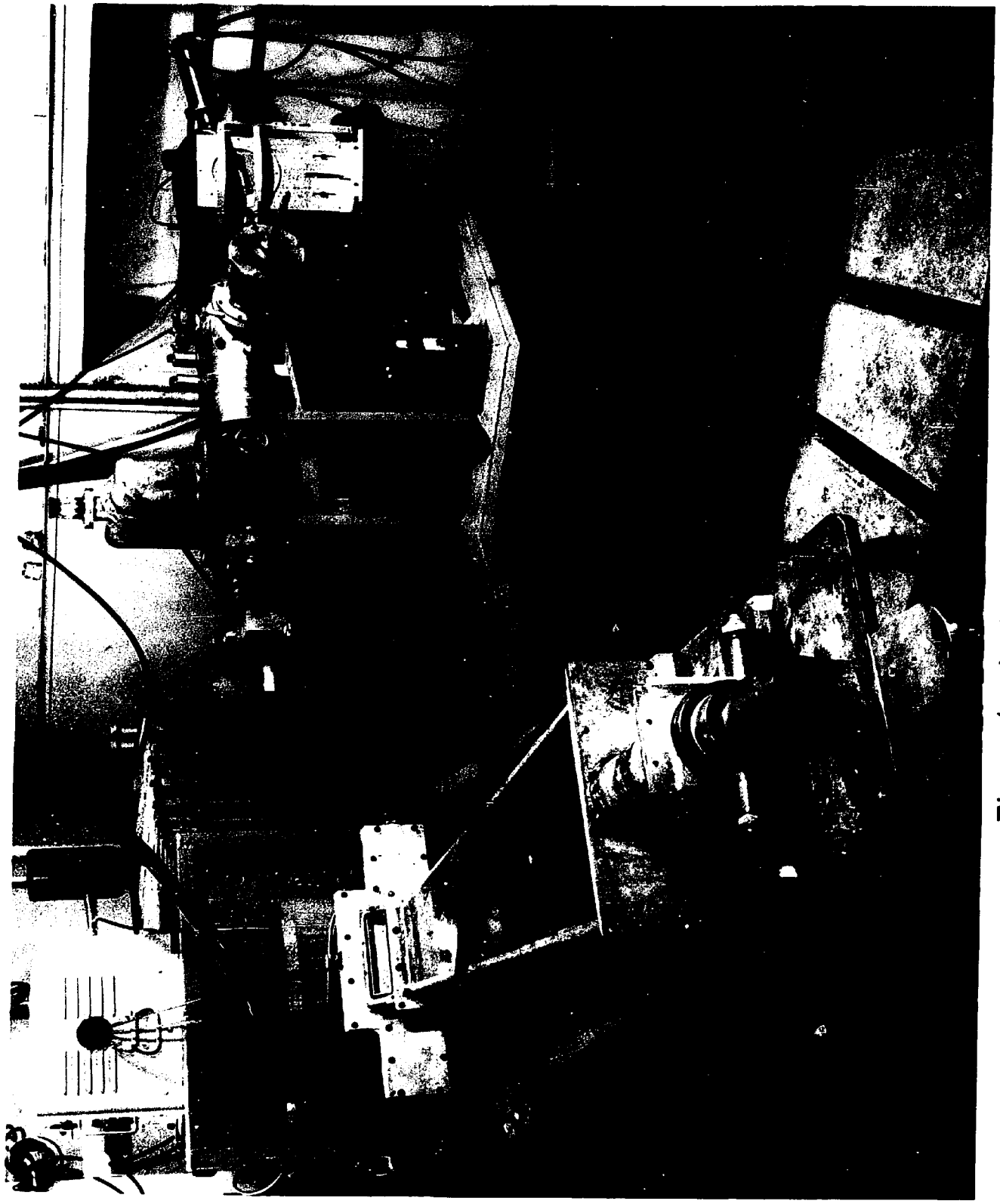


Figure 4. Analyzing magnet.

from a heterogeneous point source is ± 7 Kev for 7.8 Mev deuterons. This is a measure of the accuracy of the stretched wire measurement and does not necessarily represent the quality of focus finally attained. Measurement of the image distance made with elastic scattered deuterons gave t = 208 ± 5 cm., which is in good agreement with the value of t predicted by the first order theory.

Since n was of necessity chosen to be 0.45, the double focusing properties predicted for an n = 0.5 magnet were somewhat impaired. The predicted image distance from the exit pole face becomes 330 cm. for vertical focus whereas the radial image point is at 208 cm. However, measurements made on the vertical distribution of scattered particles in the image plane show a full width at half maximum of 28 mm. from a target having a vertical height of 9 mm. Since the detectors used can accept particles with a vertical distribution of the order of one inch or more, enough of the double focusing property is retained to prevent any appreciable loss in intensity.

Relevant data on the analyzing magnet are as follows:

Object and image distances	208 cm.
Central radius of curvature	100 cm.
n	0.45
Angle of bend	90°
Dispersion (calculated for 7.8 Mev deuterons)	4.2 Kev/mm
Dispersion (measured for 7.8 Mev deuterons)	4.37 Kev/mm
Useful radial aperture at center of magnet	10 cm.
Geometrical radial aperture at center of magnet	15 cm.
Solid angle (in steradians)	4.5×10^{-4}
Focal length	170 cm.

Distance from pole face to principal foci	38 cm. outside field region
Average gap	6.35 cm.

Particle Detectors

Conventional cylindrical proportional counters and nuclear track plates were used for particle detection. For the examination of the resolution of the over-all system, a large proportional counter (13 inches long, 3 inches in diameter) having a one by three inch window was constructed. Two smaller double proportional counters were machined from solid blocks of aluminum. One of these is used as a beam monitor and is placed inside the scattering chamber so that it is rigidly fixed in space with respect to the target and the incident deuteron beam (Figure 5). The second is used as a heavy particle detector in the image plane of the analyzing magnet. These two counters are filled with a 96 percent argon, 4 percent CO_2 mixture to a pressure of 40 cm. Hg and are operated at a central wire potential of 1500 volts.

Standard cathode follower preamplifiers in conjunction with 204-B amplifiers (34), coincidence circuits, and scalers were used with the above described proportional counters.

One by three inch 100 micron Kodak nuclear track plates were used for collection of the final data. Four of these plates can be placed along the image plane of the analyzing magnet enabling one to cover a range of relative momentum of 7 percent at one exposure. The plate method has the advantage that Q values for unknown nuclear levels can be measured relative to the Q values of known levels appearing on the same set of plates. A second reason

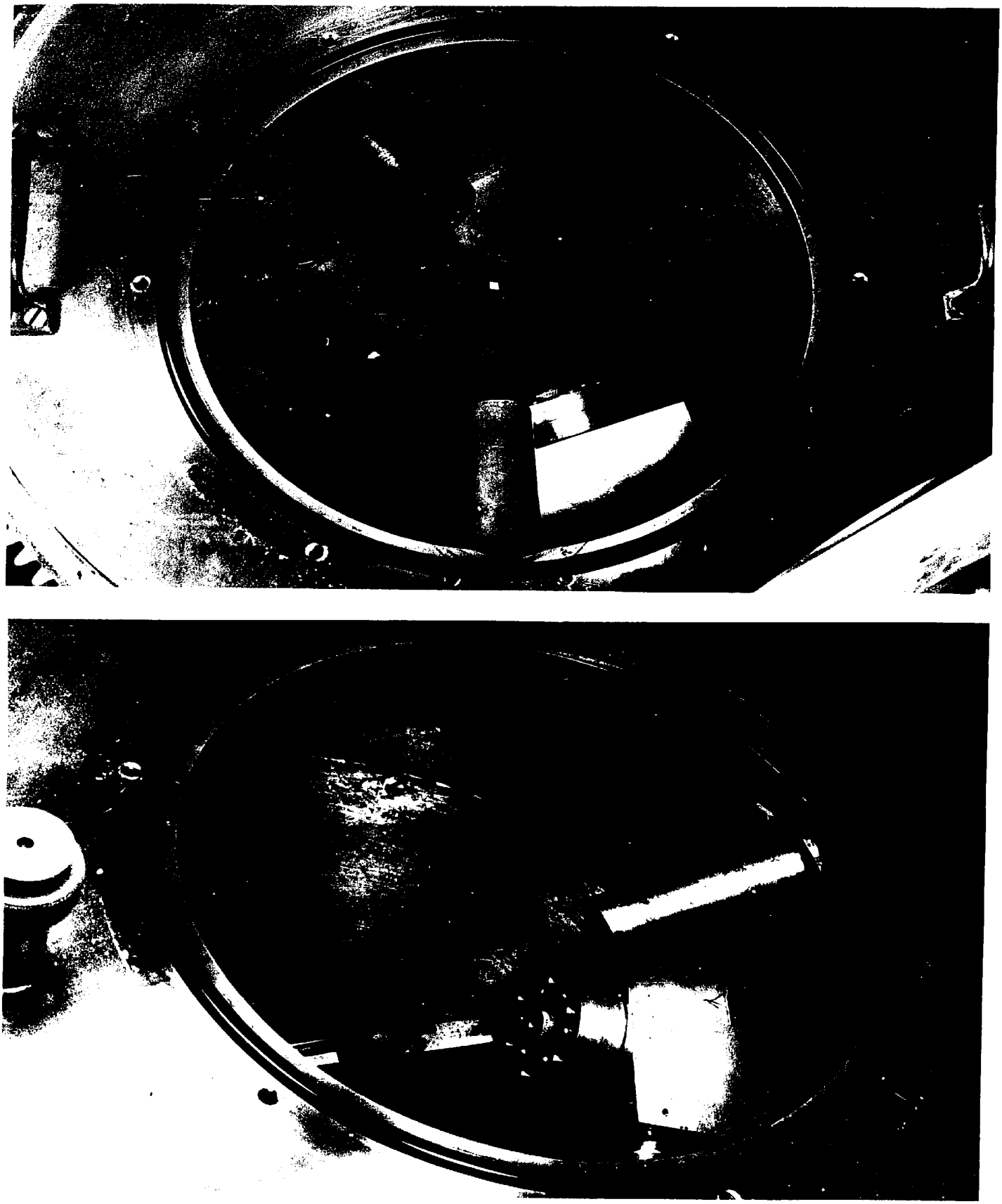


Figure 5. Monitor, target, and exit slit. Incident beam aperture visible in upper photograph.

for using plates is the great gain in data obtained per cyclotron hour.

The present analyzing magnet field regulator uses a nuclear moment device placed in a prepared field in the fringe field of the magnet. The nuclear moment probe is placed between two pieces of half-inch iron which are positioned between the magnet coils close to the poles. The magnetic field intensity in the prepared field is about one-third the intensity of the field in the analyzing magnet gap. The hysteresis loops of the iron in the prepared field and the iron in the analyzing magnet are obviously different. This means that the ratio between the two fields is not constant. It was found that differences of thirty Kev at a proton energy of 8.5 Mev are introduced by turning the analyzing magnet on and off. On the other hand, without changing the field purposely, particle groups having half widths of 20 Kev have been measured by means of one hour exposures of nuclear plates indicating that the fixed field regulation is satisfactory.

CHAPTER III

EXPERIMENTAL PROCEDURE

Preliminary Investigation

Resolution.--The resolution of the entire system was investigated by observing the lateral distribution of elastic scattered deuteron groups in the image plane of the analyzing magnet. These measurements were made by moving a 2 mm. wide slit across the window of the large proportional counter described above. Elastic scattered deuterons from various targets were counted as a function of linear position along the image plane.

In order to follow the sequence of events for this investigation, it is necessary to understand the complete slitting system (Figure 6). Slits which restrict the radial aperture (radial is used in the magnetic field sense) are denoted R slits and slits which restrict the vertical aperture are denoted Z slits.

Preliminary investigation of the focal properties of the analyzing magnet at the center of the image plane were made with a 2 mm. wide 2.54 mg/cm^2 silver strip target. The peak of the elastic scattered deuterons from this target was found to have a large low energy tail. This was interpreted as being due to deuterons passing through poor field regions of the analyzing magnet. A more symmetric line shape was obtained when the exit R slits (G, Figure 6) were closed down to give a total of 6 cm. radial aperture. This aperture was found to correspond to the useful aperture of the magnet as found by the stretched wire method.

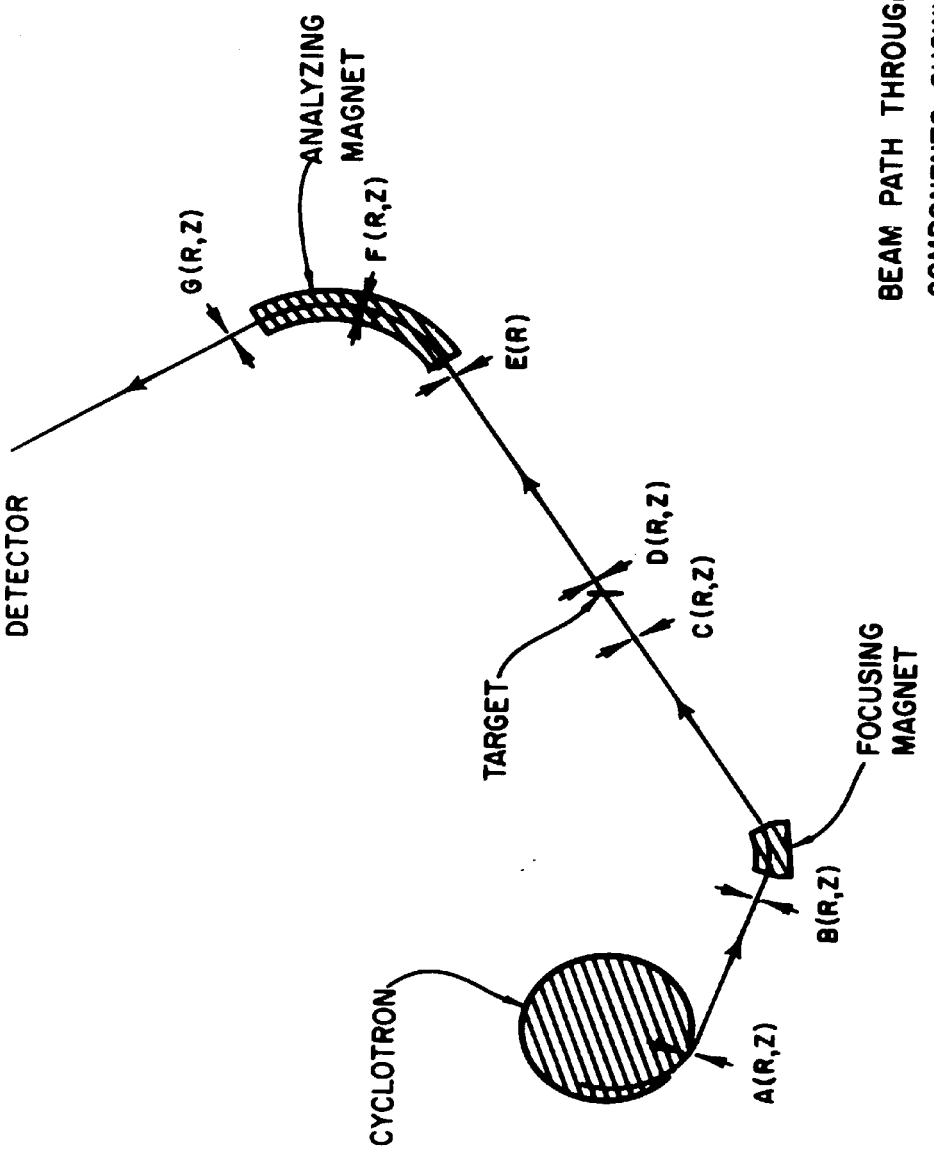

DETECTOR
G(R,Z)
ANALYZING MAGNET
F(R,Z)
E(R)
D(R,Z)
C(R,Z)
TARGET
FOCUSING MAGNET
B(R,Z)
A(R,Z)
CYCLOTRON
BEAM PATH THROUGH MAJOR COMPONENTS SHOWING POSITION OF SLITS.
R = RADIAL SLITS
Z = VERTICAL SLITS
MAGNETIC FIELD REGIONS
NOT TO SCALE

Figure 6

An additional effect of restricting the radial aperture at G is to reduce drastically the intensity of particle groups which are focused at the extreme off-center positions in the image plane. This can be most easily seen by referring to the results (Figure 7) of measurements of the trajectories of polonium alpha particles in the analyzing magnet made by O. Bilaniuk. The paths drawn represent the central rays of the alpha beams striking the detector at two off-center positions in the image plane. The slits G obviously interfere with the extreme radial rays. Slits G were therefore opened to their full aperture and a four inch radial slit was placed inside the magnet gap at position F. Particles which pass through the poor field regions of the magnet are thus not detected in the image plane and there is no unnecessary reduction of intensity.

The longitudinal image distance for the analyzing magnet at the center of the image plane was found by locating the position of minimum half width. The full width at half maximum of the elastic scattered deuteron peak from the silver target was found to be 9 mm. corresponding to 38 Kev. Restrictions made in radial aperture at the various slit positions showed no observable change in half width. The stability of the system was found to be better than 10 Kev (Figure 8) over an eight hour period with the focusing and analyzing magnet regulators left unchanged and the cyclotron kept in resonance for maximum beam. This stability was achieved only after a two hour warm-up period.

A classical (3) calculation of the energy straggling expected in the silver foil showed that a large part of the measured half width could be due to this effect. Therefore, further measurements were made with a 0.2 mg/cm^2 gold leaf target. Full widths at half maxima of the elastic scattered deuteron groups from this target

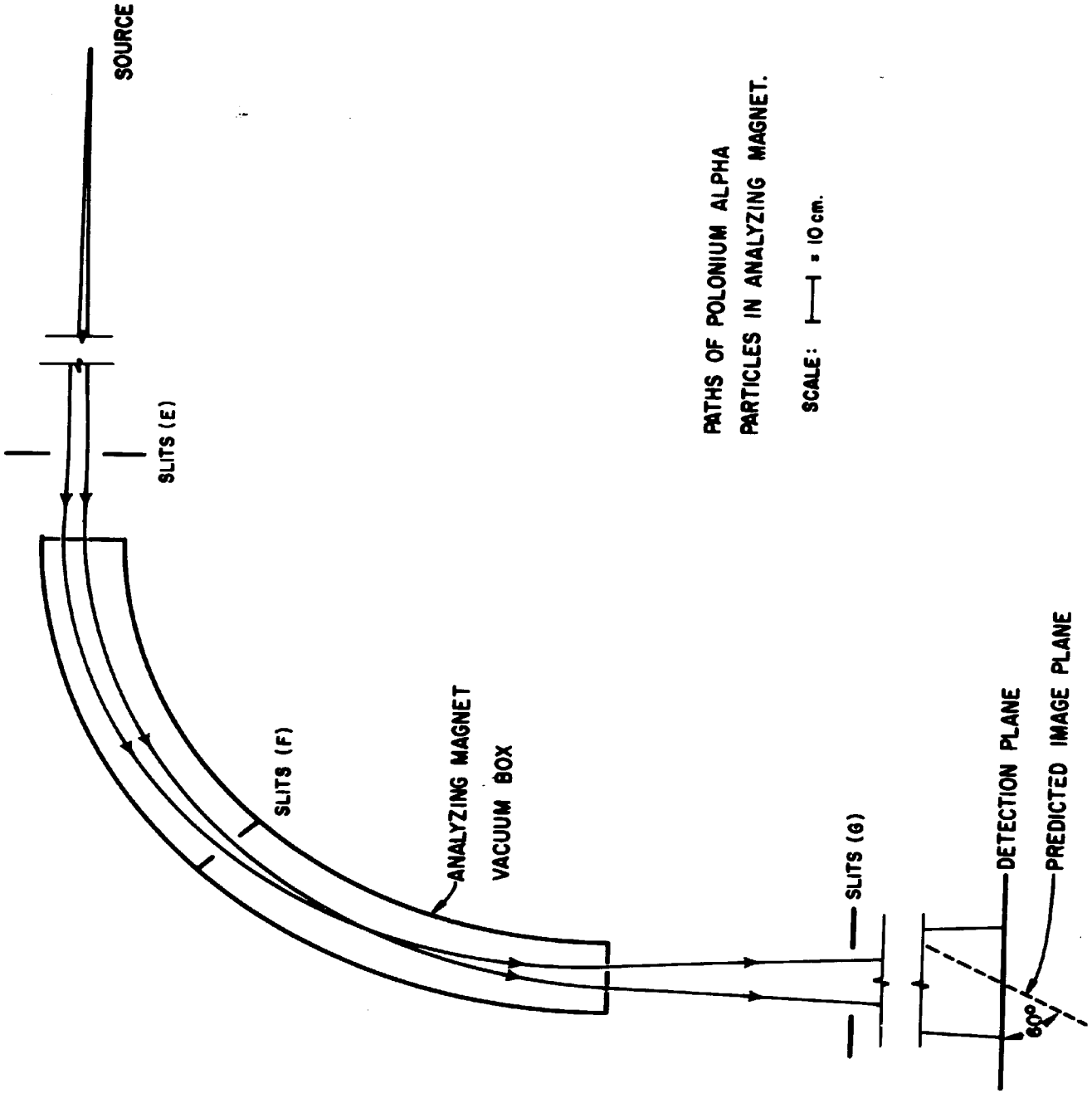

SOURCE
SLITS (E)
SLITS (F)
ANALYZING MAGNET
VACUUM BOX
SLITS (G)
DETECTION PLANE
PREDICTED IMAGE PLANE
60°
PATHS OF POLONIUM ALPHA
PARTICLES IN ANALYZING MAGNET.
SCALE: 1 = 10 cm.

Figure 7

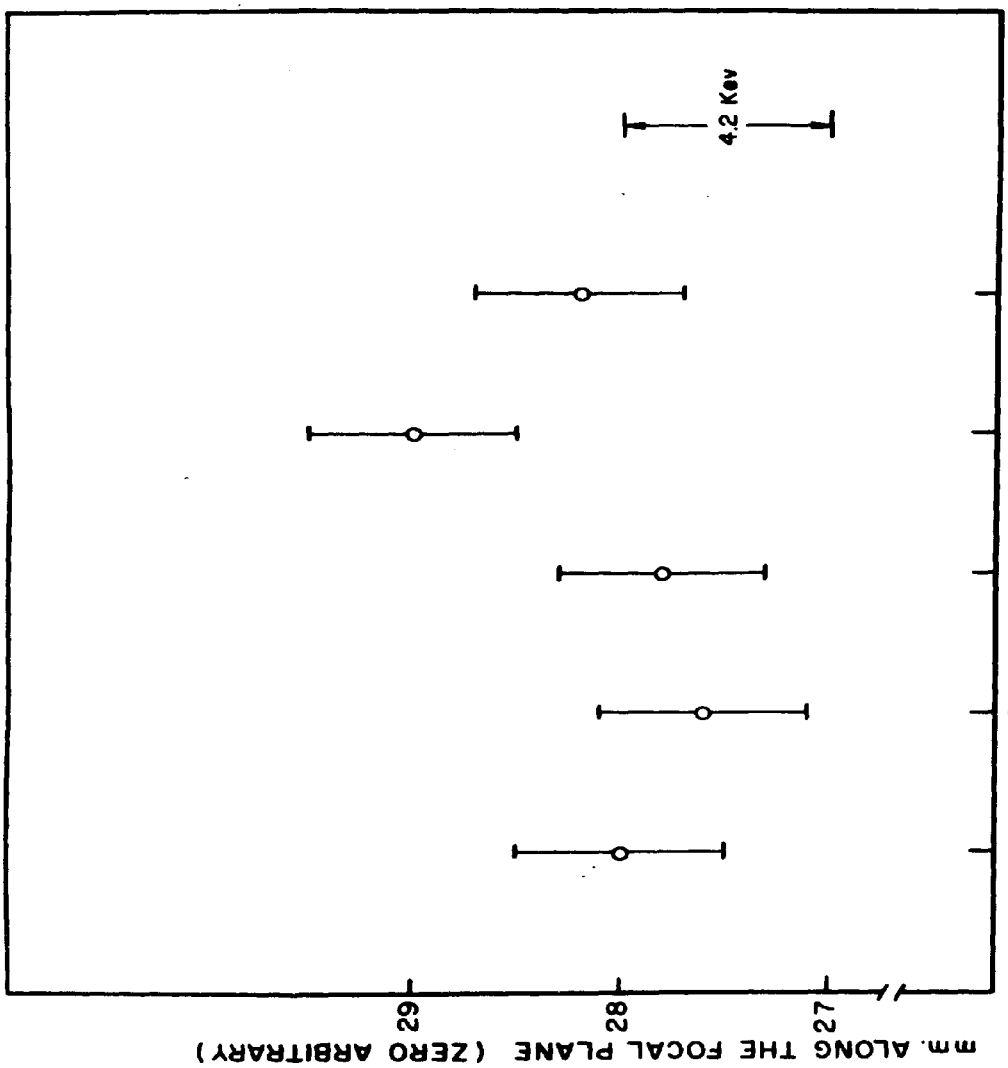


Figure 8. Data showing stability of system.

measure from 17 to 25 Kev (Figure 9). Nuclear plates were used to cover a portion of the $Al^{27}(d,p)Al^{28}$ proton spectrum from a 0.14 mg/cm^2 aluminum leaf target. Six proton groups with energies of about 10 Mev show full widths at half maxima ranging between 21 and 22 Kev (Figure 10).

Using these data, an experimental number for the resolving power, R, of the system can be derived. Such a quantity is usually defined as

$$R = P/\Delta P = 2(E/\Delta E)$$

where P and E are the particle momentum and energy; ΔP is the difference in momentum between two particle groups that are barely resolvable, and ΔE is the corresponding energy difference. If the peaks of two groups of equal intensity are separated by more than the full width at half maximum a dip in intensity between the two peaks will be observed and the groups are considered resolved. Therefore, dE is taken to be equal to the full width at half maximum and the aluminum data give a resolving power of 930 for the system.

Since the source of particles at the scattering chamber is not monoenergetic, this measure of the resolving power does not represent the resolving power of the analyzing magnet. The geometrical positions of the focusing and analyzing magnets with respect to each other cause a collapse in the dispersions of the two magnets. Deuterons of higher energy impinge on the target at larger radial positions than those of lower energy. Therefore the higher energy scattered particles are focused at smaller radial positions in the analyzing magnet image plane. The spread in energy of the scattered particles caused by the spread in energy of the deuteron beam striking the target is therefore reduced. The resolving power obtained is

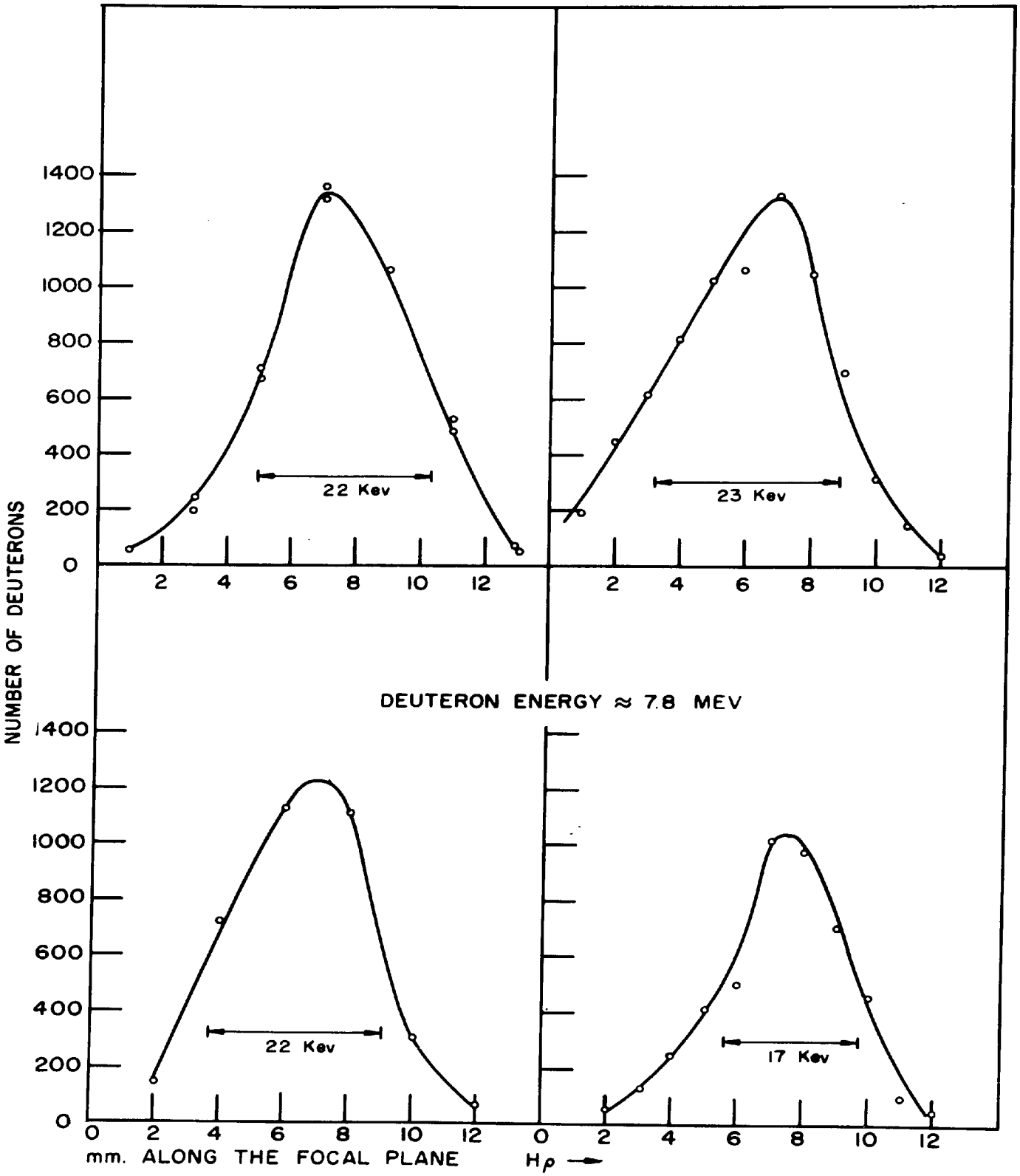


Figure 9. Elastic scattered deuterons from an Au target.

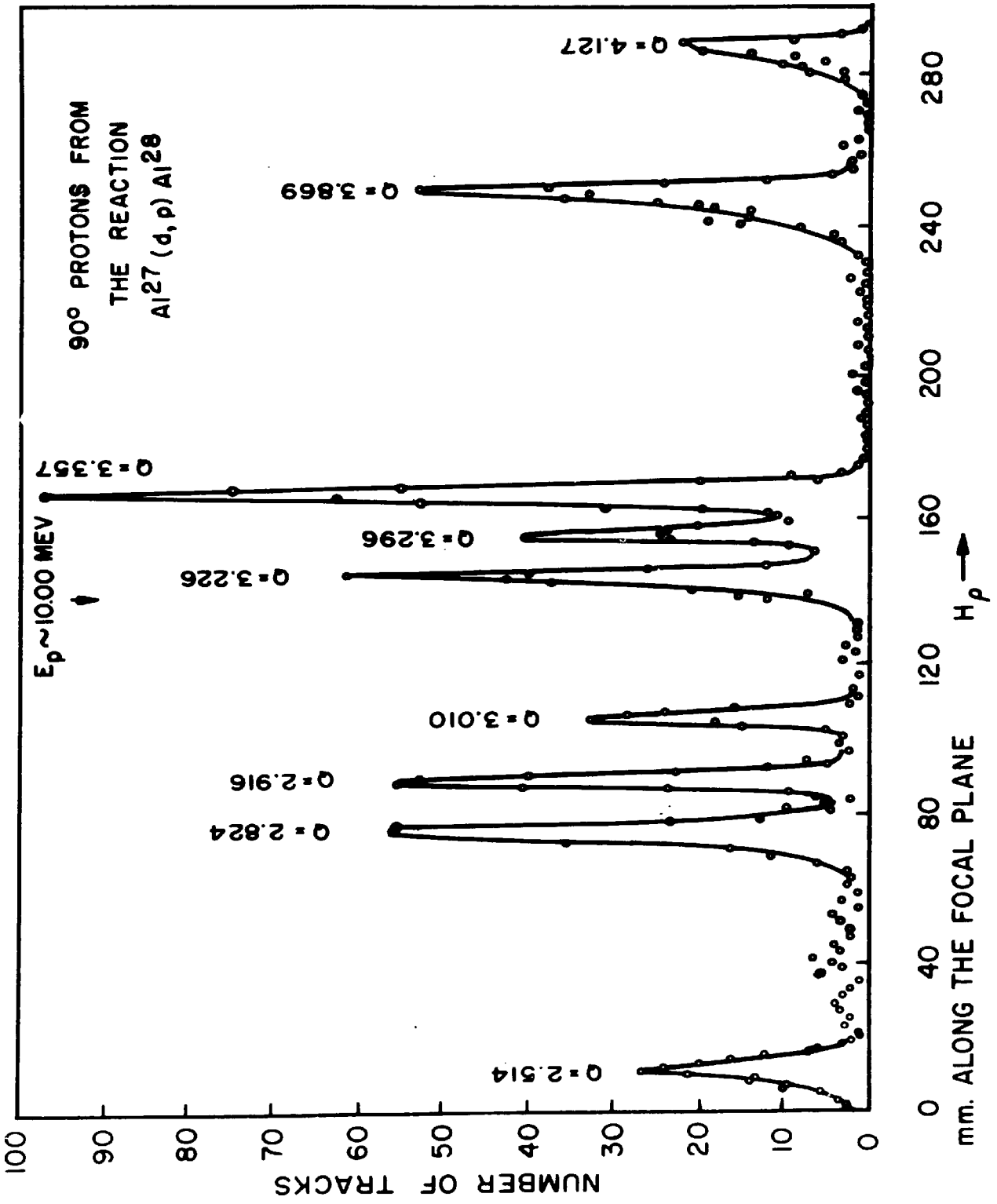

90° PROTONS FROM
THE REACTION
Al27 (d, p) Al28
Ep~10.00 MEV
Q = 4.127
Q = 3.869
Q = 3.357
Q = 3.296
Q = 3.226
Q = 3.010
Q = 2.916
Q = 2.824
Q = 2.514
NUMBER OF TRACKS
mm. ALONG THE FOCAL PLANE
Hρ

Figure 10

due to ion optical imperfections in both magnets and does not arise from source and image sizes.

Analyzing magnet dispersion.--A first order calculation for the energy dispersion of the magnet gives 4.2 Kev/mm at 7.8 Mev. This uses the constants given on page 13. The dispersion D is defined as

$$D = \frac{\delta x}{\delta P/P}$$

and can be shown (1, 2) to be equal to $\frac{1-M}{1-n}$ where δx is the radial change in the image coordinate for a δP change in momentum, p is the particle momentum, n is the first order fall-off parameter of the magnetic field or $\frac{1}{B}\frac{dB}{dr}$ and M is the magnification which is equal to -1 for an equal arm magnet. On substitution, the following result is obtained:

$$\frac{\delta E/E}{\delta x} = 0.54 \times 10^{-3} \text{ mm.}^{-1}$$

Measurements of the dispersion were made by means of a portion of the $Al^{27}(d,p)Al^{28}$ spectrum (Figure 10). Aluminum was chosen because of the simplicity of thin target preparation, the great number of closely spaced energy levels, and the well-known Q values for the reaction (4). The spectrum was taken with one set of four one by three inch photoplates in the image plane of the analyzing magnet. The scattering angle of 90° was chosen because the separation in energy between any pair of groups is then independent of the deuteron energy (see Equation III-3).

For two groups of identical particles with energies E_2, E_1, and separated by Δx mm., the dispersion function $a(x)$ is defined by:

$$a(x) = \frac{2(E_2 - E_1)}{\Delta x (E_2 + E_1)} \qquad \text{(III-1)}$$

The errors in the measurement consist of errors in the Q measurements of the $Al^{27}(d,p)Al^{28}$ excited states, errors in measurement of the peak positions on the plates, and an uncertainty in the value used for the deuteron beam energy. The last uncertainty introduces a systematic error in the dispersion measurements made from the various groups on the same set of plates. However, an assumed error of 100 Kev in the deuteron energy causes an error of only 1 percent in the dispersion function.

It was found that there is a 20 percent variation in the dispersion function across the image plane of the magnet. A plot (Figure 11) was made which shows this variation. The bars represent errors due to measurements of the peak positions and errors in the aluminum Q values. The plateholder was placed for convenience parallel to the exit pole face of the analyzing magnet. It is suggested that the variation in the dispersion function might be reduced considerably by repositioning the plateholder. The first order calculation (5) shows that the image plane should be inclined at an angle of 60° with respect to the pole face (see Figure 7). The uncertainties in the calculation indicate that the best position must be found in an empirical manner. Considerable asymmetry in the peak shapes noted at the extremes of the image plane may also be explained by this effect.

A change in the deuteron energy shifts the entire dispersion curve in the vertical coordinate direction. Since the aluminum spectrum was not taken at the same time as the final data, further measurements of the dispersion constant were made on the final spectrum from known oxygen, lithium, and carbon groups. It was necessary to place the plates for the experiment inside the magnet vacuum chamber at a position about two inches closer to the exit pole face than the position used for the aluminum spectrum. In addition to

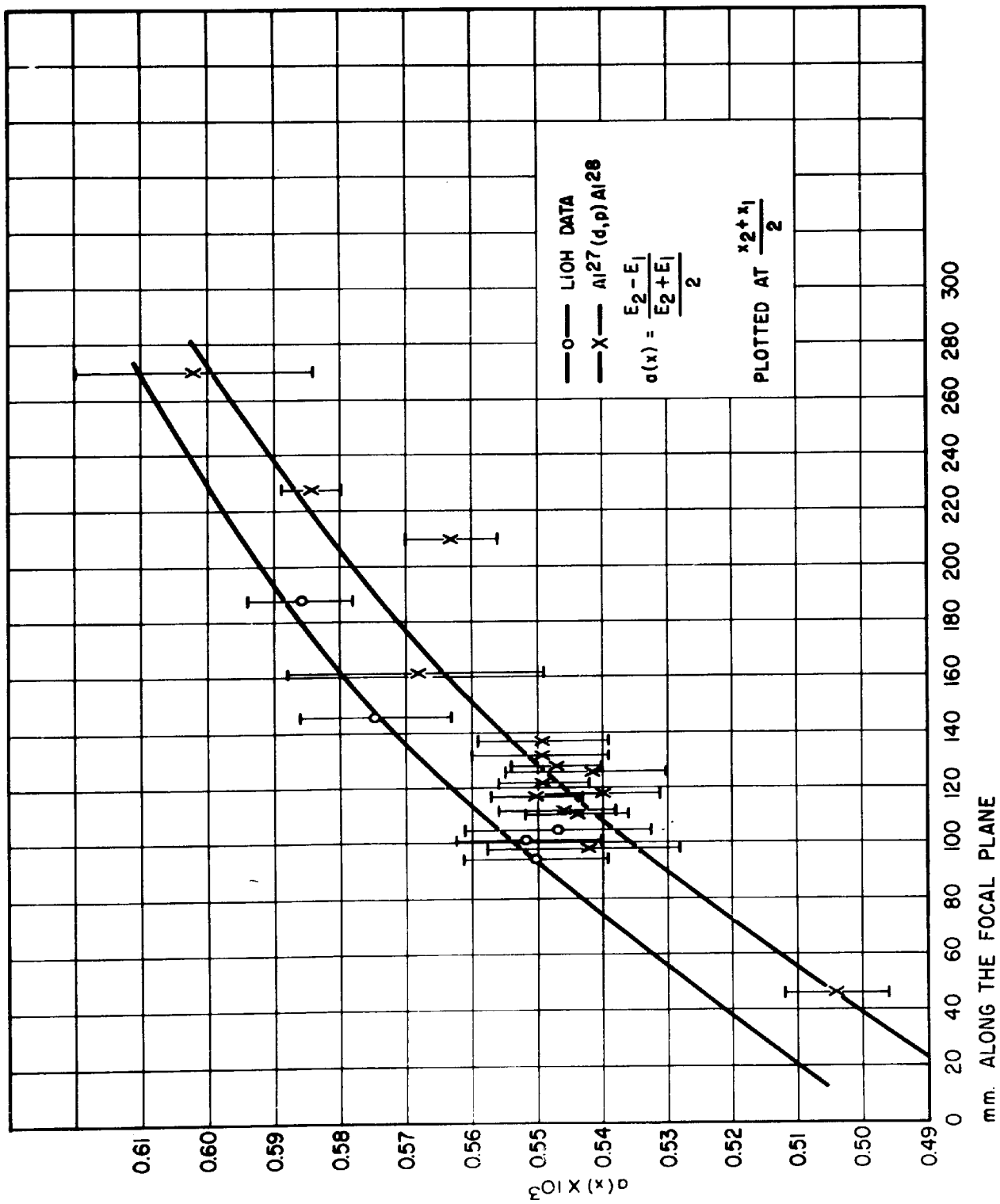


Figure 11. Analyzing magnet dispersion curve.

shifting the dispersion curve due to a possible difference in deuteron energy, the geometrical effect of moving the detector closer to the magnet would be expected to raise the dispersion function a. An examination of the particle orbits by means of polonium alpha particles shows that a should be increased by 2 percent. It was found that a was increased by 3 percent, indicating that a 1 percent change in a due to a shift in the deuteron energy had occurred.

Background reduction.--The background level is defined as the number of particles (e.g., deuterons) appearing in a spectrum as a continuum apart from regions covered by reaction product groups. Preliminary runs made with an enriched oxygen gas target demonstrated a background level of about 1/50 the intensity of the elastic scattered deuterons from O^{16}. Since enriched oxygen containing approximately equal abundances of O^{16} and O^{18} was available, the criterion of an elastic scattered deuteron intensity from O^{16} to background ratio of 2,000 to 1 was arbitrarily selected. This would make inelastic scattered deuteron groups from O^{18} of intensity 1 percent of the elastic scattered group ten times more intense than the background level.

Various targets were examined by using a proportional counter in the image plane of the analyzing magnet. The investigation demonstrated that deuterons degraded in the slit edges just ahead of the target were responsible for a large part of the deuteron background. Targets made from high Z material were found to be unsatisfactory for deuteron spectra because of the increased scattering in the target of low energy deuterons scattered from vacuum chamber walls.

In order to eliminate the effect of the slit, a strip target of 0.0005 inch mylar was tested in the cyclotron for deuteron background.

This was found to be satisfactory and gave a ratio of elastic deuterons to background of about 3,000 to 1.

The effect of nonuniform targets is to make the shape of reaction product groups asymmetric. The distortion of peak shape can be so extreme as to form a tail that decreases gradually in intensity over an energy range of several Mev. Attempts to make strip targets of LiOH resulted in extremely nonuniform targets. For this reason, a one quarter inch square of LiOH on Formvar was placed on a single layer of 0.010 mg/cm^2 Formvar mounted on a one inch square target frame (Figure 5). A further attempt to make the Formvar mounted target effectively a strip target was made by placing a slit between the target and the analyzing magnet entrance aperture. This prevents the majority of particles scattered from the large Formvar backing from entering the magnet. The ratio of elastic scattered deuterons to background on the final run is about 2,000 to 1.

On examination of the spectrum, it is found that the background level is always increased below strong groups of the same kind of particle. This is probably due to reactions in the target caused by low energy deuterons scattered from slits and vacuum chamber walls far ahead of the target. A fundamental difficulty of the present system is that, for high resolution, a small portion of the beam entering the scattering chamber must be selected either by a slit or by using a strip target. For low intensity work a strip target seems to be almost essential but extremely difficult to manufacture.

Target Preparation

The first work on the unknown spectrum of O^{18} was done with an enriched gas target. The gas chamber was machined from a solid

block of aluminum and was fitted with windows of 9.1 mg/cm^2 nickel foil. The gas used (74 percent O^{16}, 25 percent O^{18}, 1 percent O^{17}) was obtained through the courtesy of A. O. C. Nier at the University of Minnesota. Measurements of the pressure made by observing the momentum spacing between known deuteron and proton groups indicated no apparent change in gas pressure over a period of about three months. The spectrum of scattered particles observed with this target showed contamination groups from carbon, nickel, and nitrogen. These groups covered such a large portion of the spectrum that it was impossible to derive any information on the presence or absence of groups from O^{18}.

Analysis of these data demonstrated additional defects of gas targets. The windows contribute to the widths of reaction product groups without adding to the counting rate of relevant reactions. The calculation of the energy loss of different particles through portions of the target is involved and uncertain due to the bowing of window foils. For these reasons, it was decided at this point to search for a stable solid target.

Since the enriched oxygen was obtained in the form of oxygen gas, attempts were made to form oxide layers on various substances including lithium and bismuth. These were unsuccessful mainly because the oxide layers formed were too thin. For intensity reasons it was considered desirable to have at least 0.20 mg/cm^2 of oxygen in the target.

The chemical reaction finally used was:

$$Li + H_2O \longrightarrow LiOH + (1/2)\ H_2$$

This reaction takes place at room temperature and reasonable pressures.

It was first necessary to explode the enriched oxygen with hydrogen in order to form the water required for the above reaction. Since only about 20 mg. of oxygen was available, the major difficulty of this operation was one of the efficiency of the explosion and of water collection. A glass system consisting of a mercury transfer pump and a connecting explosion chamber was constructed (Figure 12). It was found necessary to clean the interior of the explosion chamber after each explosion in order to prevent adsorption of water vapor on the walls. After filling the explosion chamber with one volume of O_2, about four volumes of H_2 were added and the explosion was triggered by a Tesla coil connected to a platinum spark gap in the interior of the chamber. A rather mild "pop" and a brilliant blue flash is observed when the reaction takes place. The total pressure in the explosion chamber before explosion is about 40 cm. of Hg. It was found unnecessary to keep a level of mercury in the chamber to act as a buffer for the explosion.

The water vapor was condensed in a glass bottle connected to the explosion chamber and surrounded by liquid air. During the collection process, the explosion chamber and connecting glassware was heated gently with a gas air flame in order to remove as much water as possible from the walls. Test runs made with nonenriched oxygen demonstrated an efficiency of between 50 and 80 percent for the explosion and collection process, depending largely on the cleanliness of the system. The yield of the enriched oxygen explosion was about 11 mg. of H_2O.

Tests were made on various types of containers to determine the quantity of water lost through surface adsorption. The results showed a negligible amount of water loss in clean glass systems, but a prohibitive amount in a brass system sealed with "O" rings. For this reason, a small glass hydroxidation chamber was constructed

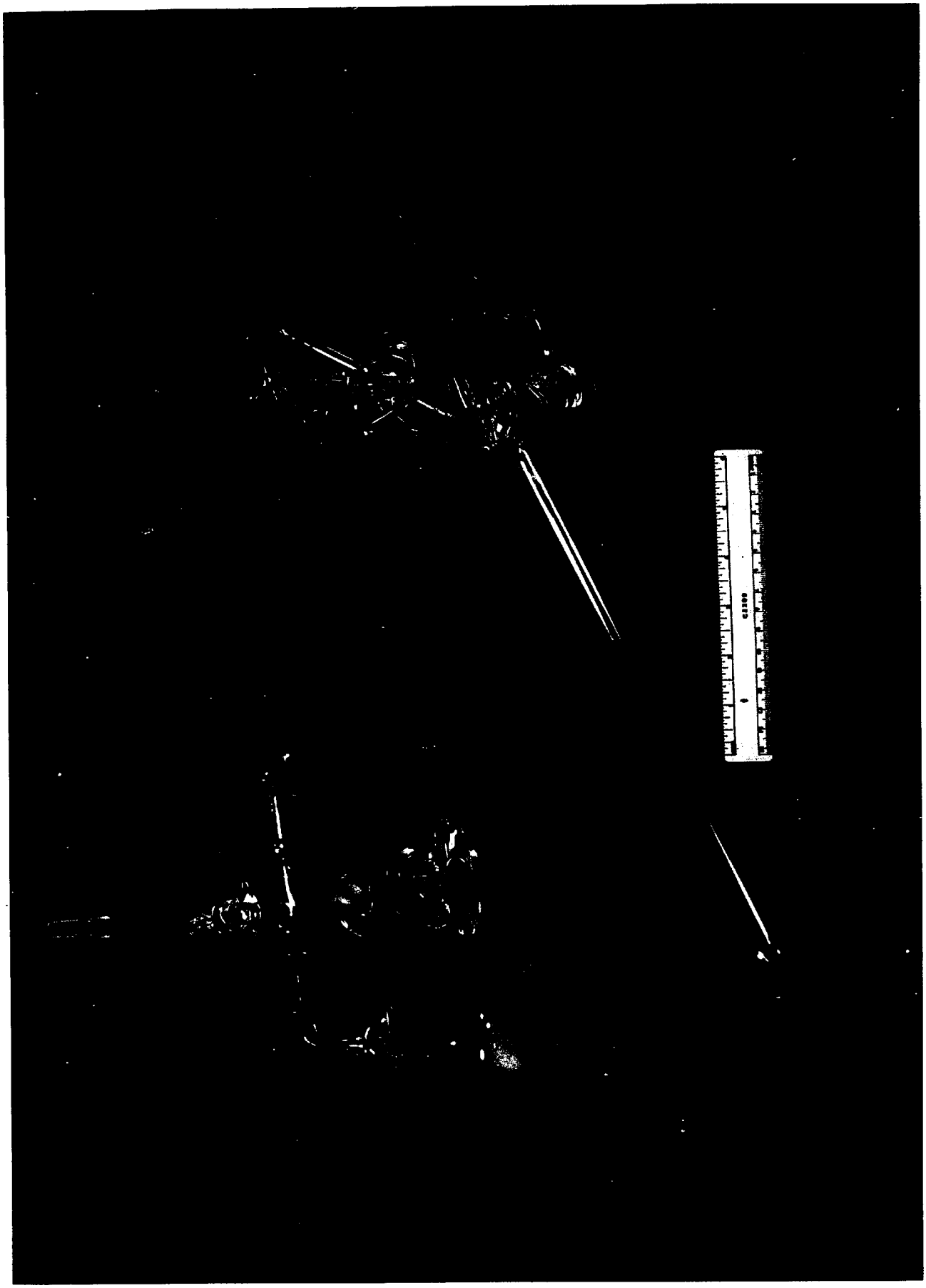


Figure 12. Explosion and hydroxidation chambers.

(Figure 12). Lithium is evaporated through a large (one cm. diameter) stopcock onto the target foil. After evaporation, the stopcock is closed and water vapor from the enriched water bottle is admitted to the system. It is necessary to cool the water bottle to a temperature somewhat below room temperature (10-20° C.) in order to prevent excess water from condensing on the target. Since LiOH is deliquescent, the enriched water bottle must be placed in liquid air as soon as the white hydroxide has formed in order to prevent destruction of the target.

The nature of the background problem (see page 28) requires that a rather thick layer of LiOH be supported by a thin backing. The simple technique of hydroxidation of a thin layer of Li on a thin backing results in complete distortion of the foil because of the difference in densities of the evaporated Li and the LiOH. Only when the backing material is made considerably thicker than the evaporated layer can smooth targets be obtained. Several nonenriched targets on 0.8 mg/cm^2 mylar were made in this manner.

The technique for making thick targets on thin backings that was finally developed is as follows: A clean piece of smooth glass is covered with a dry layer of about 0.020 mg/cm^2 Formvar (1 percent by weight Formvar in ethylene dichloride dropped on water and picked up by frame). The Formvar must adhere smoothly to the glass over the target area. Lithium is evaporated onto the Formvar covered glass and the hydroxide formed. A razor blade is then used to peel up portions of the LiOH covered Formvar. A piece is then placed, Formvar side down, onto a layer of Formvar supported by a one inch square target frame (Figure 5). Slight pressure applied with a smooth, round-ended metal object is enough to make the target stick to the Formvar. A second layer of Formvar is then placed over the target and frame.

An obvious defect of this target preparation is the mechanical operation described above. The removal from the glass plate is not always successful and the delicate foil can curl enough to be useless if the transfer is not made quickly. Another defect, not restricted to this particular target, is instability under deuteron bombardment. The backing layer of Formvar can melt or break due to excessive heating caused by the energy loss of particles passing through the foil and by electrostatic forces which arise from the charging of the foil by secondary electron emission.

Attempts were made to improve the stability of the targets both by keeping the cyclotron beam current to the scattering chamber as small as practicable and by making use of a filament close to the target in order to keep the target discharged. The last run was made under these conditions and indicated that the situation was definitely improved.

Collection of Data

Of major importance in obtaining particle spectra by means of nuclear plates is the constancy of the deuteron energy. For this reason the focusing magnet regulator is left untouched during a run in order to keep the deuteron energy into the scattering chamber fixed.

A total of 84 one by three inch photoplates were exposed in two runs. The 50° and 90° plates were taken during run No. 1 and the remainder were taken during run No. 2.

Preliminary investigation with counters had given a rough calibration of the analyzing magnet nuclear moment field meter frequency in terms of particle momentum. It was thus possible to set the field to a correct value by noting the frequency position of some

strong well-known group of reaction particles. Plates were exposed with about one plate overlap in order to lessen the danger of missing groups.

The plates were placed at an angle of 45° with respect to the magnet Z axis. Where necessary, absorber foils were placed in front of the plates in order to make particle identification by track length possible. Microscope scanning was done in half mm. vertical strips using an 8 mm. oil immersion lens.

Data Analysis

Target thickness.--Measurements of target thickness were made by examination of the $C^{12}(d,p)C^{13}$ ground and first excited state peak shapes. From the structure of the targets used (see page 29 and Figure 13), carbon protons can arise in four different ways. These are: (1) by protons produced in and passing through the thin Formvar layer alone; (2) by protons produced in the front Formvar layer and passing through the LiOH target; (3) by protons produced in the LiOH target due to a uniform carbon contamination; and (4) by protons produced in the back Formvar layer.

Because of the great difference in thickness of the Formvar layers and the LiOH target, it is possible to estimate the relative half widths of the proton peaks in each of the four cases. Case (1) should give a high resolution peak with a half width of 20 Kev or less; cases (2) and (4) should show peak widths due to straggling of proton and deuterons respectively, plus a contribution due to target nonuniformity; and case (3) should exhibit a thick target width comparable to that of the single peaks from oxygen in the LiOH.

Two difficulties must be noted: (a) The intensity of the sharp peak (1) depends on the size of the LiOH target relative to the aperture

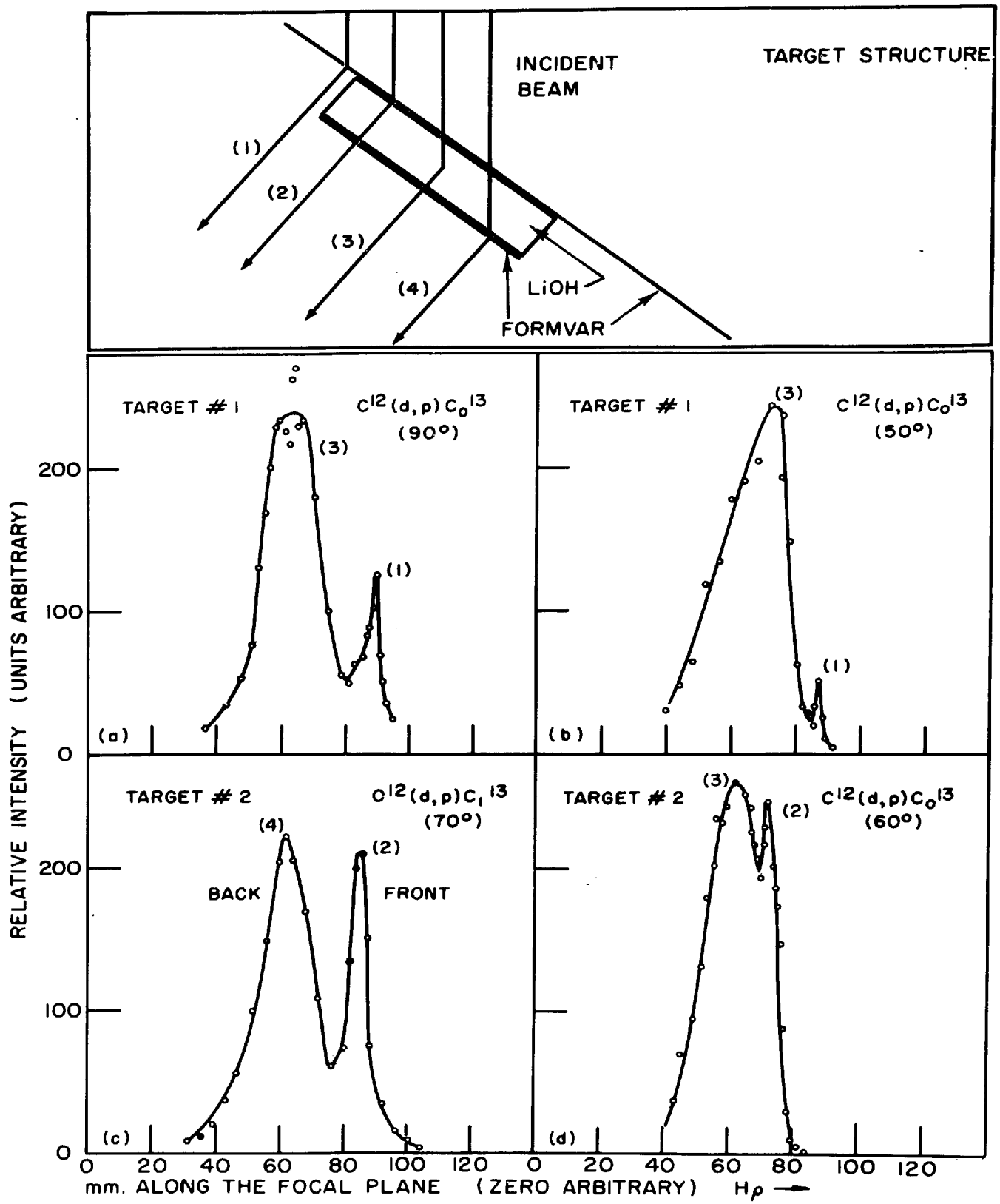


Figure 13. Target structure and $C^{12}(d,p)C^{13}$ peaks.

of slit D (Figure 6). When the target is larger than the aperture, the peak must be missing; as the target becomes smaller the peak appears and becomes more intense. (b) Because of the low melting point of Formvar any of the layers adjacent to the thick target can be destroyed by the passage of deuterons through it.

For this reason the carbon level structure is unfortunately a function of bombardment time. The first plate exposed during run No. 2 (c, Figure 13) shows cases (2) and (4) with well-defined front and back layers. A plate taken six hours later during the same run (d) shows complete deterioration of the back layer and only a small part of the front layer remaining. This indicates that some of the Formvar has melted and penetrated into the LiOH. A measurement of the energy separation of the front and back layers in (c) gives a half target thickness of 0.65 ± 0.05 mg/cm^2. A similar measurement from the structure shown in (d) gives 0.65 ± 0.1 mg/cm^2 assuming that the wide peak is of type (3).

Definite spikes of type (1) are demonstrated in the carbon structure obtained from target No. 1. The difference in the intensity of the pure Formvar peak relative to the large peak in the two curves (a) and (b) is due to a difference in target sizes. The 50° and 90° targets were obtained from the same evaporation and the measurements give half thicknesses of 0.58 ± 0.05 and 0.62 ± 0.05 mg/cm^2, respectively.

Variation of scattering angle with image plane position.--Reference is made to Figure 7, which shows trajectories of alpha particles striking different points in the image plane of the analyzing magnet. It is seen that particles of higher energy have a smaller scattering angle than particles of lower energy. A measurement of this effect was made by examination of the ground and first excited

state separation of Li^7 as seen by protons from the reaction $Li^6(d,p)Li^7$. The protons from these two levels have a large change of energy with respect to scattering angle because of the low nuclear mass. The measured separation is therefore sensitive to a difference in scattering angle between the two groups. Measurements made of the separation at three angles indicate a change in scattering angle of 1.0 ± 0.25 degrees across 304 mm. of the image plane. This is in good agreement with 1.1 ± 0.25 degrees which was obtained by examination of the alpha orbits.

Reaction kinematics (6).--Consider a nuclear reaction in which a nucleus, particle 0, is bombarded by particle 1. The reaction products are the recoil nucleus, particle 3, and particle 2 which has a direction making an angle θ with the original direction of the bombarding particle. By making use of momentum and energy conservation the following equations can be derived:

$$Q = E_2 + E_3 - E_0 - E_1 = E_2 + E_3 - E_1 \qquad \text{(III-2)}$$

$$E_2^{1/2} = \frac{(M_1 M_2 E_1)^{1/2} \cos\theta}{M_2 + M_3} + \left(\frac{M_3 Q}{M_2 + M_3} + \frac{M_3 - M_1}{M_2 + M_3} E_1 + \frac{M_1 M_2 E_1 \cos^2\theta}{M_2 + M_3} \right)^{1/2} \qquad \text{(III-3)}$$

$$E_3 = \frac{M_2 E_2}{M_3} + \frac{M_1 E_1}{M_3} - 2\xi \cos\theta \qquad \text{where } \xi = \frac{(M_1 M_2 E_1 E_2)^{1/2}}{M_3} \qquad \text{(III-4)}$$

$$Q = \frac{M_2 + M_3}{M_3} E_2 - \frac{M_3 - M_1}{M_3} E_2 - 2\xi \cos\theta \qquad \text{(III-5)}$$

Other useful relations which follow from these equations are:

$$\frac{\partial E_2}{\partial Q} = \frac{M_3}{M_2 + M_3 - \left(M_3 \varepsilon / E_2\right) \cos\theta} \qquad \text{(III-6)}$$

$$\frac{\partial E_2}{\partial \theta} = - \frac{2 M_3 \varepsilon \sin\theta}{M_2 + M_3 - \left(M_3 \varepsilon / E_2\right) \cos\theta} \qquad \text{(III-7)}$$

$$\frac{\partial E_2}{\partial E_1} = \frac{M_3 - M_1 + \left(M_3 \varepsilon / E_1\right) \cos\theta}{M_2 + M_3 - \left(M_3 \varepsilon / E_2\right) \cos\theta} \qquad \text{(III-8)}$$

$$\frac{\partial Q}{\partial \theta} = 2 \varepsilon \sin\theta \qquad \text{(III-9)}$$

$$\frac{\partial Q}{\partial E_1} = - \frac{M_3 - M_1}{M_3} - \frac{\varepsilon}{E_1} \cos\theta \qquad \text{(III-10)}$$

$$\frac{\partial Q}{\partial E_2} = \frac{M_2 + M_3}{M_3} - \frac{\varepsilon}{E_2} \cos\theta \qquad \text{(III-11)}$$

$$\frac{\partial Q}{\partial M_1} = \frac{E_1}{M_3} - \frac{\varepsilon}{M_1} \cos\theta \qquad \text{(III-12)}$$

$$\frac{\partial Q}{\partial M_2} = \frac{E_2}{M_3} - \frac{\varepsilon}{M_2} \cos\theta \qquad \text{(III-13)}$$

$$\frac{\partial Q}{\partial M_3} = - \frac{E_3}{M_3} \qquad \text{(III-14)}$$

$$\frac{\partial E_2}{\partial M_1} = - \left(\frac{E_1}{M_3} - \frac{\varepsilon}{M_1} \cos\theta \right) \left(\frac{M_3}{M_2 + M_3 - \left(M_3 \varepsilon / E_2\right) \cos\theta} \right) \qquad \text{(III-15)}$$

$$\frac{\partial E_2}{\partial M_2} = -\left(\frac{E_2}{M_3} - \frac{\mathcal{E}}{M_2}\cos\theta\right)\left(\frac{M_3}{M_2 + M_3 - \left(M_3\mathcal{E}/E_2\right)\cos\theta}\right) \qquad \text{(III-16)}$$

$$\frac{\partial E_2}{\partial M_3} = \frac{E_3}{M_3}\left(\frac{M_3}{M_2 + M_3 - \left(M_3\mathcal{E}/E_2\right)\cos\theta}\right) \qquad \text{(III-17)}$$

Equations 6 through 17 are useful for estimating the effect of small corrections and for evaluation of the probable errors in a measurement. It must be remembered, however, that the partial derivatives can only be applied to errors in a measurement involving independent determinations of E_2, E_1, and θ.

Relativistic effects can be included by noting that the correct relation between the energy and momentum of a particle is:

$$p^2 = 2M_0E + \frac{E^2}{c^2} \qquad \text{(III-18)}$$

Equation (III-2) is relativistically correct. Equations (III-3), (III-4), and (III-5) can be made relativistically correct by replacing each mass by an effective mass:

$$M_{eff} = M_0 + \frac{E}{2c^2} \qquad \text{(III-19)}$$

Determination of deuteron energy and scattering angle.--In its present state, the analyzing magnet is capable of making accurate measurements of the separation in energy between particle groups detected in the image plane. By means of the measured separations of certain types of known groups, it is possible to make an adequate measurement of the deuteron energy and the scattering angle.

The linear separation at the image plane between a known deuteron group and a known proton group is a rapidly varying function of the incident deuteron energy. For a given change in the deuteron energy, the change in the linear position of the deuteron group is approximately twice that of the proton group since the momenta are approximately equal. The scattering angle, on the other hand, can be measured by means of the separation between two particle groups emitted by nuclei of quite different mass. This is because the change of reaction product energy with angle is approximately proportional to the mass of the recoil nucleus (see equation [III-7]).

Available on the spectra were proton groups from (d,p) stripping reactions together with elastic and inelastic deuteron groups resulting in the recoil nuclei Li^6, Li^7, C^{12}, C^{13}, O^{16}, O^{17}, O^{18}, and O^{19}. Pairs of these levels appearing on the same set of plates were used to determine the beam energy and the scattering angle for both runs.

The energies of two groups appearing on the same set of plates are calculated utilizing an assumed incident deuteron energy and scattering angle. The measured separation of the two groups on the plates gives a separation in energy different from the calculated value. This difference is interpreted in terms of corrections to the assumed deuteron energy and scattering angle. Obviously, for the determination of both the scattering angle and incident deuteron energy, two pairs of groups must be used.

For two reaction product groups of identical particles with energies E_2' and E_2 (see equation [III-1]):

$$E_2' - E_2 = \left(\frac{E_2' + E_2}{2}\right) a \, \Delta x$$

where a is the value of the dispersion function at the linear position

midway between the two peaks and Δx the separation in mm. as measured from the plates. On rearrangement, this becomes

$$E_2' = E_2\left(1 + \frac{a\Delta x}{2}\right)\left(1 - \frac{a\Delta x}{2}\right)^{-1} \cong E_2\left(1 + a\Delta x + \frac{(a\Delta x)^2}{2}\right)$$

Or,

$$E_2 = bE_2 . \qquad \text{where} \qquad b = 1 + a\Delta x + \frac{(a\Delta x)^2}{2} \qquad \text{(III-20)}$$

In the special case where E_2' is the energy of a deuteron group and must be measured from a proton group of energy $\bar{E}_2$ appearing on the same set of plates, (III-20) requires modification. $\bar{E}_2$ is known and therefore the momentum $\bar{P}_2$ of the proton group can be determined. The energy E_2 of a deuteron group with the same momentum $P_2 = \bar{P}_2$ can then be calculated and used in (III-20). The relativistically correct relation between momentum and energy must be used as the nonrelativistic expression introduces errors of the order of 30 Kev. This is:

$$\bar{P}_2^2 = 2\bar{E}_2\bar{M}_2 + \frac{\bar{E}_2^2}{c^2} = P_2^2 = 2E_2M_2 + \frac{E_2^2}{c^2}$$

From which:

$$E_2 = \frac{\bar{E}_2\bar{M}_2}{M_2} + \frac{\bar{E}_2^2}{2M_2c^2} - \frac{E_2^2}{2M_2c^2} \cong \frac{\bar{E}_2\bar{M}_2}{M_2} + \frac{3}{16}\frac{\bar{E}_2^2}{c^2}$$

Since $\frac{M_2}{M_2} = \frac{1}{2}\left(1 + 0.75\times10^{-3}\right)$

$$E_2 = \frac{\bar{E}_2}{2} + \frac{\bar{E}_2}{2}\times 0.75\times10^{-3} + \frac{3}{16}\frac{\bar{E}_2^2}{c^2} \qquad \text{(III-21)}$$

Substituting this result into (III-20):

$$E_2' = \frac{b}{2}\bar{E}_2\left(1 + 0.75 \times 10^{-3} + \frac{3}{8}\frac{\bar{E}_2}{c^2}\right)$$

Or,

$$E_2' = \bar{b}\,\bar{E}_2 \qquad \text{where} \quad \bar{b} = \frac{b}{2}\left(1 + 0.75 \times 10^{-3} + \frac{3}{8}\frac{\bar{E}_2}{c^2}\right) \qquad \text{(III-22)}$$

In order to make the angle and energy measurements, target thickness corrections must be considered. Reaction product group positions are measured at the peak, and therefore the reaction is assumed to occur at midfoil. The energies of the reaction products E'_{20} and E_{20} are calculated in a relativistically correct manner for an assumed scattering angle θ_o and incident deuteron energy E_{10}. θ_o and E_{10} are estimated as carefully as possible. Since the two groups occur at different linear positions in the image plane the reaction angles θ' and θ are different. The half target losses $\Delta E'_{2t}$ and ΔE_{2t} are found from the energy loss curve calculated for LiOH (Figure 14) and the measured target thickness. Consideration of these effects results in the following expressions for the energies E'_{2m} and E_{2m} of the two groups in the magnet:

$$E'_{2m} = E'_{20} + \frac{\partial E'_{20}}{\partial E_{10}}\Delta E_1 - \Delta E'_{2t} + \frac{\partial E'_{20}}{\partial \theta}(\theta' - \theta_o)$$

$$E_{2m} = E_{20} + \frac{\partial E_{20}}{\partial E_{10}}\Delta E_1 - \Delta E_{2t} + \frac{\partial E_{20}}{\partial \theta_o}(\theta - \theta_o)$$

Since the magnet energies are related by (III-20) or (III-22), a simple calculation shows that:

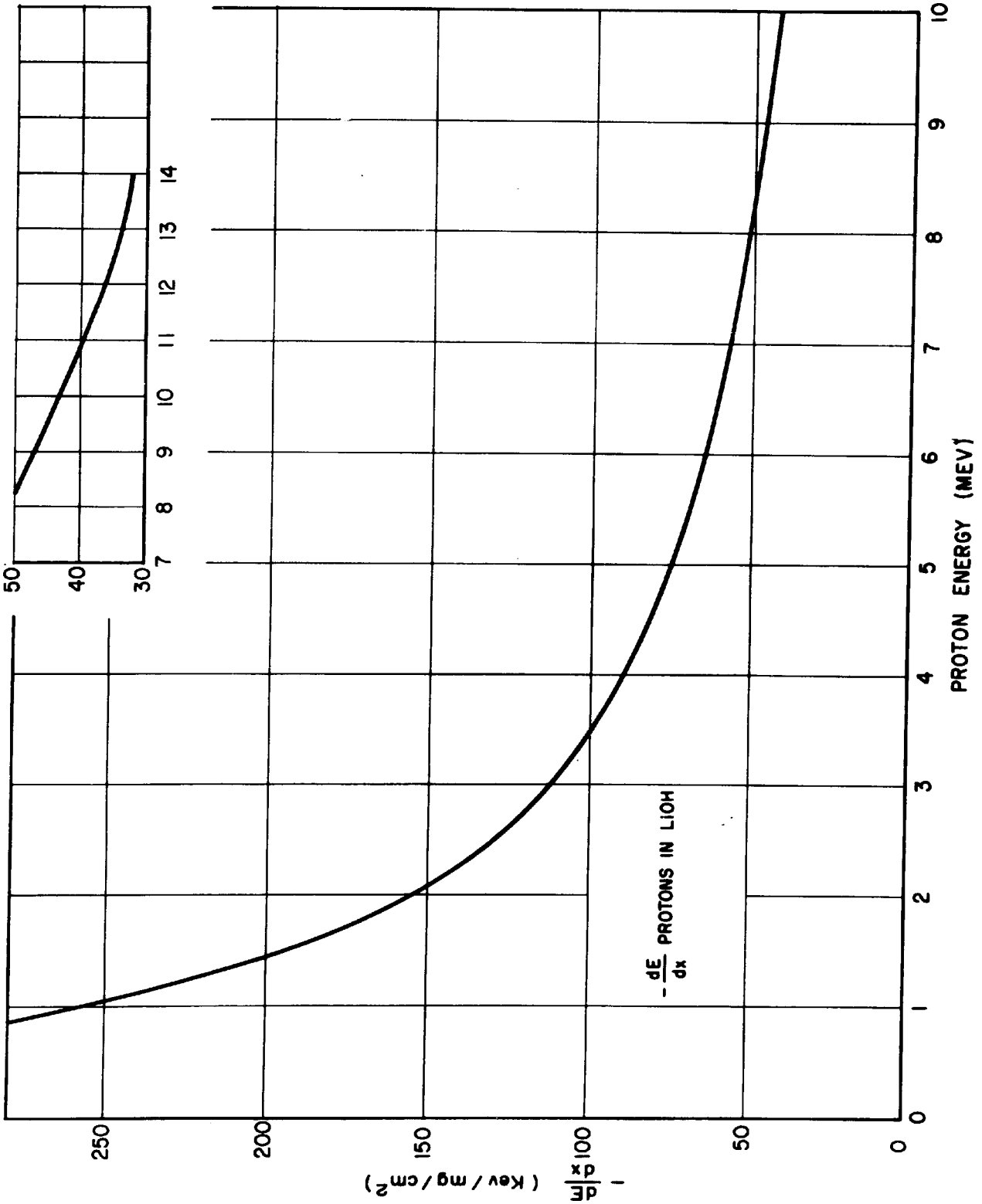

$-\frac{dE}{dx}$ PROTONS IN LiOH
$-\frac{dE}{dx}$ (kev / mg / cm^2)
PROTON ENERGY (MEV)
0
50
100
150
200
250
1
2
3
4
5
6
7
8
9
10
30
40
50
7
8
9
10
11
12
13
14

Figure 14

$$\alpha \Delta E_1 + \beta(\theta' - \theta_0) = \gamma \qquad \text{(III-23)}$$

where $\alpha = \frac{\partial E'_{20}}{\partial E_{10}} - b\frac{\partial E_{20}}{\partial E_{10}}$ $\qquad \beta = \frac{\partial E'_{20}}{\partial \theta_0} - b\frac{\partial E_{20}}{\partial \theta}$

$$\gamma = b\left(E_{20} - \Delta E_{2t} + \delta \frac{\partial E_{20}}{\partial \theta}\right) - E'_{20} + \Delta E_{2t}$$

$$\delta = \theta - \theta'$$

δ and b are measured by the peak separation on the plates.

If the scattering angle is known, (III-23) gives ΔE_1, or a correction to the assumed deuteron energy. On the other hand, if E_1 is known θ' is determined. For a determination of both the angle and the deuteron energy a second pair of levels must be used. In exact analogy with (III-23) then:

$$\alpha^* \Delta E_1 + \beta^*(\theta^* - \theta_0) = \gamma^* \qquad \text{(III-24)}$$

where $\theta^* = \epsilon + \theta'$

ϵ can be measured by the separations of the peak positions on the plates, allowing equations (III-23) and (III-24) to be solved simultaneously with the result:

$$\theta' - \theta_0 = \frac{\gamma\alpha^* + \epsilon\beta^*\alpha - \gamma^*\alpha}{\beta\alpha^* - \alpha\beta^*} \qquad \text{(III-25)}$$

$$\Delta E_1 = \frac{\gamma}{\alpha} - \frac{\beta}{\alpha}(\theta' - \theta_0) \qquad \text{(III-26)}$$

The separation between a proton group and a deuteron group from nuclei of approximately equal mass is relatively insensitive to changes in the scattering angle and therefore is useful for determination of the bombarding deuteron energy. The angle measurement is best made by the separation of groups of identical particles from nuclei of as different mass as possible.

The results of the measurements of the midfoil energies E_1 and the central scattering angle θ_c together with the groups responsible for each measurement are as follows:

Run No. 1

$Li^7(d,d')Li^7$ and $O^{18}(d,d')O_1^{18}$	$E_1 = 7.678 \pm 0.041$ Mev
$O^{16}(d,p)O_0^{17}$ and $O^{18}(d,d')O_1^{18}$	$\theta_c = 50.14° \pm 0.5°$
$O^{16}(d,p)O_0^{17}$ and $O^{18}(d,d')O_1^{18}$	$E_1 = 7.681 \pm 0.041$ Mev
$Li^6(d,d')Li_1^6$ and $O^{18}(d,p)O_2^{19}$	$\theta_c = 49.30° \pm 0.5°$

Run No. 2

$O^{16}(d,p)O_0^{17}$ and $O^{18}(d,d')O_1^{18}$	$E_1 = 7.835 \pm 0.041$ Mev
$Li^6(d,p)Li_1^7$ and $O^{17}(d,p)O_1^{18}$	$\theta_c = 28.5° \pm 0.5°$

The probable errors in the above measurements were calculated following the steps involved in the energy and angle calculations and also by an approximate method described on page 47.

Determination of an unknown Q.--Measurement of an unknown Q is made by comparison with a known group on the same set of plates. Let E_2' be the midfoil energy of the unknown group and E_2 the relativistically correct energy calculated for the known group using the measured midfoil energy E_1 and the measured scattering angle θ. Equations (III-20) and (III-22) become:

$$E'_{2m} = bE_{2m} = b(E_2 - \Delta E_{2t}) \qquad \text{for identical particles} \qquad \text{(III-27)}$$

$$E'_{2m} = \bar{b}(\bar{E}_2 - \Delta E_{2t}) \qquad \text{prime deuteron, barred proton} \qquad \text{(III-28)}$$

The unknown midfoil energy is given by:

$$E_2' = E'_{2m} + \Delta E_{2t}$$

E_2', E_1, and the measured θ' for the unknown group are then substituted into equation (III-5) using masses corrected by (III-19) giving the desired result for the unknown Q.

Probable errors in the measurements.--Using the Q equation and assuming $\theta' = \theta$ a measurement is made of an unknown Q' from a known Q. Writing the Q equations for both groups:

$$Q' = \frac{M_2' + M_3'}{M_3'} E_2' - \frac{M_3' - M_1'}{M_3'} E_1' - 2\varepsilon' \cos\theta \qquad \text{(III-29)}$$

$$Q = \frac{M_2 + M_3}{M_3} E_2 - \frac{M_3 - M_1}{M_3} E_1 - 2\varepsilon \cos\theta \qquad \text{(III-30)}$$

where the energies refer to midfoil.

The relation between the magnet energies is given by:

$$E'_{2m} = E'_2 - \frac{t}{2}\left(\frac{dE'_2}{dx}\right) = bE_{2m} = b\left[E_2 - \frac{t}{2}\left(\frac{dE_2}{dx}\right)\right]$$

t/2 is the half target thickness and dE/dx is the energy loss per unit target thickness. This equation can be written:

$$E'_2 = fE_2 \qquad \text{where } f = b + \frac{t}{2E_2}\left[\frac{dE'_2}{dx} - b\frac{dE_2}{dx}\right] \qquad \text{(III-31)}$$

Substituting (III-31) and

$$E'_1 = E_1 \qquad \mathcal{E}' = \frac{M_3}{M'_3}\left(\frac{M'_1 M'_2}{M_1 M_2}\right) f^{1/2}\mathcal{E} = \mu\frac{M_3}{M'_3} f^{1/2}\mathcal{E}$$

where $\mu = \left(\frac{M'_1 M'_2}{M_1 M_2}\right)^{1/2}$

into (III-29) and removing the cosθ term from (III-29) by substitution from (III-30), (III-29) becomes:

$$Q' = E_2\left\{\frac{f(M'_2+M'_3) - \mu f^{1/2}(M_2+M_3)}{M'_3}\right\} + E_1\left\{\frac{\mu f^{1/2}(M_3-M_1) - (M'_3-M'_1)}{M'_3}\right\} \qquad \text{(III-32)}$$

$$+ \frac{M_3}{M'_3}\mu f^{1/2} Q$$

The present system of measurement requires that E_2 be regarded as a function of E_1, Q, and θ. b is independent of these quantities and the dependence of f on E_1, Q, and θ can be neglected for the calculation of errors.

The following partial derivatives are obtained from (III-32):

$$\frac{\partial Q'}{\partial\theta} = \frac{\partial E_2}{\partial\theta}\left\{\frac{f(M'_2+M'_3) - \mu f^{1/2}(M_2+M_3)}{M'_3}\right\} \qquad \text{(III-33)}$$

$$\frac{\partial Q'}{\partial E_1} = \frac{\partial E_2}{\partial E_1}\left\{\frac{f(M_2'+M_3') - \mu b^{1/2}(M_2+M_3)}{M_3'}\right\} + \frac{\mu f^{1/2}(M_3-M_1) - (M_3' - M_1')}{M_3'} \qquad \text{(III-34)}$$

$$\frac{\partial Q'}{\partial Q} = \frac{M_3}{M_3'}\mu f^{1/2} + \frac{\partial E_2}{\partial Q}\left\{\frac{f(M_2'+M_3') - \mu f^{1/2}(M_2+M_3)}{M_3'}\right\} \qquad \text{(III-35)}$$

$$\frac{\partial Q'}{\partial f} = \frac{E_2}{M_3'}\left\{(M_2'+M_3') - \frac{\mu}{2f^{1/2}}(M_2+M_3)\right\} + \frac{E_1\mu}{2M_3' f^{1/2}}(M_3-M_1) + \frac{M_3}{2M_3' f^{1/2}}\mu Q \qquad \text{(III-36)}$$

The partial derivatives remaining on the right side of these equations are given by equations (III-6) through (III-17).

The probable error attached to a Q' measurement is:

$$\Delta Q' = \sqrt{\left(\frac{\partial Q'}{\partial \theta}\Delta\theta\right)^2 + \left(\frac{\partial Q'}{\partial E_1}\Delta E_1\right)^2 + \left(\frac{\partial Q'}{\partial Q}\Delta Q\right)^2 + \left(\frac{\partial Q'}{\partial f}\Delta f\right)^2} \qquad \text{(III-37)}$$

$\Delta\theta$ and E_1 are given by the uncertainties in the angle and energy determination. ΔQ is the probable error in the known Q value. Δf is compounded from uncertainties in the dispersion constant, peak positions, and target thickness. The dispersion constant and peak position contributions occur in f in an obvious manner. The target thickness uncertainty Δf_t is found in the following way:

$$\Delta f_t = \frac{\partial f}{\partial t}\Delta t = \frac{1}{2E_2}\left(\frac{dE_2'}{dx} - b\frac{dE_2}{dx}\right)\Delta t \qquad \text{(III-38)}$$

For the errors of a deuteron energy determination, E_1 in (III-32) is regarded as the unknown quantity. The partial derivatives of E_1 with respect to the independent quantities are calculated from (III-32). The results are:

$$\frac{\partial E_1}{\partial \theta} = -\frac{\partial E_2}{\partial \theta}\frac{f(M_2'+M_3') - \mu f^{1/2}(M_2+M_3)}{\mu f^{1/2}(M_3-M_1) - (M_3'-M_1') + \frac{\partial E_2}{\partial E_1}\left[f(M_2'+M_3') - \mu f^{1/2}(M_2+M_3)\right]} \qquad \text{(III-39)}$$

$$\frac{\partial E_1}{\partial Q'} = \frac{-M_3'}{\frac{\partial E_2}{\partial E_1}\left[f(M_2'+M_3') - \mu f^{1/2}(M_2+M_3)\right] + \mu f^{1/2}(M_3-M_1) - (M_3'-M_1')} \qquad \text{(III-40)}$$

$$\frac{\partial E_1}{\partial Q} = -\frac{M_3 \mu f^{1/2}}{M_3'} \frac{\partial E_1}{\partial Q'} \qquad \text{(III-41)}$$

$$\frac{\partial E_1}{\partial f} = \frac{-E_2\left[M_2'+M_3' - \frac{H}{2f^{1/2}}(M_3+M_2)\right] - \frac{E_1\mu}{2f^{1/2}}(M_3-M_1) - \frac{M_3\mu}{2f^{1/2}}Q}{\frac{\partial E_2}{\partial E_1}\left[f(M_2'+M_3') - \mu f^{1/2}(M_2+M_3)\right] + \mu f^{1/2}(M_3-M_1) - (M_3'-M_1')} \qquad \text{(III-42)}$$

The partial derivatives on the right side of these equations are given by equations (III-6) through (III-17).

The probable error attached to a measurement of the deuteron energy is given by:

$$\Delta E_1 = \sqrt{\left(\frac{\partial E_1}{\partial \theta}\Delta\theta\right)^2 + \left(\frac{\partial E_1}{\partial Q'}\Delta Q'\right)^2 + \left(\frac{\partial E_1}{\partial Q}\Delta Q\right)^2 + \left(\frac{\partial E_1}{\partial f}\Delta f\right)^2} \qquad \text{(III-43)}$$

Reduction of errors.--Referring to equation (III-37) which gives the contributions to the error of an unknown Q measurement, several improvements can be pointed out. Measurement of the scattering angle by the method used is difficult and inaccurate. A direct measurement of the trajectories of the incident deuterons and scattered particles should lead to a more accurate angle determination.

The deuteron energy can also be measured directly by a calibration of the analyzing magnet field in terms of the well-known

energies of polonium alpha particles. This requires measurement of the field in the analyzing magnet by means of a nuclear moment magnetic field meter placed directly in the magnet gap. The linearity of the field meter with respect to particle momentum can be checked by measuring the momenta of known groups. Measurement of the field required to focus the elastic scattered deuterons from a standard target at a fixed position in the analyzing magnet image plane should give an accurate measure of the deuteron energy.

The remaining error consists mainly of uncertainties in measurement of peak positions on the plates and can only be improved by utilizing thinner and more uniform targets.

CHAPTER IV

EXPERIMENTAL RESULTS

Spectra

The spectra obtained from the O^{17} and O^{18} enriched LiOH targets are exhibited in Figures 15 through 22. The track counts are plotted against linear positions along the image plane of the analyzing magnet and the changes in vertical scale represent differences in counting areas in order that more counts be obtained in the regions of low background. Both the ordinates and abscissae are subject to correction; the former because of the variation in solid angle across the image plane and the latter because of the change in dispersion discussed on page 26.

An examination of the spectra reveals deuteron and proton groups from the recoil nuclei Li^6, Li^7, C^{12}, C^{13}, O^{16}, O^{17}, O^{18}, and O^{19}. A moderately thick target spectrum such as this has the advantage that reaction product groups from thin layers of surface contaminants are too weak to be detected. In searching for new levels, this advantage seems to outweigh the loss in resolution.

Because the nucleus of interest is O^{18}, only groups leaving O^{18} in its ground or excited states will be discussed, except where other groups are used for calibration purposes.

The first excited state of O^{18} with an excitation energy of 1.986 Mev (7, 8) was observed from the reaction $O^{18}(d,d')O_1^{18}$ at 49.7° and 58.5° and from the reaction $O^{17}(d,p)O_1^{18}$ at 28.5° and 89.7°.

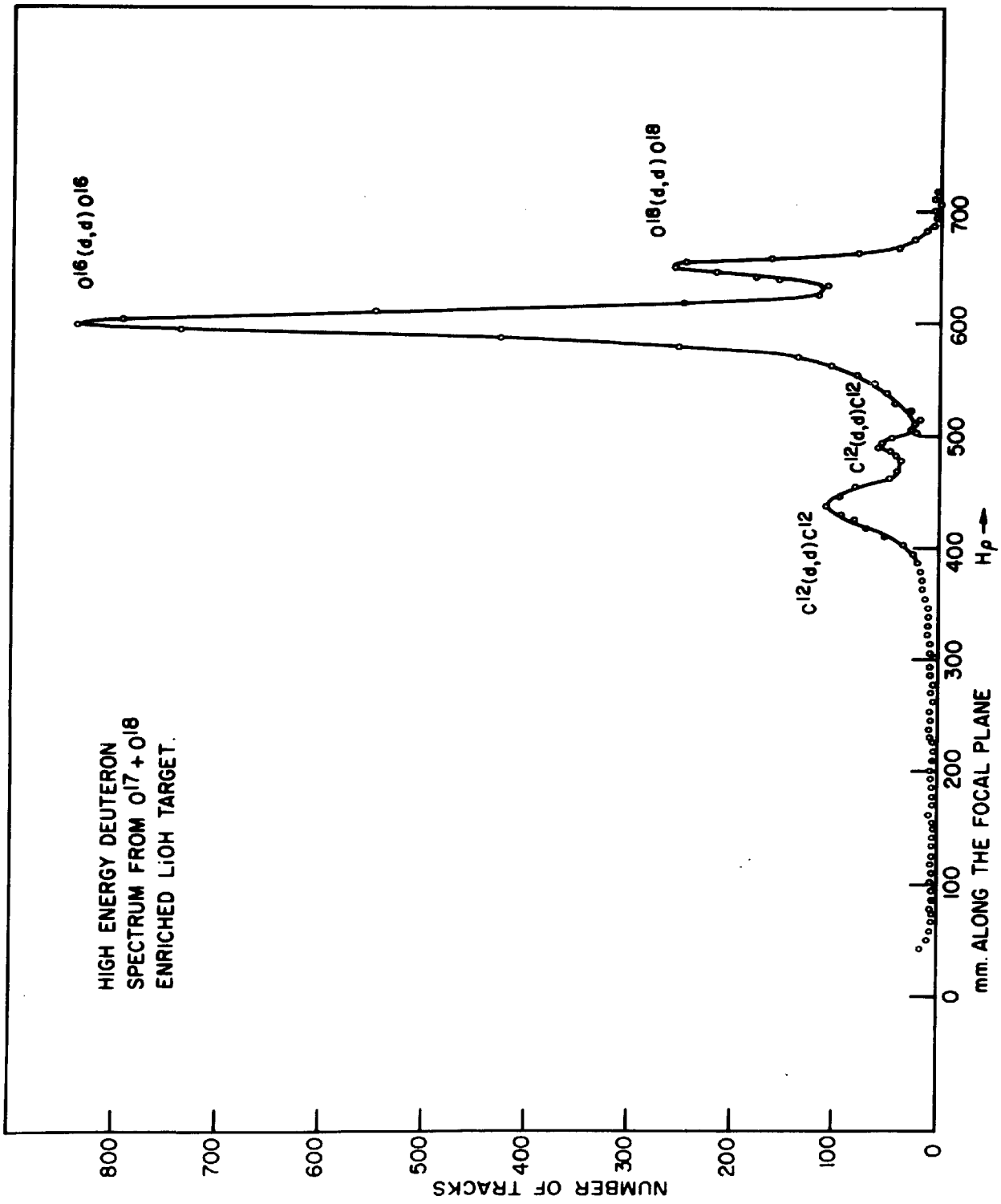

HIGH ENERGY DEUTERON
SPECTRUM FROM $O^{17}+O^{18}$
ENRICHED LiOH TARGET.
$O^{16}(d,d)O^{16}$
$O^{18}(d,d)O^{18}$
$C^{12}(d,d)C^{12}$
$C^{12}(d,d)C^{12}$
NUMBER OF TRACKS
mm. ALONG THE FOCAL PLANE
Hρ →
0
100
200
300
400
500
600
700
800

Figure 15

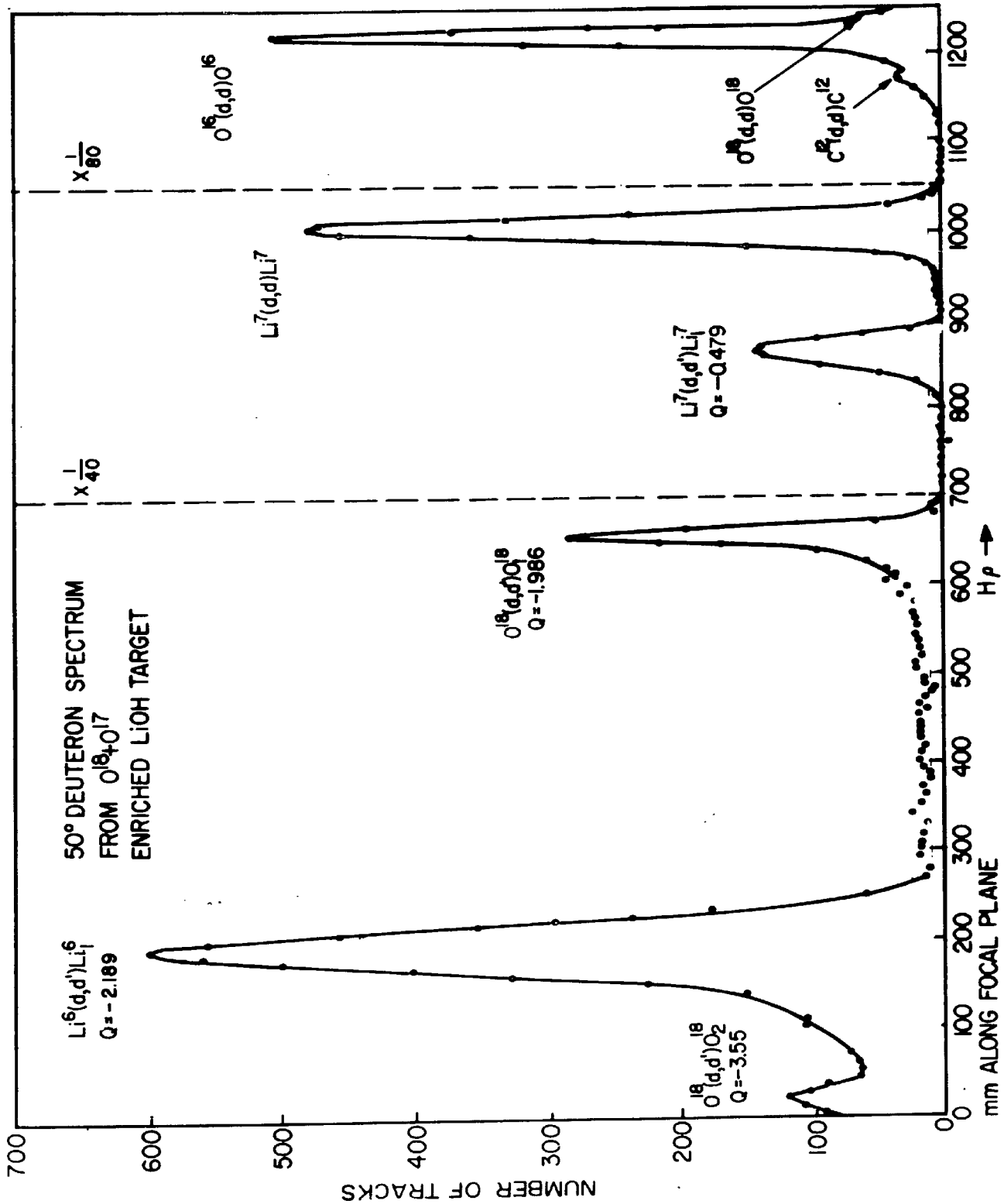

50° DEUTERON SPECTRUM
FROM O18+O17
ENRICHED LiOH TARGET
Li6(d,d')Li6
Q=-2.189
O18(d,d')O18
Q=-3.55
O18(d,d')O18
Q=-1.986
Li7(d,d')Li7
Q=-0.479
Li7(d,d)Li7
O16(d,d)O16
O18(d,d)O18
C12(d,d)C12
X 1/40
X 1/80
NUMBER OF TRACKS
mm ALONG FOCAL PLANE
Hρ →

Figure 16

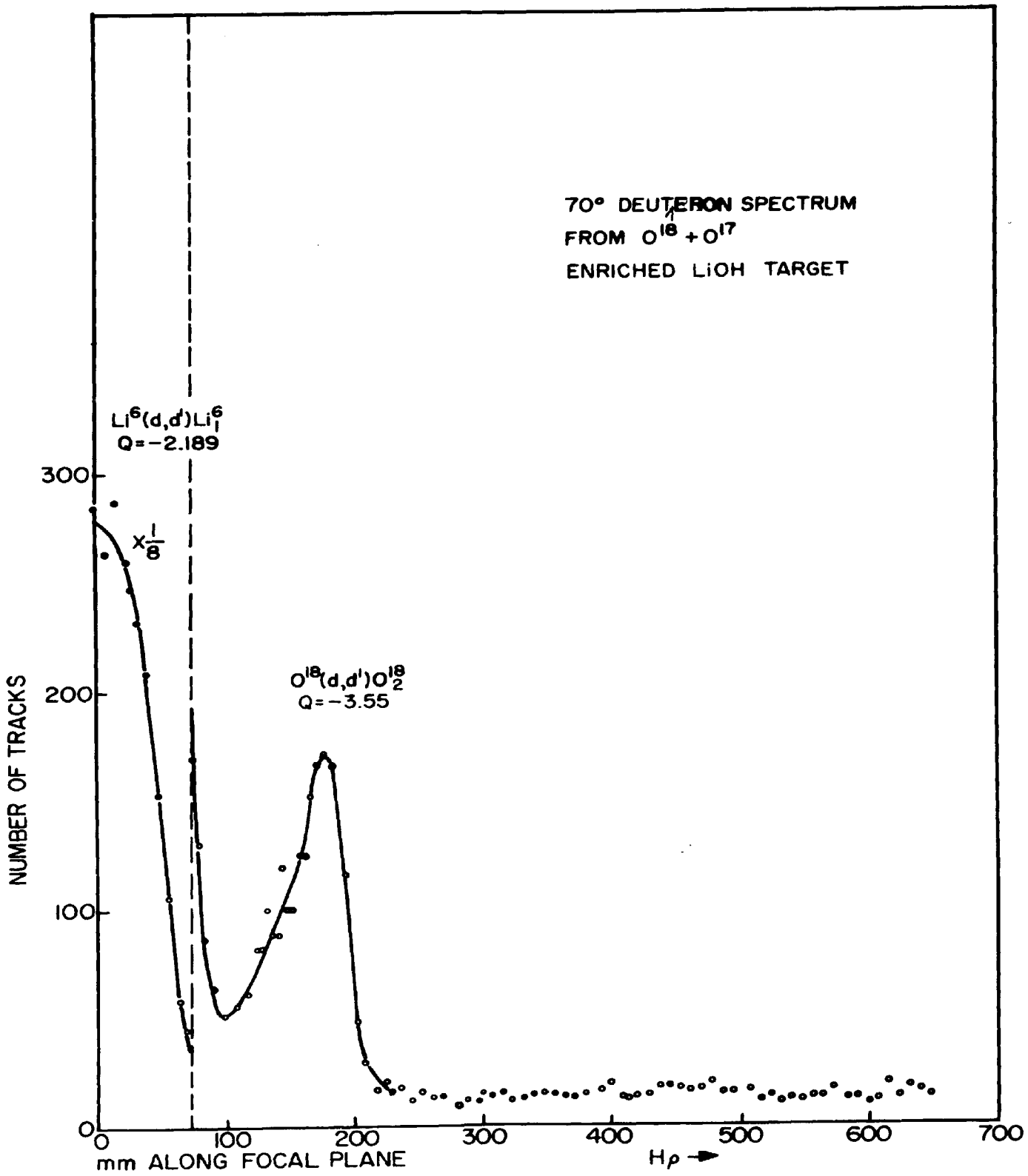

70° DEUTERON SPECTRUM
FROM O18 + O17
ENRICHED LiOH TARGET
Li6(d,d')Li6
Q=-2.189
X 1/8
O18(d,d')O18
Q=-3.55
NUMBER OF TRACKS
300
200
100
0
0
100
200
300
400
500
600
700
mm ALONG FOCAL PLANE
Hρ

Figure 17

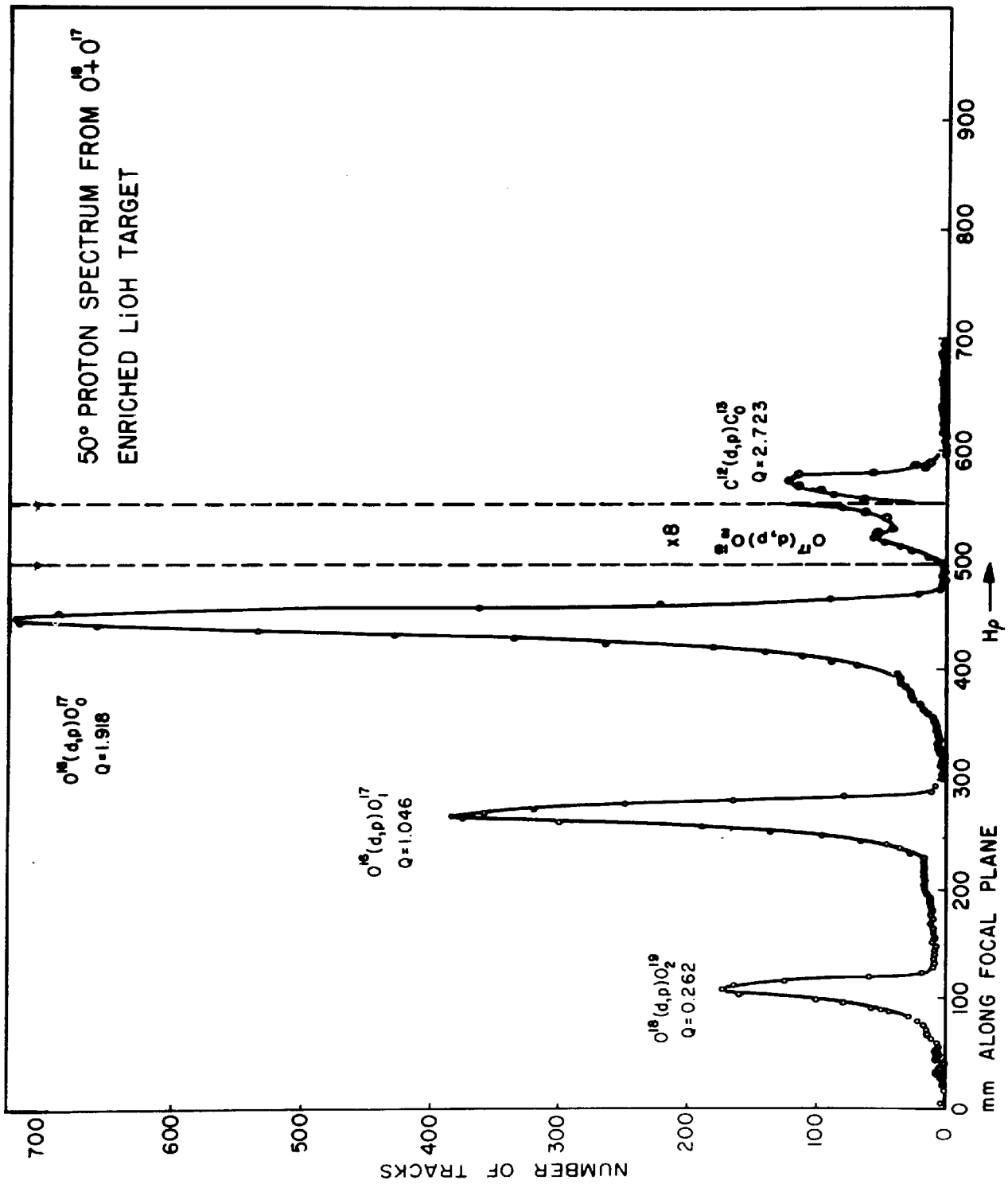

50° PROTON SPECTRUM FROM O¹⁸+O¹⁷
ENRICHED LiOH TARGET
O¹⁸(d,p)O₀¹⁷
Q=1.918
O¹⁸(d,p)O₁¹⁷
Q=1.046
O¹⁸(d,p)O₂¹⁹
Q=0.262
O¹⁷(d,p)O₀¹⁸
C¹²(d,p)C₀¹³
Q=2.723
x8
NUMBER OF TRACKS
mm ALONG FOCAL PLANE
Hρ

Figure 18

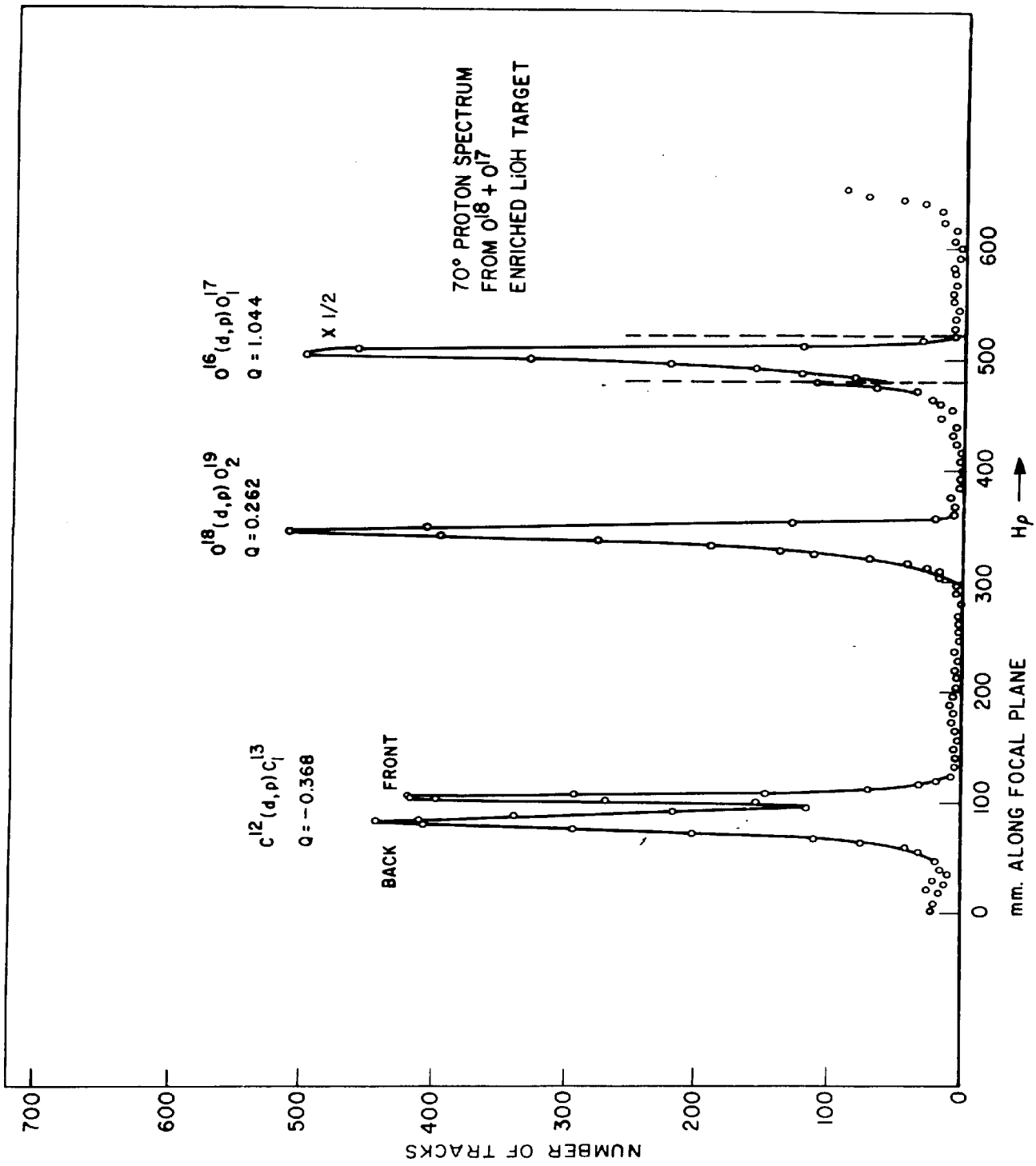

70° PROTON SPECTRUM
FROM O18 + O17
ENRICHED LiOH TARGET
O16(d,p)O17
Q = 1.044
X 1/2
O18(d,p)O19
Q = 0.262
C12(d,p)C13
Q = -0.368
FRONT
BACK
NUMBER OF TRACKS
mm. ALONG FOCAL PLANE
Hρ

Figure 19

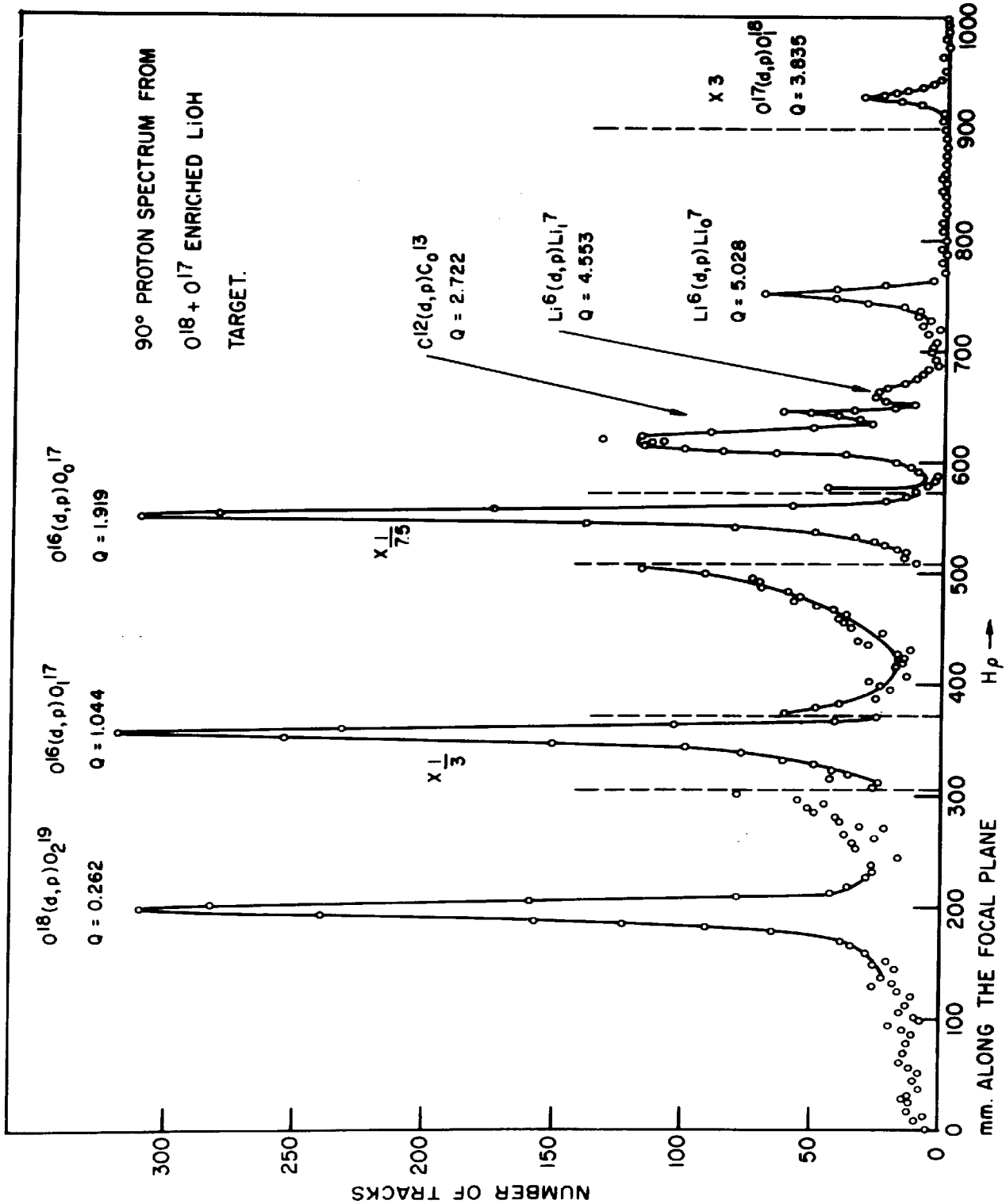

90° PROTON SPECTRUM FROM
O18 + O17 ENRICHED LiOH
TARGET.
O18(d,p)O2 19
Q = 0.262
O16(d,p)O1 17
Q = 1.044
O16(d,p)O0 17
Q = 1.919
C12(d,p)C0 13
Q = 2.722
Li6(d,p)Li1 7
Q = 4.553
Li6(d,p)Li0 7
Q = 5.028
O17(d,p)O1 8
Q = 3.835
X 1/3
X 1/7.5
X 3
NUMBER OF TRACKS
mm. ALONG THE FOCAL PLANE
Hρ →

Figure 20

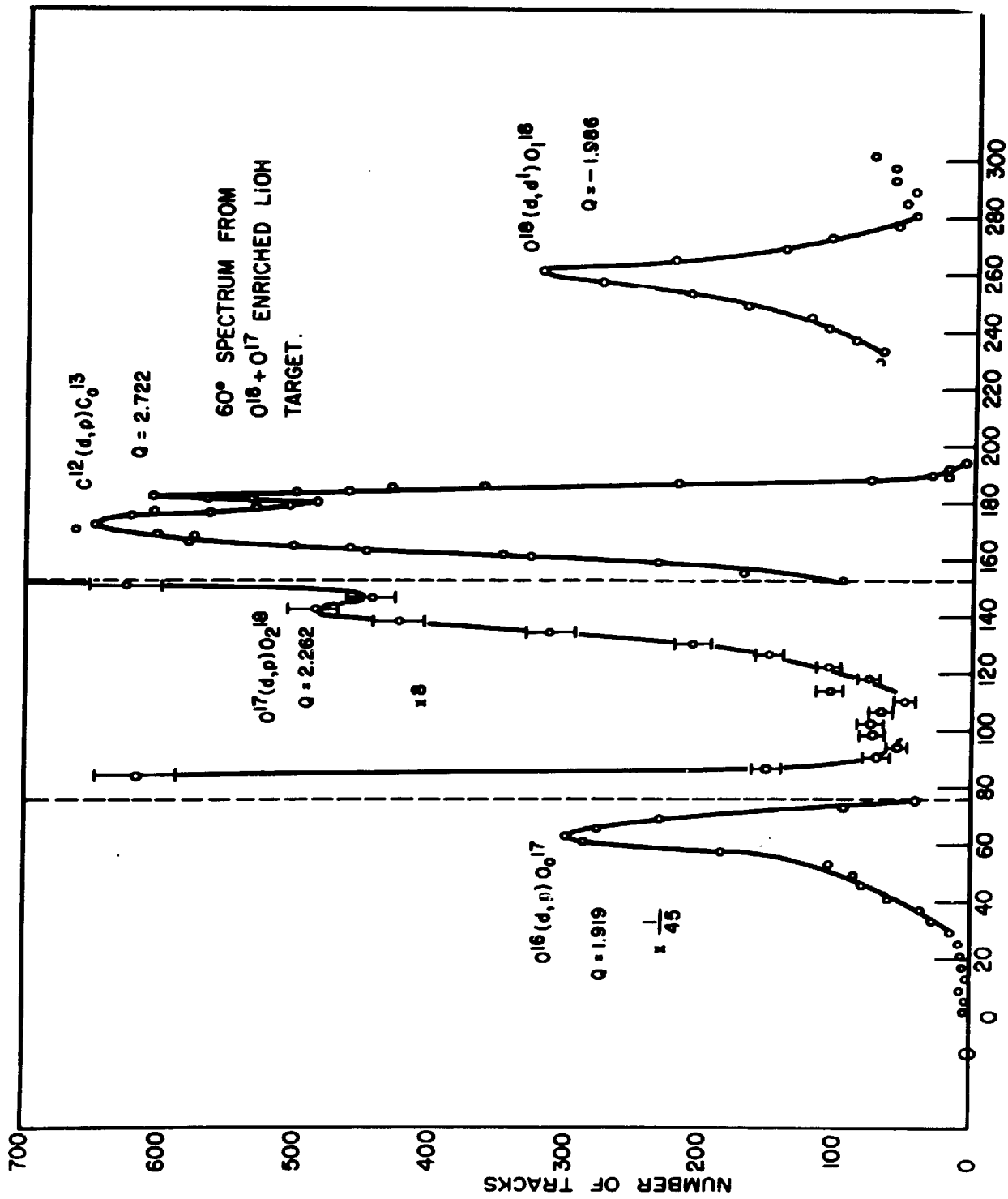

60° SPECTRUM FROM
O18 + O17 ENRICHED LiOH
TARGET.
C12(d,p)C13
Q = 2.722
O17(d,p)O18
Q = 2.262
x8
O16(d,p)O17
Q = 1.919
x 1/45
O18(d,d')O18
Q = -1.986
NUMBER OF TRACKS
mm. ALONG THE FOCAL PLANE
Hρ

Figure 21

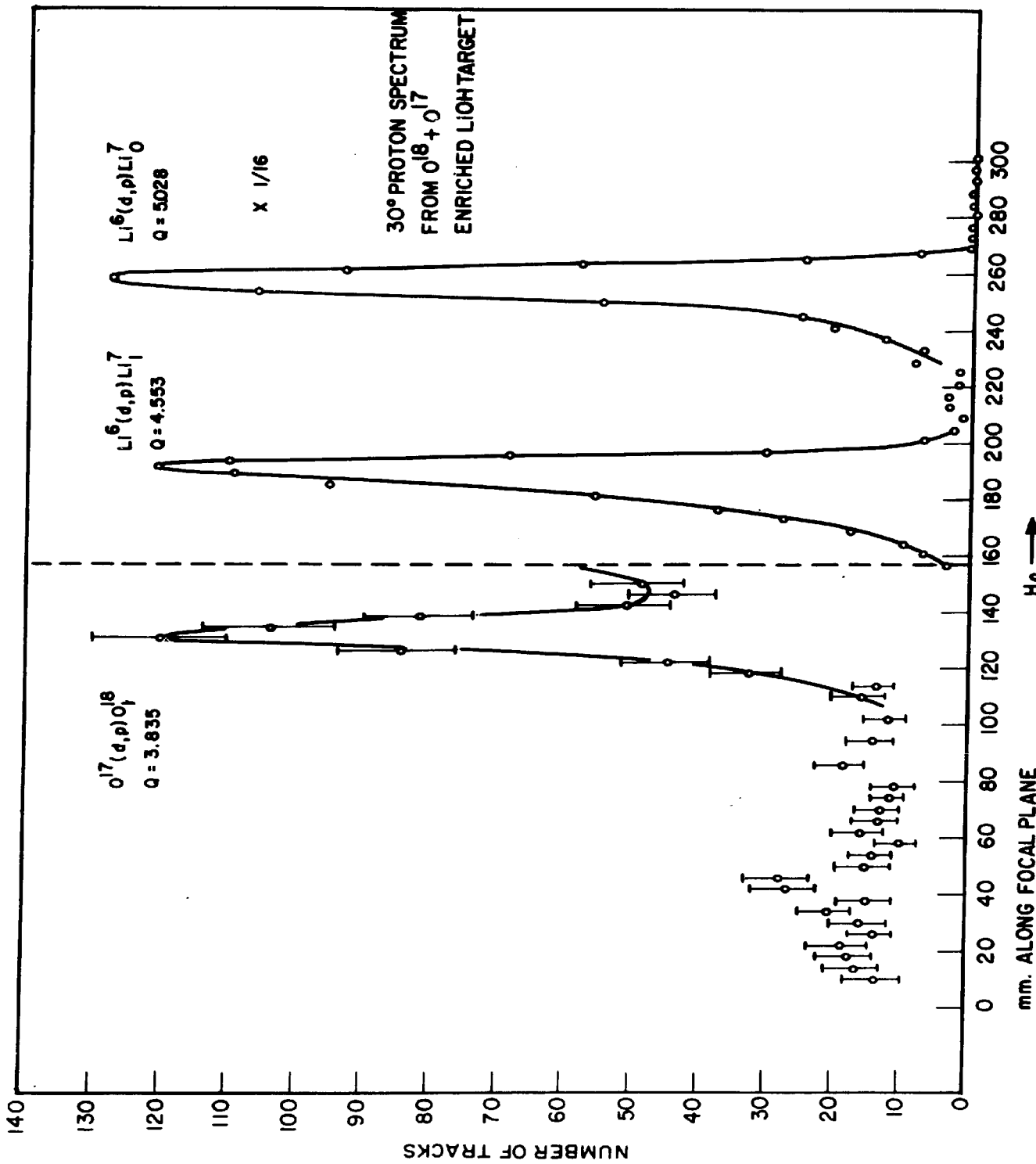

30° PROTON SPECTRUM
FROM $O^{18} + O^{17}$
ENRICHED LiOH TARGET
X 1/16
$Li^6(d,p)Li^7_0$
Q = 5.028
$Li^6(d,p)Li^7_1$
Q = 4.553
$O^{17}(d,p)O^{18}_1$
Q = 3.835
NUMBER OF TRACKS
mm. ALONG FOCAL PLANE
Hρ

Figure 22

A search was made for a previously reported (8) level at an excitation energy of 2.445 Mev which should appear on the spectrum shown in Figure 22 along with the protons from the first excited state. No level was found at this energy with an intensity greater than 20 percent of the intensity of the first excited state. A search of the corresponding region of excitation in the deuteron spectrum at 49.7° and 68.5° shows no groups greater than 3 percent of the intensity of the inelastic scattered deuterons from the first excited state at 49.7°.

A level not previously reported in O^{18} was found at an excitation energy of 3.55 Mev by means of the reaction $O^{17}(d,p)O^{18}$ at 49.7° and 58.5° and by means of the reaction $O^{18}(d,d')O^{18}$ at 49.7° and 68.5°. The Q values, excitation energies E*, and groups from which this level was measured are given in Table I. The average of these energy determinations gives 3.550 ± 0.010 Mev for the excitation energy of the new level.

The mass of the nucleus responsible for this level is 18 ± 1 a.m.u. which was measured by observing the change in energy of the deuteron group with respect to scattering angle. The lack of groups from target nuclei of the mass range 17 to 19 other than O^{17} and O^{19}, together with the fact that O^{17} has no excited state at this energy, indicates that the new level must certainly be due to O^{18}.

Complete coverage of 3.5 Mev excitation energy in O^{18} cannot be claimed. However, the 49.7° deuteron spectrum shows no groups of intensity greater than 3 percent of the intensity of the deuterons from $O^{18}(d,d')O_1^{18}$ in the region of excitation from 1.986 Mev to 2.55 Mev. The 68.5° deuteron spectrum shows no groups of intensity greater than 3 percent of the intensity of the first excited state deuterons at 49.7° in the excitation region from 2.5 Mev to the level at 3.5 Mev. The 90° deuteron spectrum shows no groups of intensity

TABLE I

RESULTS OF Q MEASUREMENTS ON THE SECOND EXCITED STATE OF O^{18}

Reference Group (9)	(d,d') Q' (Mev)	Excitation Energy	Contributions to Error			
			$\frac{\partial Q'}{\partial \theta}\Delta\theta$	$\frac{\partial Q'}{\partial E_1}\Delta E_1$	$\frac{\partial Q'}{\partial Q}\Delta Q$	$\frac{\partial Q'}{\partial f}\Delta f$
$Li^6(d,d')Li^6_1$ (49.7°) . .	-3.551 ± 0.019	3.551 ± 0.019	0.017	0.007	0.002	0.005
$O^{18}(d,p)O^{19}_2$ (49.7°) . .	-3.532 ± 0.021	3.532 ± 0.021	0.004	0.019	0.006	0.007
$O^{18}(d,p)O^{19}_2$ (68.5°) . .	-3.551 ± 0.022	3.551 ± 0.022	0.005	0.019	0.006	0.008
	(d,p) Q'					
$O^{17}(d,p)O^{17}_0$ (49.7°) . .	2.262 ± 0.015	3.559 ± 0.018	0.005	0.002	0.004	0.014

greater than 3 percent of the intensity of the elastic scattered deuterons from O^{18} in the excitation region from 1.00 to 1.98 Mev.

Relative Intensities

The relative intensities measured from the plates were corrected for the change in solid angle across the image plane. Use was made of the known angular distribution (10) of the protons from the reaction $O^{16}(d,p)O_0^{17}$ in order to normalize run No. 2 to run No. 1. The intensity ratios of the $O^{17}(d,p)O^{18}$ proton groups are rather poor because of the low intensity and the background correction that must be applied. A measure of the sensitivity of the method to weak proton groups is given by the fact that the intensities of the O^{18} proton groups are about 0.1 percent of the intensity of the ground state protons from the reaction $O^{16}(d,p)O_0^{17}$. The weak proton groups are about six times as intense as the proton background. This is true only at energies higher than the energies of groups from isotopes that are more than about 50 percent abundant. The results of the intensity measurements are given in Table II.

TABLE II

RELATIVE INTENSITIES

Reactions	Angles	Intensity Ratio
$O^{18}(d,d')O_1^{18}$ / $O^{18}(d,d')O_2^{18}$	49.7° / 49.7°	5.7 ± 1.4
$O^{16}(d,p)O_0^{17}$ / $O^{17}(d,p)O_2^{18}$	49.7° / 49.7°	930 ± 160
$O^{17}(d,p)O_1^{18}$ / $O^{17}(d,p)O_2^{18}$	28.5° / 58.5°	3.0 ± 1
$O^{17}(d,p)O_1^{18}$ / $O^{17}(d,p)O_2^{18}$	28.5° / 49.7°	1.8 ± 0.4

CHAPTER V

THEORY

Nuclear Spectroscopic Calculations

In recent years the methods of atomic spectroscopy have found application to a great extent in attempts at solution of the varied problems of nuclear spectroscopy (11-17). In atomic spectroscopy it is possible to evaluate the various parameters appearing in the calculations by comparison with the great amount of experimental data. The nuclear calculations require actual evaluation of the interaction matrix elements because of the small amount of experimental data available. The general method of these calculations will be described below and then particularized to calculations of certain tensor force interaction energies.

Consider a Hamiltonian for a number of nucleons outside a closed shell:

$$H = \sum_i H(\vec{r}_i) + \sum_{i \neq j} V_{ij}(\vec{r}_{ij}) + \sum_i \xi(\vec{r}_i)\vec{l}_i \cdot \vec{s}_i \qquad \text{(V-1)}$$

$H(\vec{r}_i)$ is the potential due to a central field, $V_{ij}(\vec{r}_{ij})$ is the interaction potential between nucleons, and $\xi(\vec{r}_i)\vec{l}_i \cdot \vec{s}_i$ is the potential due to the spin orbit force. Nucleons outside closed shells are assumed to move in orbits produced by a central field due to the closed shell. The strength of the spin orbit force term in the Hamiltonian, $\xi(\vec{r}_i)$, is determined empirically from the spin orbit splitting measured for

the closed shell plus one nucleon nucleus. The interaction potential $V_{ij}(\vec{r}_{ij})$ is generally assumed to be of a type that fits the deuteron data.

Consider a complete orthonormal set of eigenfunctions ψ_N and their eigenvalues E_N, where the subscript N refers to several quantum numbers. The problem is to find the E_N and ψ_N by means of the Schrodinger equation:

$$H\psi_N(\vec{r}) = E_N \psi_N(\vec{r}) \qquad \text{(V-2)}$$

The eigenfunctions ψ_N can be expanded in terms of a second known complete orthonormal set of functions χ_m ; or:

$$\psi_N = \sum_m a_{Nm} \chi_m \qquad \text{(V-3)}$$

In the jj coupling scheme, the χ_m are specified by the quantum numbers $n_i l_i j_i JM$.

Inserting the expansion into (V-1), multiplying by χ_l^* , integrating over all space, and carrying out spin sums:

$$\int \sum_m a_{Nm} \chi_l^* H \chi_m d\tau = E_N \int \sum_m a_{Nm} \chi_l^* \chi_m d\tau$$

$$= E_N \sum_m a_{Nm} \delta_{lm} = E_N a_{Nl}$$

Or:

$$\sum_m a_{Nm} H_{lm} - E_N a_{Nl} = 0 \quad \text{where } H_{lm} = \int \chi_l^* H \chi_m d\tau \qquad \text{(V-4)}$$

The condition for a solution of the homogeneous set of linear equations given by (V-4) is that the determinant of the coefficients

of the a_{ij} vanish or that:

$$\begin{vmatrix} H_{11}-E_N & H_{12} & \cdots \\ H_{21} & H_{22}-E_N & \cdots \\ \vdots & \vdots & \end{vmatrix} = 0 \qquad \text{(V-5)}$$

The roots of this equation, the E_{Ni}, are the eigenvalues of the Hamiltonian. Using these, (V-4) can be solved for the transformation coefficients a_{ij} since the H_{lm} are determined by means of the assumed wave functions χ_m. (V-3) then gives the unknown eigenfunctions ψ_N in terms of the a_{ij} and χ_m.

The matrix of H is diagonal with respect to the wave functions ψ_N and therefore the operation just described is called diagonalization of the Hamiltonian matrix. This gives an exact solution to the problem. In practice, however, only a finite number of the wave functions χ_m are used and in this sense the solution is only approximate. In a first order perturbation calculation the off diagonal matrix elements are neglected and the eigenvalues are given by the diagonal elements of the perturbation Hamiltonian.

It is necessary at this point to clarify the spectroscopic language to be used. In the LS coupling representation, configurations are specified by the n and l of each nucleon and terms are given by the L and S for the system of nucleons. For example, the ld^2 configuration for identical nucleons leads to the terms ^1D, ^3P, ^1S, ^3F, and ^1G. Each term may give rise to one or more levels (e.g., $^3F_{2,3,4}$) where the subscript denotes the J of each level. In the jj representation configurations are again specified by the n and l of each nucleon (e.g., ld^2 for two ld nucleons) and terms are specified

by giving the n, l, and j for each nucleon. For example, the ld^2 configuration in the first d shell gives rise to the jj terms $(|d_{5/2})^2$, $(|d_{3/2})^2$, and $(|d_{5/2}|d_{3/2})$. Each term may lead to one or more levels (e.g., $[|d_{5/2}]^2_{J=0}$). It must be pointed out that the usual practice is to call each jj term a jj configuration.

Specializing the eigenvalue problem, consider the jj coupling representation where each nucleon state is labeled by the quantum numbers nljmj. Terms giving rise to low lying two nucleon T = 1 states outside the O^{16} core are $(d_{5/2})^2$, $(d_{3/2})^2$, $(d_{5/2}\ d_{3/2})$, $(d_{5/2}\ S_{1/2})$, $(d_{3/2}\ S_{1/2})$, and $(S_{1/2})^2$. The experimental spectrum of O^{17} suggests limiting the number of terms in this way and the infinite Hamiltonian matrix is reduced to a practical size. The matrix elements H_{ij} are of the type $(j_1 j_2\ J|V|j_3 j_4 J)$. The matrix made up of these elements with an x marked in each position corresponding to a nonzero matrix element is shown in Figure 23. Matrix elements occur only between levels having the same J value. Therefore, the secular equation factors into a product of secular equations, one for each J value.

The results desired from such a calculation are the energies of all the states for each J value and the relative amounts of each term responsible for each state. Calculation of the eigenvalues is accomplished by diagonalization of the submatrices belonging to the same J. For example, the submatrix for T = 1 and J = 0 has the form:

$j_1 j_2$ \ $j_3 j_4$	$d^2_{5/2}$	$d^2_{3/2}$	$S^2_{1/2}$
$d^2_{5/2}$	×	×	×
$d^2_{3/2}$	×	×	×
$S^2_{1/2}$	×	×	×

(V-6)

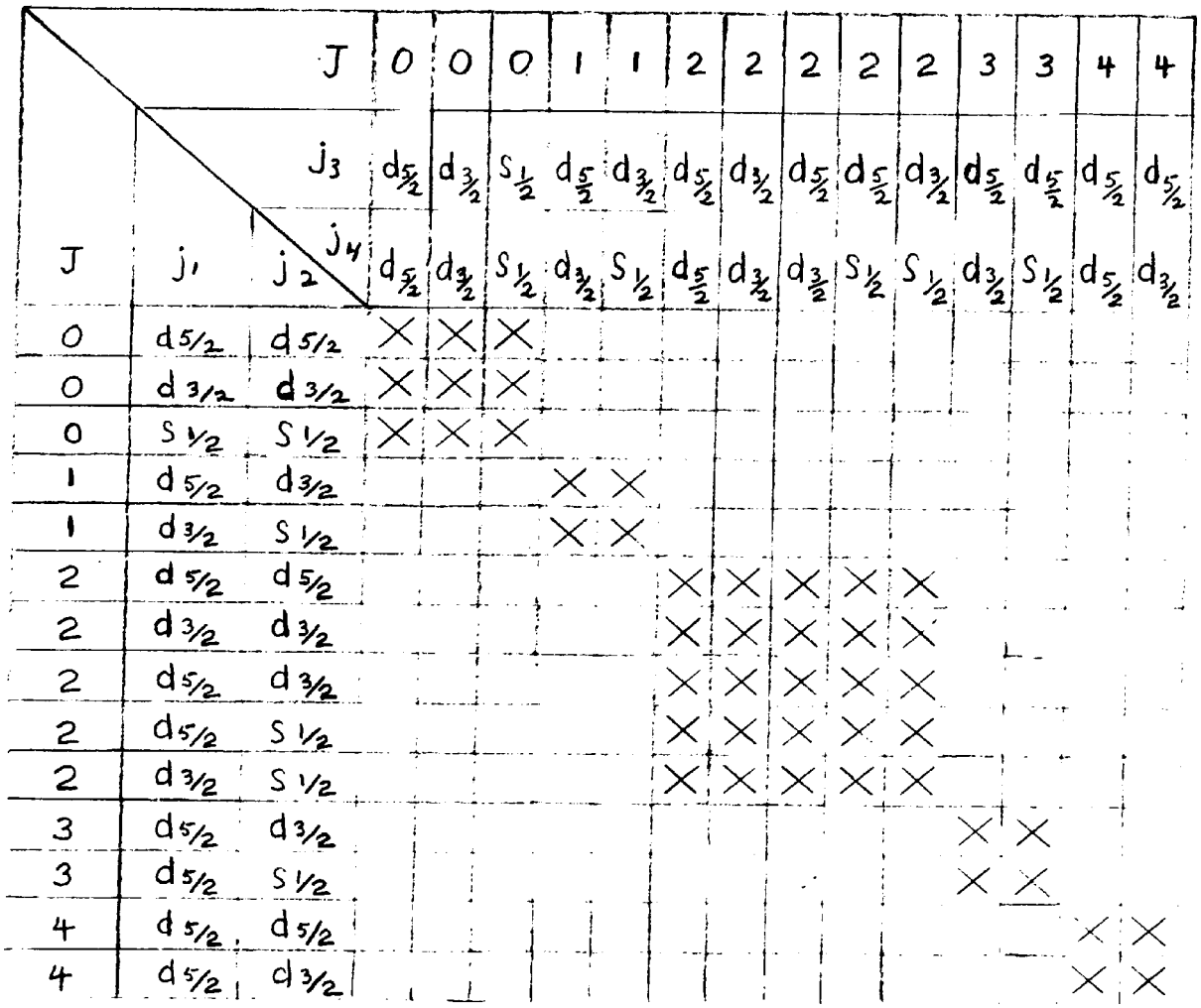


Figure 23. The matrix $(j_1 j_2 JT|V|j_3 j_4 JT)$ for T = 1.

The secular equation (V-5) gives the three eigenvalues E_{N1}, E_{N2}, and E_{N3} for J = 0, and the transformation (V-3) gives the unknown eigenfunction for each eigenstate in terms of the assumed wave functions, or:

$$\psi\begin{pmatrix} E_{N1} \\ J=0 \\ T=1 \end{pmatrix} = \alpha\chi\left(d_{5/2}^2\right) + \beta\chi\left(d_{3/2}^2\right) + \gamma\chi\left(s_{1/2}^2\right) \qquad \text{(V-7)}$$

Pure jj coupling results when the Hamiltonian contains no interparticle potential. If the interaction term $V_{ij}(\vec{r}_{ij})$ is equal to zero, then the matrix elements are made up of terms due to the spin orbit force alone which are diagonal in the jj representation. Pure LS coupling results when the Hamiltonian contains no spin orbit potential. If the χ_m are chosen in the LS scheme and ξ = 0, the Hamiltonian matrix is made up of elements due to the interparticle potential and is diagonal.

Diagonalization of the Hamiltonian matrix when both spin orbit and central forces are included leads to intermediate coupling. The choice of the LS or jj representation for calculation of the matrix does not affect the result and is usually made for ease of calculation. Many of the $\vec{l}_i \cdot \vec{s}_i$ matrix elements have been calculated (24, 25) in the LS scheme and for this reason the LS representation is generally employed. Recent work by Elliott and Flowers (16) indicates that intermediate coupling is closer to the true physical picture for the two and three nucleon systems outside the O^{16} core than either of the two extremes.

The results obtained by diagonalization of (V-6) if the potential is assumed to contain both spin orbit and interparticle terms are the eigenfunctions and eigenvalues of the J = 0 states including configuration interaction and given in intermediate coupling.

When configuration interaction is neglected, the matrix (V-6) does not include interaction terms between the d and s nucleons and has the form:

$j_1 j_2$ \ $j_3 j_4$	$d^2_{5/2}$	$d^2_{3/2}$	$S^2_{1/2}$
$d^2_{5/2}$	×	×	0
$d^2_{3/2}$	×	×	0
$S^2_{1/2}$	0	0	×

(V-8)

Diagonalization of this matrix then gives the eigenvalues and eigenfunctions including "term interaction"; i.e., in intermediate coupling.

A first order perturbation calculation neglects "term interaction" and involves calculation of the energies for the different J values for each term (e.g., $[\ d_{5/2}\ ]^2$). The submatrix (V-8) is clearly diagonal and the energies are given by the diagonal elements. This is the poorest approximation to the problem and gives a solution in either of the two coupling schemes. When no two levels with the same J occur in the term, the diagonal sum method (18) can be used to calculate the energies. The matrix elements which must be calculated are diagonal elements of the type $(j_1 j_2 m_{j_1} m_{j_2} | V | j_1 j_2 m_{j_1} m_{j_2})$.

Tensor Interaction Energies

Tensor force interaction energies were calculated for each of the T = 1 terms $(d_{5/2})^2$, $(d_{5/2}\ d_{3/2})$, $(d_{5/2}\ S_{1/2})$, and $(d_{3/2}\ S_{1/2})$. The eigenvalue of the tensor force for the configuration $(S_{1/2})^2$ is zero since the only state possible is a spin singlet state. The method used is due to Talmi (12) and will be described briefly.

Since no one of the terms listed above has two equal J values, the diagonal sum method can be used for calculation of the energies. The matrix elements $(j_1 j_2 m_{j_1} m_{j_2} | V | j_1 j_2 m_{j_1} m_{j_2})$ are expressed in terms of spin and space matrix elements and the sums over spins carried out. Talmi (12) demonstrated the usefulness of harmonic oscillator wave functions by showing that the two nucleon harmonic oscillator wave functions are separable into a center of gravity coordinate $\vec{R}$ and a relative coordinate $\vec{r}$. Since the interparticle potential depends only on the relative coordinate, the space integrals on $\vec{R}$ give 0 or 1 by orthogonality and normalization and the energies can be expressed in terms of the Talmi radial integrals $I_\ell(r)$, which are defined below.

The formulas for the matrix elements together with the expansion of various two particle wave functions which were calculated by Talmi (19) are listed in Appendix I. These formulas have been checked in various ways and are believed to be without error.

The tensor interaction energies given in terms of the $I_\ell(r)$ were also calculated by C. R. Lubitz (20) using the Racah (21) method and are in agreement with those found by the method outlined above. Using the notation E_J^T, where the superscript refers to the tensor force and the subscript to the J value for each state, the results are as follows:

$(d_{5/2})^2$

$$E_4^T = \frac{1}{5}(I_1 - I_3)$$

$$E_2^T = \frac{1}{5} I_1 - \frac{4}{5} I_2 + \frac{23}{25} I_3$$

$$E_0^T = \frac{7}{5} I_1 - 2 I_2 + \frac{7}{5} I_3$$

$d_{3/2}\, s_{1/2}$

$$E_2^T = \frac{21}{40}(I_1 + I_3) - \frac{9}{20} I_2$$

$$E_1^T = -\frac{7}{8}(I_1 + I_3) + \frac{3}{4} I_2$$

$d_{5/2}\, d_{3/2}$

$$E_4^T = \frac{1}{20}(I_1 - I_3)$$

$$E_3^T = -\frac{3}{4}(I_1 - I_3)$$

$$E_2^T = \frac{33}{100} I_1 + \frac{9}{10} I_2 - \frac{159}{100} I_3$$

$$E_1^T = -\frac{7}{4} I_1 + \frac{5}{2} I_2 - \frac{7}{4} I_3$$

$d_{5/2}\, s_{1/2}$

$$E_3^T = -\frac{1}{4} I_1 + \frac{3}{14} I_2 - \frac{1}{4} I_3$$

$$E_2^T = \frac{7}{20} I_1 - \frac{3}{10} I_2 + \frac{7}{20} I_3$$

$$I_\ell = \int_0^\infty R_\ell^2(r)\, V(r)\, dr \qquad R_\ell = \left(\frac{\sqrt{\nu}\, \nu^{\ell+1}\, 2^{\ell+1}}{\sqrt{\pi}\; 1 \cdot 3 \cdot \cdots \cdot (1+2\ell)} \right)^{1/2} e^{-\frac{\nu}{2} r^2}\, r^{\ell+1}$$

$\nu = \frac{\omega m}{\hbar}$ for the Hamiltonian:

$$H = \frac{1}{2m}\left(p^2 + m^2 \omega^2 r^2\right)$$

Central Interaction Energies

Central force interaction energies were calculated for each of the T = 1 terms $(d_{5/2})^2$, $(d_{5/2}\, d_{3/2})$, $(d_{3/2}\, s_{1/2})$, $(d_{5/2}\, s_{1/2})$, and $(s_{1/2})^2$. The Wigner force energies were calculated in three ways: First by the diagonal sum method as in the tensor calculation, second by use of the jj tables (20) given by Condon and Shortley (26), and last by using the well-known LS coupling energies (15, 27) and making the transformation from the LS representation to the jj representation (28).

The last method simplifies the problem of deriving the Majorana energies. The generalized Pauli principle requires that the wave functions for T = 1 states be antisymmetric in space and spin since the T = 1, or isotopic spin triplet wave functions, are symmetric. This means that the effect of the space exchange operator P^x on the potential is to change the sign of the energy for spin triplet (symmetric) states and to leave the energies of spin singlet (antisymmetric) states unchanged.

The last two methods require that expressions be obtained for the Slater F's in terms of the Talmi radial integrals I_ℓ. These transformations can be calculated by a method due to Talmi and the relations necessary for the present work are given in Appendix II.

Each of the Wigner and Majorana energies was calculated by two independent methods. A further check on the energies is given by numerical agreement with those calculated by Redlich (14) upon substitution of the parameters used by him. Using the notation E_J^W for Wigner energies and E_J^M for Majorana energies, the results are as follows:

$d^2_{5/2}$

$$E^W_4 = \frac{3}{40}(I_0 + I_4) + \frac{2}{5}(I_1 + I_3) + \frac{1}{20} I_2$$

$$E^W_2 = \frac{9}{50}(I_0 + I_4) + \frac{27}{50}(I_1 + I_3) - \frac{11}{25} I_2$$

$$E^W_0 = \frac{63}{80}(I_0 + I_4) - \frac{21}{20}(I_1 + I_3) + \frac{61}{40} I_2$$

$$E^M_4 = \frac{3}{40}(I_0 + I_4) - \frac{2}{5}(I_1 + I_3) + \frac{1}{20} I_2$$

$$E^M_2 = \frac{9}{50}(I_0 + I_4) - \frac{11}{10}(I_1 + I_3) + \frac{9}{5} I_2$$

$$E^M_0 = \frac{63}{80}(I_0 + I_4) - \frac{49}{20}(I_1 + I_3) + \frac{141}{40} I_2$$

$d_{5/2}\, d_{3/2}$

$$E^W_4 = \frac{3}{10}(I_0 + I_4) + \frac{1}{10}(I_1 + I_3) + \frac{1}{5} I_2$$

$$E^W_3 = \frac{1}{2}(I_1 + I_3)$$

$$E^W_2 = \frac{9}{100}(I_0 + I_4) + \frac{87}{100}(I_1 + I_3) - \frac{23}{25} I_2$$

$$E^W_1 = \frac{7}{4}(I_1 + I_3) - \frac{5}{2} I_2$$

$$E^M_4 = \frac{3}{10}(I_0 + I_4) - \frac{1}{10}(I_1 + I_3) + \frac{1}{5} I_2$$

$$E^M_3 = -\frac{1}{2}(I_1 + I_3)$$

$$E^M_2 = \frac{9}{100}(I_0 + I_4) - \frac{23}{20}(I_1 + I_3) + \frac{8}{5} I_2$$

$$E^M_1 = -\frac{7}{4}(I_1 + I_3) + \frac{5}{2} I_2$$

$d_{5/2}\, s_{1/2}$

$$E_3^W = \frac{7}{8} I_1 - \frac{3}{4} I_2 + \frac{7}{8} I_3$$

$$E_2^W = \frac{3}{16} I_0 + \frac{13}{40} I_1 + \frac{23}{40} I_2 - \frac{7}{8} I_3 + \frac{63}{80} I_4$$

$$E_3^M = -\frac{7}{8} I_1 + \frac{3}{4} I_2 - \frac{7}{8} I_3$$

$$E_2^M = \frac{3}{16} I_0 - \frac{3}{8} I_1 + \frac{141}{120} I_2 - \frac{63}{40} I_3 + \frac{63}{80} I_4$$

$d_{3/2}\, s_{1/2}$

$$E_2^W = \frac{1}{8} I_0 + \frac{61}{120} I_1 + \frac{2}{15} I_2 - \frac{7}{24} I_3 + \frac{21}{40} I_4$$

$$E_1^W = \frac{7}{8} (I_1 + I_3) - \frac{3}{4} I_2$$

$$E_2^M = \frac{1}{8} I_0 - \frac{13}{14} I_1 + \frac{31}{30} I_2 - \frac{161}{120} I_3 + \frac{21}{40} I_4$$

$$E_1^M = -\frac{7}{8} (I_1 + I_3) + \frac{3}{4} I_2$$

$s_{1/2}^2$

$$E_0^N = E_0^M = \frac{41}{64} I_0 - \frac{79}{48} I_1 + \frac{5 \times 77}{96} I_2 - \frac{175}{45} I_3 + \frac{105}{64} I_4$$

Radial Integrals

Theoretical jj coupling level schemes for the excited states of O^{18} can be constructed by evaluation of the radial integrals and substitution into the formulas for the interaction energies. The term separations are derived from the experimental d-s and spin orbit splitting in O^{17}.

With this procedure, choices can be made of the exchange character and radial dependence of the potential. The parameters appearing in the calculation are ν, which measures the extension of the harmonic oscillator wave functions and the range r_o and depth V_o of the chosen potential.

For the present work, the Yukawa potential was chosen for the radial dependence of the potential with constants which give the correct binding energy, quadrupole moment, and triplet effective range for the deuteron (29) One set of levels using a Gaussian radial dependence was calculated in order to determine the effect of a change in potential shape on the level structure.

The harmonic oscillator parameter ν was determined by calculating the mean square radius of a d nucleon and equating this to the radius given by the $1.43 \times A^{1/3}$ formula (14). A table of the numerical values for the I_ℓ used is given in Appendix III.

Theoretical Spectra

The theoretical spectra obtained by the methods described above are exhibited in Figures 24 and 25. The zero of the energy scale is taken as the energy of the O^{16} nucleus with two neutrons at infinity. Binding one of the two neutrons to the O^{16} core gives O^{17} and one neutron at infinity. Binding both neutrons to the O^{16}

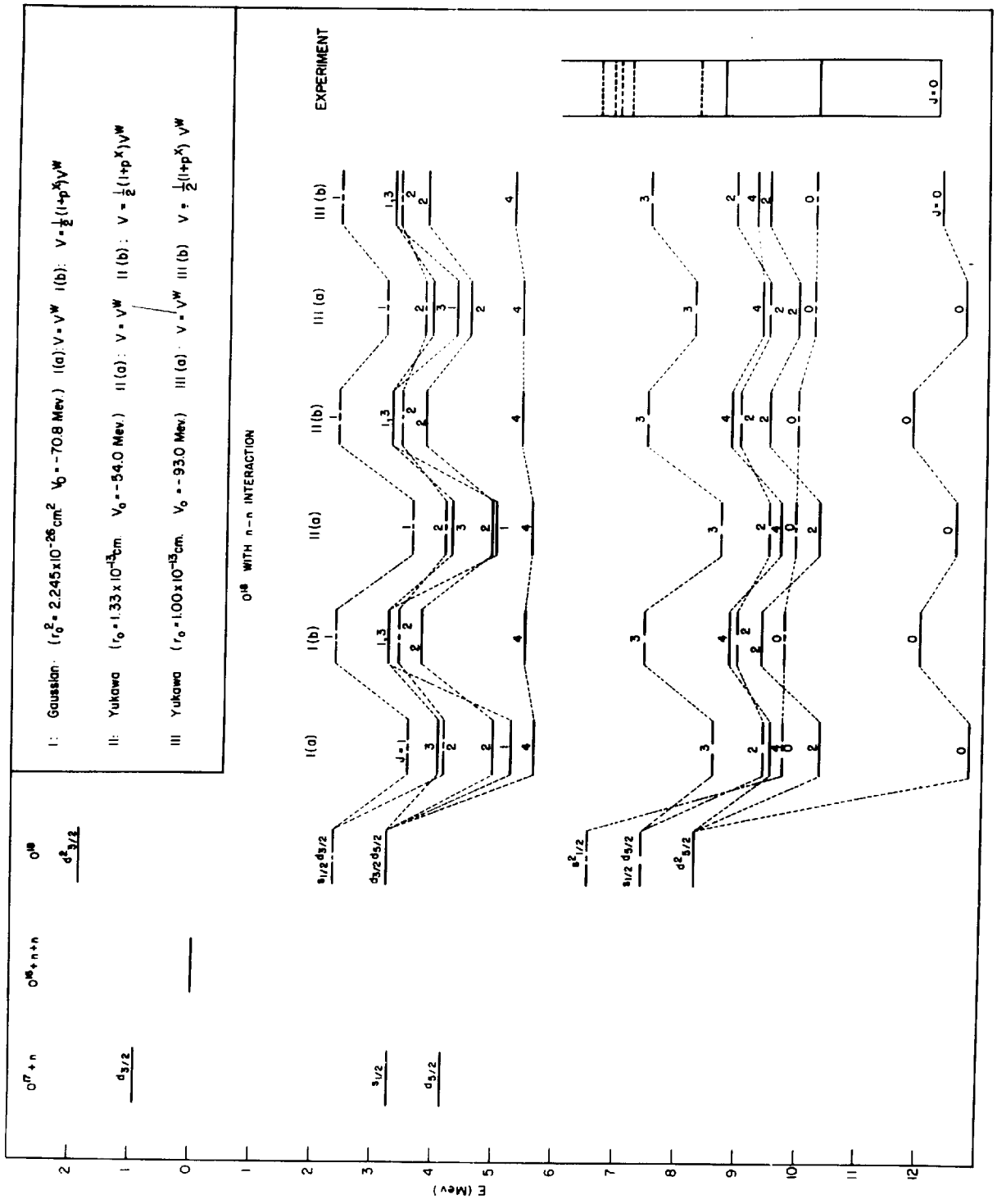


Figure 24. Central force level diagram of O^{18}.

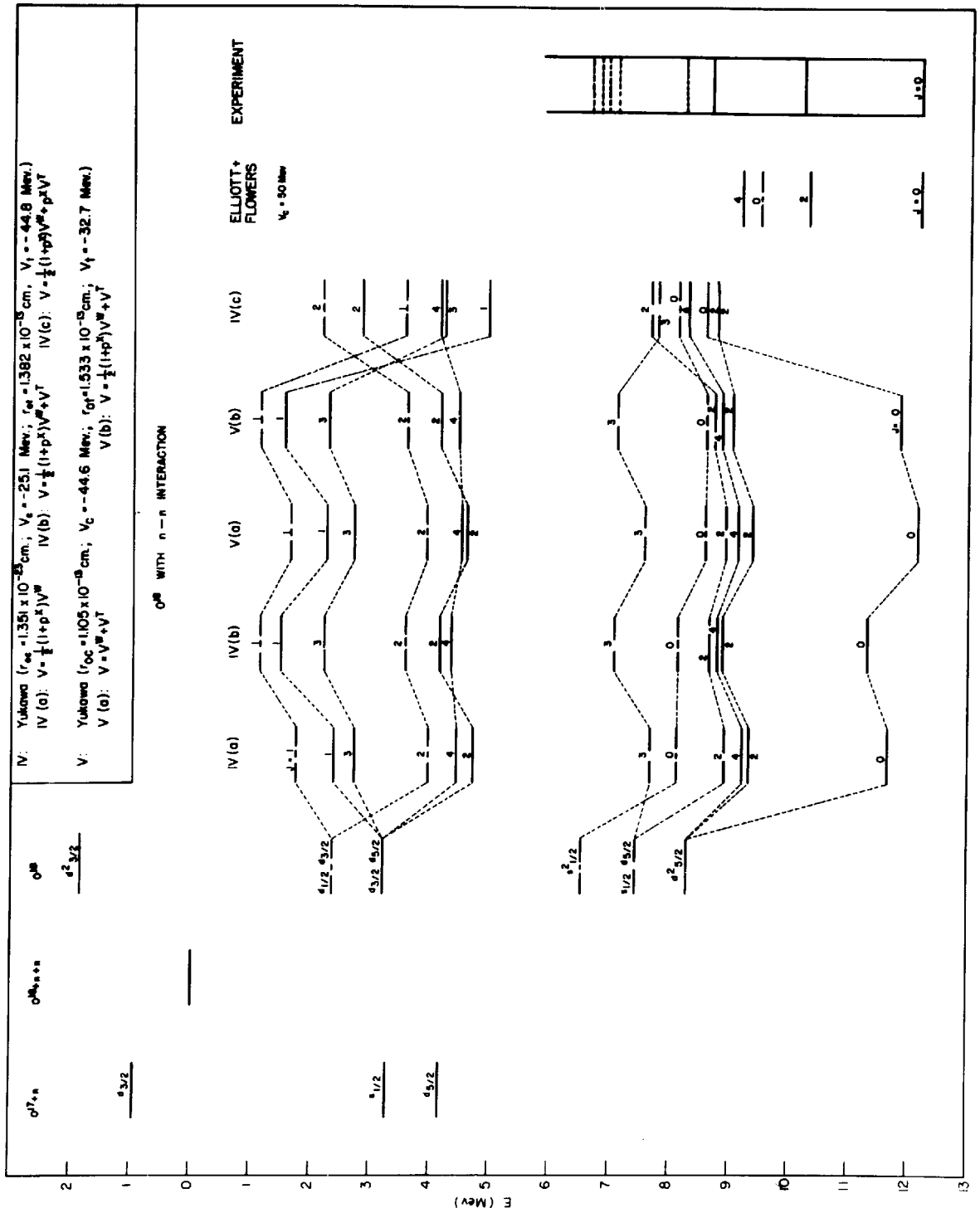


Figure 25. Central + tensor force level diagram of O^{18}.

core gives O^{18} without any interaction between the two neutrons. Including the n-n interaction gives the theoretical level structure of O^{18} and the position of the ground state can be compared with the experimental position. Knowing the $O^{17}(d,p)O^{18}$ ground state Q and the binding energy of the deuteron, the experimental ground state of O^{18} can be positioned relative to the ground state of O^{17}.

CHAPTER VI

CONCLUSIONS

Experimental Conclusions

The first work on the level structure of O^{18} was done by Ahnlund (7), who measured the ground and first excited state Q values by the reaction $O^{17}(d,p)O^{18}$. Her spectrum shows that the region from the ground state to the first excited state contains no groups of intensity greater than about 10 percent of the intensity of the ground state protons. Holmgren et al. (8), by the same reaction, report a Q value for the first excited state which is in agreement with that quoted by Ahnlund. They also report a level at an excitation energy of 2.445 Mev.

The present work has verified the existence of the first excited state which was seen both by inelastic deuteron scattering on O^{18} and by deuteron stripping on O^{17}. A second excited state was found at an excitation energy of 3.55 Mev. Between the first and second excited states, the deuteron spectrum shows no groups of intensity greater than 3 percent of the intensity of the deuterons from the first excited state. The region of the reported 2.445 Mev level was also examined by means of the 30° proton spectrum. No group of intensity greater than 20 percent of the intensity of the protons from the first excited state was observed. The 90° deuteron spectrum shows no groups of intensity greater than 3 percent of the intensity of the elastic scattered deuterons from O^{18} in the excitation region from 1.00 to 1.98 Mev.

Preliminary results by Jarmie (30) from the reaction $F^{19}(t,\alpha)O^{18}$ indicate excited states in O^{18} with excitation energies 1.96 Mev, 3.57 Mev, and several higher energies. The angular distribution of the pickup reaction $F^{19}(n,d)O^{18}$ to the ground state of O^{18} has been measured by Ribe (31), and is consistent with a value of J = 0 for the ground state. Direct measurement of J = 0 for the ground state has been reported by Miller et al. (32).

In conclusion, the positive results to date demonstrate the existence of excited states in O^{18} at the excitation energies 1.986 ± 0.014 Mev and 3.550 ± 0.010 Mev. These are the only strong levels in the excitation region from 0 to 3.55 Mev.

Theoretical Conclusions

Reference at this point must be made to the jj coupling level schemes shown in Figures 24 and 25, together with the structure predicted by Elliott and Flowers (16). The experimental levels are shown on the far right of each figure with levels measured by more than one observer drawn with solid lines and those measured by only one observer represented by dashed lines.

The level schemes calculated by means of a Wigner Gaussian interaction and Wigner Yukawa interaction are remarkably similar except for a crossing of the J = 2 level of the ($s_{1/2}$ $d_{3/2}$) term and the J = 3 level of the ($d_{3/2}$ $d_{5/2}$) term. The effect of a change in the nuclear radius and a change of the range of the nuclear force on the ($d_{5/2}$)^2 term has been investigated by Redlich (14) for the Gaussian interaction. A decrease in the nuclear radius increases the level spacing and the binding energy. Decreasing the range of the force increases the level spacing and decreases the binding energy.

Including half space exchange into the central part of the potential has the general effect of shifting the entire spectrum in the direction of less binding. Addition of the tensor force without exchange gives less binding by about half an Mev. The only case which gives complete disagreement with the experimental binding is the one including a tensor force with space exchange. Here the binding is too low by three Mev and the J = 0 and J = 2 levels of the $(d_{5/2})^2$ term are inverted. The effect of the tensor force without exchange is to bring these two levels closer together.

Comparison of the jj coupling levels with the experimental levels demonstrates the failure of the approximation. The only predictions made by the theory that agree with experiment are that an approximately correct binding energy is obtained and that a spacing of two Mev or more should occur between the ground and first excited states.

The calculation of Elliott and Flowers (16), which includes configuration interaction in intermediate coupling, is in better agreement with experiment. The largest V_c given on their curve for the two nucleon levels was chosen in order to fit the experimental levels as closely as possible. They show that the correct binding energy is obtained with V_c = 44.5 Mev. Since the dependence of the binding energy on V_c is not quoted, the ground state has been arbitrarily placed in Figure 25 at the position of the experimental ground state. It is evident, however, that a still larger spacing is needed between the J = 2 and J = 4 levels than given by Elliott and Flowers.

The cross sections of the proton groups from the first and second excited states as found in the present work by the reactions $O^{17}(d,p)O^{18}_{1,2}$ are of comparable magnitude. The higher J = 0 level in the work of Elliott and Flowers arises mainly from the $(s_{1/2})^2$ term. Since the ground state of O^{17} consists of a $d_{5/2}$ neutron

outside the O^{16} core, stripping cannot take place to a pure $(S_{1/2})^2$ state in O^{18}. The stripping cross section to this J = 0 level can only be due to admixture of other states and therefore is expected to be smaller by an order of magnitude than stripping to states made up of d nucleons. If the first excited state is the J = 2 or J = 4 level of the $(d_{5/2})^2$ term, it seems unlikely that the 3.55 Mev level is the $(S_{1/2})^2$ J = 0 state.

This indicates that the higher J = 0 level probably lies above instead of below the J = 4 state, contrary to the prediction made by Elliott and Flowers. It is possible that still more configurations must be considered. Until a calculation including tensor force configuration interaction in intermediate coupling has been made, it does not seem likely that tensor forces can be ruled out.

The necessity for determination of the spins and parities of the excited states is obvious. Without this information, it is difficult to draw any conclusions concerning the potentials and exchange mixtures. It is possible that levels arising from core excitation may appear at fairly low excitation energies as is the case in O^{17}. This points out the futility of fitting the theoretical spectrum to the experimental spectrum until more information about each state is obtained.

Future Work

The identification of the proton groups from the reactions $O^{17}(d,p)O^{18}_{1,2}$ has demonstrated that it is possible to obtain angular distributions for these reactions with the present target and equipment. Angular distribution and identification of the higher excited states seen by Jarmie (30) can probably only be accomplished with more enrichment in O^{17} because of the large number of contaminant levels in the lower energy region.

Inelastic alpha particle scattering on O^{18} can also provide information on the excited states. Lane and Thomas (33) have suggested that this reaction may take place at the nuclear surface. The angular distributions are given in terms of Bessel functions j_l, where the order l depends on the angular momentum transfer taking place in the reaction. Since the ground state of O^{18} has J = 0, the $O^{18}(\alpha, \alpha')O^{18*}$ angular distributions should give a measure of the J values for some of the excited states of O^{18}.

APPENDIX I

THE TRANSFORMATIONS (19)

$$\psi^{m_1}_{n_1 l_1}(\vec{r}_1)\,\psi^{m_2}_{n_2 l_2}(\vec{r}_2) \longrightarrow \psi^{M}_{NL}(\vec{R})\;\psi^{m}_{n\Lambda}(\vec{r})$$

n_1, n_2, N, and n refer to the number of radial nodes in the wave functions. In the following compilation, n will be omitted when equal to zero and the (r_1, r_2) wave functions will be denoted by (m_1,m_2) with n_1, l_1, n_2, and l_2 given at the head of each table. The vector symbols in $\vec{R}$ and $\vec{r}$ are omitted. The subscripts $\underline{s}$ and $\underline{a}$ refer to symmetric and antisymmetric combinations, respectively.

Od Od :

$$(2,2)_S = \tfrac{1}{2}\sqrt{\tfrac{3}{2}}\left(\psi^4_4(R)\psi^0_0(r) + \psi^4_4(r)\psi^0_0(R)\right) - \tfrac{1}{2}\,\psi^2_2(R)\,\psi^2_2(r)$$

$$(2,1)_S = \tfrac{1}{2}\sqrt{\tfrac{3}{2}}\left(\psi^3_4(R)\psi^0_0(r) + \psi^3_4(r)\psi^0_0(R)\right) - \frac{1}{2\sqrt{2}}\left(\psi^2_2(R)\psi^1_2(r) + \psi^2_2(r)\,\psi^1_2(R)\right)$$

$$(1,1)_S = \sqrt{\tfrac{3}{4}}\left(\psi^2_4(R)\psi^0_0(r) + \psi^2_4(r)\psi^0_0(R)\right) - \frac{1}{\sqrt{6}}\left(\psi^2_2(R)\psi^0_2(r) + \psi^2_2(r)\psi^0_2(R)\right)$$

$$+\frac{1}{2\sqrt{3}}\left(\psi^2_2(R)\psi^0_{10}(r) + \psi^2_2(r)\psi^0_{10}(R)\right) - \frac{1}{2\sqrt{7}}\left(\psi^2_{12}(R)\psi^0_0(r) + \psi^2_{12}(r)\psi^0_0(R)\right)$$

$$(2,0)_S = \frac{3}{2\sqrt{14}}\left(\psi^2_4(R)\psi^0_0(r) + \psi^2_4(r)\psi^0_0(R)\right) + \frac{1}{6\sqrt{2}}\left(\psi^2_2(R)\psi^0_2(r) + \psi^2_2(r)\psi^0_2(R)\right)$$

$$-\frac{1}{\sqrt{3}}\psi^1_2(R)\psi^1_2(r) - \frac{1}{3}\left(\psi^2_2(R)\psi^0_{10}(r) + \psi^2_2(r)\psi^0_{10}(R)\right)$$

$$+\frac{1}{\sqrt{21}}\left(\psi^2_{12}(R)\psi^0_0(r) + \psi^2_{12}(r)\psi^0_0(R)\right)$$

$$(1,0)_S = -\frac{3}{2\sqrt{7}}\left(\psi_4^1(R)\psi_0^0(r) + \psi_4^1(r)\psi_0^0(R)\right) - \frac{\sqrt{2}}{6}\left(\psi_2^1(R)\psi_2^0(r) + \psi_2^1(r)\psi_2^0(R)\right)$$

$$- \frac{\sqrt{3}}{6}\left(\psi_2^2(R)\psi_2^{-1}(r) + \psi_2^2(r)\psi_2^{-1}(R)\right) + \frac{1}{6}\left(\psi_2^1(R)\psi_{10}^0(r) + \psi_2^1(r)\psi_{10}^0(R)\right)$$

$$- \frac{1}{2\sqrt{21}}\left(\psi_{12}^1(R)\psi_0^0(r) + \psi_{12}^1(r)\psi_0^0(R)\right)$$

$$(2,-1)_S = -\frac{1}{4}\sqrt{\frac{6}{7}}\left(\psi_4^1(R)\psi_0^0(r) + \psi_4^1(r)\psi_0^0(R)\right) - \frac{\sqrt{3}}{6}\left(\psi_2^1(R)\psi_2^0(r) + \psi_2^1(r)\psi_2^0(R)\right)$$

$$+ \frac{\sqrt{2}}{4}\left(\psi_2^2(R)\psi_2^{-1}(r) + \psi_2^2(r)\psi_2^{-1}(r)\right) - \frac{1}{\sqrt{6}}\left(\psi_2^1(R)\psi_{10}^0(r) + \psi_2^1(r)\psi_{10}^0(R)\right)$$

$$+ \frac{1}{\sqrt{14}}\left(\psi_{12}^1(R)\psi_0^0(r) + \psi_{12}^1(r)\psi_0^0(R)\right)$$

$$(2,-2)_S = \frac{1}{4}\sqrt{\frac{6}{35}}\left(\psi_4^0(R)\psi_0^0(r) + \psi_4^0(r)\psi_0^0(R)\right) + \frac{\sqrt{2}}{4}\left(\psi_2^2(R)\psi_2^{-2}(r) + \psi_2^2(r)\psi_2^{-2}(R)\right)$$

$$- \frac{\sqrt{2}}{6}\psi_2^0(R)\psi_2^0(r) - \frac{1}{3}\left(\psi_2^0(R)\psi_{10}^0(r) + \psi_2^0(r)\psi_{10}^0(R)\right) - \frac{\sqrt{2}}{3}\psi_{10}^0(R)\psi_{10}^0(r)$$

$$+ \frac{1}{\sqrt{21}}\left(\psi_{12}^0(R)\psi_0^0(r) + \psi_{12}^0(r)\psi_0^0(R)\right) + \frac{1}{\sqrt{15}}\left(\psi_{20}^0(R)\psi_0^0(r) + \psi_{20}^0(r)\psi_0^0(R)\right)$$

$$(1,-1)_S = \sqrt{\frac{6}{35}}\left(\psi_4^0(R)\psi_0^0(r) + \psi_4^0(r)\psi_0^0(R)\right) - \frac{1}{6}\left(\psi_2^0(R)\psi_2^0(r) + \psi_2^0(r)\psi_{12}^0(R)\right)$$

$$- \frac{\sqrt{2}}{3}\psi_2^0(R)\psi_2^0(r) - \frac{\sqrt{2}}{3}\psi_{10}^0(R)\psi_0^0(r) + \frac{1}{2}\frac{1}{\sqrt{21}}\left(\psi_{12}^0(R)\psi_0^0(r) + \psi_{22}^0(r)\psi_0^0(R)\right)$$

$$- \frac{1}{\sqrt{15}}\left(\psi_{20}^0(R)\psi_0^0(r) + \psi_{20}^0(r)\psi_0^0(R)\right)$$

$$(0,0)_S = \frac{3}{2}\sqrt{\frac{3}{35}}\left(\psi_4^0(R)\psi_0^0(r) + \psi_4^0(r)\psi_0^0(R)\right) - \frac{1}{6}\left(\psi_2^2(R)\psi_2^{-2}(r) + \psi_2^2(r)\psi_2^{-2}(R)\right)$$

$$- \frac{1}{3}\left(\psi_2^1(R)\psi_2^{-1}(r) + \psi_2^1(r)\psi_2^{-1}(R)\right) + \frac{1}{3\sqrt{2}}\left(\psi_2^0(R)\psi_{10}^0(r) + \psi_2^0(r)\psi_{10}^0(R)\right)$$

$$- \frac{1}{\sqrt{12}}\left(\psi_{12}^0(R)\psi_0^0(r) + \psi_{12}^0(r)\psi_0^0(R)\right) - \frac{1}{3}\psi_{10}^0(R)\psi_{10}^0(r) + \frac{1}{\sqrt{30}}\left(\psi_{20}^0(R)\psi_0^0(r) + \psi_{20}^0(r)\psi_0^0(R)\right)$$

$$(2,1)_a = \frac{\sqrt{6}}{4}\left(\psi_3^3(R)\psi_1^0(r) + \psi_3^3(r)\psi_1^0(R)\right) - \frac{\sqrt{2}}{4}\left(\psi_3^2(R)\psi_1^1(r) + \psi_3^2(r)\psi_1^1(R)\right)$$

$$(2,0)_a = \frac{1}{2\sqrt{2}}\left(\psi_3^3(R)\psi_1^{-1}(r) + \psi_3^3(r)\psi_1^{-1}(R)\right) + \frac{1}{\sqrt{6}}\left(\psi_3^2(R)\psi_1^0(r) + \psi_3^2(r)\psi_1^0(R)\right)$$

$$-\frac{1}{2}\sqrt{\frac{5}{6}}\left(\psi_3^1(R)\psi_1^1(r) + \psi_3^1(r)\psi_1^1(R)\right)$$

$$(1,0)_a = \frac{1}{2\sqrt{3}}\left(\psi_3^2(R)\psi_1^{-1}(r) + \psi_3^2(r)\psi_1^{-1}(R)\right) + \frac{1}{2\sqrt{15}}\left(\psi_3^1(R)\psi_1^0(r) + \psi_3^1(r)\psi_1^0(R)\right)$$

$$-\frac{1}{\sqrt{10}}\left(\psi_3^0(R)\psi_1^1(r) + \psi_3^0(r)\psi_1^1(R)\right) - \frac{1}{2}\sqrt{\frac{3}{5}}\left(\psi_{11}^1(R)\psi_1^0(r) + \psi_{11}^1(r)\psi_1^0(R)\right)$$

$$+\frac{1}{2}\sqrt{\frac{3}{5}}\left(\psi_{11}^0(R)\psi_1^1(r) + \psi_{11}^0(r)\psi_1^1(R)\right)$$

$$(2,-2)_a = \frac{1}{2\sqrt{5}}\left(\psi_3^1(R)\psi_1^{-1}(r) + \psi_3^1(r)\psi_1^{-1}(R)\right) - \frac{1}{2\sqrt{5}}\left(\psi_3^{-1}(R)\psi_1^1(r) + \psi_3^{-1}(r)\psi_1^1(R)\right)$$

$$+\frac{1}{\sqrt{5}}\left(\psi_{11}^1(R)\psi_1^{-1}(r) + \psi_{11}^1(r)\psi_1^{-1}(R)\right) - \frac{1}{\sqrt{5}}\left(\psi_{11}^{-1}(R)\psi_1^1(r) + \psi_{11}^{-1}(r)\psi_1^1(R)\right)$$

$$(1,-1)_a = \frac{1}{\sqrt{5}}\left(\psi_3^1(R)\psi_1^{-1}(r) + \psi_3^1(r)\psi_1^{-1}(R)\right) - \frac{1}{\sqrt{5}}\left(\psi_3^{-1}(R)\psi_1^1(r) + \psi_3^{-1}(r)\psi_1^1(R)\right)$$

$$-\frac{1}{2\sqrt{5}}\left(\psi_{11}^1(R)\psi_1^{-1}(r) + \psi_{11}^1(r)\psi_1^{-1}(R)\right) + \frac{1}{2\sqrt{5}}\left(\psi_{11}^{-1}(R)\psi_1^1(r) + \psi_{11}^{-1}(r)\psi_1^1(R)\right)$$

$$(2,-1)_a = \frac{\sqrt{2}}{4}\left(\psi_3^2(R)\psi_1^{-1}(r) + \psi_3^2(r)\psi_1^{-1}(R)\right) + \frac{1}{2\sqrt{10}}\left(\psi_3^1(R)\psi_1^0(r) + \psi_3^1(r)\psi_1^0(R)\right)$$

$$-\frac{1}{2}\sqrt{\frac{3}{5}}\left(\psi_3^0(R)\psi_1^1(r) + \psi_3^0(r)\psi_1^1(R)\right) + \frac{1}{\sqrt{10}}\left(\psi_{11}^1(R)\psi_1^0(r) + \psi_{11}^1(r)\psi_1^0(R)\right)$$

$$-\frac{1}{\sqrt{10}}\left(\psi_{11}^0(R)\psi_1^1(r) + \psi_{11}^0(r)\psi_1^1(r)\right)$$

Odls:

$$(2,0)_S = -\frac{1}{3}\left(\psi_2^2(R)\psi_2^0(r) + \psi_2^2(r)\psi_2^0(R)\right) + \frac{1}{\sqrt{6}}\psi_2^1(R)\psi_2^1(r)$$

$$-\frac{1}{6\sqrt{2}}\left(\psi_2^2(R)\psi_{10}^0(r) + \psi_2^2(r)\psi_{10}^0(R)\right) + \frac{1}{2}\sqrt{\frac{7}{6}}\left(\psi_{12}^2(R)\psi_0^0(r) + \psi_{12}^2(r)\psi_0^0(R)\right)$$

$$(1,0)_S = \frac{1}{6}\left(\psi_2^1(R)\psi_2^0(r) + \psi_2^1(r)\psi_2^0(R)\right) - \frac{1}{\sqrt{6}}\left(\psi_2^2(R)\psi_2^{-1}(r) + \psi_{12}^2(r)\psi_2^{-1}(R)\right)$$

$$-\frac{1}{6\sqrt{2}}\left(\psi_2^1(R)\psi_{10}^0(r) + \psi_2^1(r)\psi_{10}^0(R)\right) + \frac{1}{2}\sqrt{\frac{7}{6}}\left(\psi_{12}^1(R)\psi_0^0(r) + \psi_{12}^1(r)\psi_0^0(R)\right)$$

$$(0,0)_S = \frac{1}{3}\psi_2^0(R)\psi_2^0(r) - \frac{1}{6}\left(\psi_2^1(R)\psi_2^{-1}(r) + \psi_2^1(r)\psi_2^{-1}(R)\right)$$

$$-\frac{1}{3}\left(\psi_2^2(R)\psi_2^{-2}(r) + \psi_2^2(r)\psi_2^{-2}(R)\right) - \frac{1}{6\sqrt{2}}\left(\psi_2^0(R)\psi_{10}^0(r) + \psi_2^0(r)\psi_{10}^0(R)\right)$$

$$+\frac{1}{2}\sqrt{\frac{7}{6}}\left(\psi_{12}^0(R)\psi_0^0(r) + \psi_{12}^0(r)\psi_0^0(R)\right)$$

$$(2,0)_a = \frac{1}{2}\left(\psi_3^3(R)\psi_1^{-1}(r) + \psi_3^3(r)\psi_1^{-1}(R)\right) - \frac{1}{2\sqrt{3}}\left(\psi_3^2(R)\psi_1^0(r) + \psi_3^2(r)\psi_1^0(R)\right)$$

$$+\frac{1}{2\sqrt{15}}\left(\psi_3^1(R)\psi_1^1(r) + \psi_3^1(r)\psi_1^1(R)\right) - \frac{1}{2}\sqrt{\frac{3}{5}}\left(\psi_{11}^1(R)\psi_1^1(r) + \psi_{11}^1(r)\psi_1^1(R)\right)$$

$$(1,0)_a = \frac{1}{\sqrt{16}}\left(\psi_3^2(R)\psi_1^{-1}(r) + \psi_3^2(r)\psi_1^{-1}(R)\right) - \frac{2}{5}\sqrt{\frac{5}{6}}\left(\psi_3^1(R)\psi_1^0(r) + \psi_3^1(r)\psi_1^0(R)\right)$$

$$+\frac{1}{2\sqrt{5}}\left(\psi_3^0(R)\psi_1^1(r) + \psi_3^0(r)\psi_1^1(R)\right) - \frac{1}{2}\sqrt{\frac{3}{10}}\left(\psi_{11}^1(R)\psi_1^0(r) + \psi_{11}^1(r)\psi_1^0(R)\right)$$

$$-\frac{1}{2}\sqrt{\frac{3}{10}}\left(\psi_{11}^0(R)\psi_1^1(r) + \psi_{11}^0(r)\psi_1^1(R)\right).$$

$$(0,0)_a = \frac{1}{\sqrt{10}}\left(\mathcal{Y}_3^1(R)\mathcal{Y}_1^{-1}(r) + \mathcal{Y}_3^1(r)\mathcal{Y}_1^{-1}(R)\right) - \frac{3}{2\sqrt{15}}\left(\mathcal{Y}_3^0(R)\mathcal{Y}_1^0(r) + \mathcal{Y}_3^0(r)\mathcal{Y}_1^0(R)\right)$$

$$+ \frac{1}{\sqrt{10}}\left(\mathcal{Y}_3^{-1}(R)\mathcal{Y}_1^1(r) + \mathcal{Y}_3^{-1}(r)\mathcal{Y}_1^1(R)\right) - \frac{1}{2\sqrt{10}}\left(\mathcal{Y}_{11}^{-1}(R)\mathcal{Y}_1^1(r) + \mathcal{Y}_{11}^{-1}(r)\mathcal{Y}_1^1(R)\right)$$

$$- \frac{1}{\sqrt{10}}\left(\mathcal{Y}_{11}^0(R)\mathcal{Y}_1^0(r) + \mathcal{Y}_{11}^0(r)\mathcal{Y}_1^0(R)\right) - \frac{1}{2\sqrt{10}}\left(\mathcal{Y}_{11}^1(R)\mathcal{Y}_{11}^{-1}(r) + \mathcal{Y}_{11}^1(r)\mathcal{Y}_1^{-1}(R)\right)$$

TABLE III

THE DIAGONAL T = 1 TENSOR FORCE MATRIX ELEMENTS
$(j_1 j_2 m_{j_1} m_{j_2} | S_{12} | j_1 j_2 m_{j_1} m_{j_2})$

n_1	l_1	j_1	m_{j_1}	n_2	l_2	j_2	m_{j_2}	Coefficients of I_1	I_2	I_3
0	2	5/2	5/2	0	2	5/2	3/2	1/5	0	-1/5
0	2	5/2	5/2	0	2	5/2	1/2	1/5	0	-1/5
0	2	5/2	5/2	0	2	5/2	-1/2	1/5	-2/7	1/5
0	2	5/2	5/2	0	2	5/2	-3/2	1/5	-4/7	3/5
0	2	5/2	5/2	0	2	5/2	-5/2	3/5	-8/7	1
0	2	5/2	3/2	0	2	5/2	1/2	1/5	-18/35	13/25
0	2	5/2	3/2	0	2	5/2	-1/2	1/5	-48/175	3/25
0	2	5/2	3/2	0	2	5/2	-3/2	3/5	-24/35	19/25
0	2	5/2	1/2	0	2	5/2	-1/2	3/5	-68/70	19/25
0	2	5/2	5/2	0	2	3/2	3/2	1/20	0	-1/20
0	2	5/2	5/2	0	2	3/2	1/2	-9/20	0	9/20
0	2	5/2	5/2	0	2	3/2	-1/2	-3/20	3/7	-9/20
0	2	5/2	5/2	0	2	3/2	-3/2	-17/20	11/7	-27/20
0	2	5/2	3/2	0	2	3/2	3/2	-1/4	0	1/4
0	2	5/2	3/2	0	2	3/2	1/2	9/100	12/35	-57/100
0	2	5/2	1/2	0	2	3/2	3/2	-31/100	9/70	13/100
0	2	5/2	3/2	0	2	3/2	-1/2	-81/100	27/35	-27/100
0	2	5/2	-1/2	0	2	3/2	3/2	-31/100	29/70	-27/100
0	2	5/2	1/2	0	2	3/2	1/2	-3/20	9/14	-3/4

TABLE III--Continued

n_1	l_1	j_1	m_{j_1}	n_2	l_2	j_2	m_{j_2}	Coefficients of		
								I_1	I_2	I_3
0	2	5/2	5/2	1	0	1/2	1/2	-1/4	3/14	-1/4
0	2	5/2	5/2	1	0	1/2	-1/2	1/4	-3/14	1/4
0	2	5/2	3/2	1	0	1/2	1/2	-3/20	9/70	-3/20
0	2	3/2	3/2	1	0	1/2	1/2	21/40	-9/20	21/40
0	2	3/2	3/2	1	0	1/2	-1/2	-21/40	9/20	-21/40
0	2	3/2	1/2	1	0	1/2	1/2	7/40	-3/20	7/40

APPENDIX II

SLATER PARAMETERS IN TERMS OF TALMI RADIAL INTEGRALS (12, 15, 20)

Two p nucleons:

$$F^0 = \frac{5}{12}\left(I_0 + I_2\right) + \frac{1}{6} I_1$$

$$F^2 = \frac{25}{12}\left[\left(I_0 + I_2\right) - 2 I_2\right]$$

Two d nucleons:

$$15 F^0 = \frac{63}{16}\left(I_0 + I_4\right) + \frac{7}{4}\left(I_1 + I_3\right) + \frac{29}{8} I_2$$

$$\frac{21}{49} F^2 = \frac{9}{16}\left(I_0 + I_4\right) - \frac{1}{2}\left(I_1 + I_3\right) - \frac{1}{5} I_2$$

$$\frac{35}{441} F^4 = \frac{3}{16}\left(I_0 + I_4\right) - \frac{3}{4}\left(I_1 + I_3\right) + \frac{9}{8} I_2$$

One d and one s nucleon:

$$F^0 = \frac{5}{32} I_0 + \frac{5}{12} I_1 + \frac{17}{48} I_2 - \frac{7}{12} I_3 + \frac{21}{32} I_4$$

$$G^2 = \frac{35}{32} I_0 - \frac{55}{24} I_1 + \frac{265}{48} I_2 - \frac{175}{24} I_3 + \frac{105}{32} I_4$$

APPENDIX III

NUMERICAL VALUES FOR THE I_l USED FOR $\sqrt{\mathcal{S}} = 0.499 \times 10^{13}$

Potential	$r_o \times 10^{13}$	V_o (Mev)	Coefficients x(-1)(Mev) of:				
			I_0	I_1	I_2	I_3	I_4
Gaussian . .	1.50	-70.8	7.28	1.59	0.35	0.076	0.017
Yukawa . . .	1.33	-54.0	6.53	1.73	0.73	0.33	0.18
Yukawa . . .	1.00	-93.0	6.32	1.12	0.46	0.14	0.05
Yukawa . . .	1.35	-25.1	3.14	0.85	0.36	0.17	0.09
Yukawa . . .	1.38	-44.8	5.62	1.66	0.70	0.33	0.18
Yukawa . . .	1.105	-44.6	3.70	0.73	0.31	0.11	0.02

The constants for the Gaussian potential are those used by Redlich (14) The Yukawa constants are those given by Sachs (29). Note that since the $I_l(r)$ are integrals on the relative coordinate r, they are $I_l(\gamma/2)$.

LIST OF REFERENCES

1. E. S. Rosenblum, Rev. Sci. Inst. 21, 586 (1950).
2. D. L. Judd, Rev. Sci. Inst. 21, 213 (1950).
3. M. S. Livingston and H. A. Bethe, Revs. Mod. Phys. 9, 283 (1937).
4. H. A. Enge, W. W. Buechner, and A. Sperduto, Phys. Rev. 88, 963 (1952).
5. D. R. Bach, W. J Childs, R. Grismore, R. W. Hockney, P. V. C. Hough, and W. C. Parkinson, Rev. Sci. Inst. (unpublished).
6. A. B. Brown, C. W. Snyder, W. A. Fowler, and C. C. Lauritsen, Phys. Rev. 82, 159 (1951).
7. K. Ahnlund, Phys. Rev. 96, 999 (1954).
8. H. D. Holmgren, T. D. Hanscome, and D. K. Willett, Bull. Am. Phys. Soc. 29, No. 7- R6 (1954).
9. F. Ajzenberg and T. Lauritsen, Revs. Mod. Phys. 27, 77 (1955).
10. W. J. Childs, "Study of the O^{17} Nucleus by the (d,p) Stripping Process" (unpublished Ph.D. dissertation, Dept. of Physics, University of Michigan, 1955).
11. D. Kurath, Phys. Rev. 80, 138 (1950).
12. I. Talmi, Helv. Phys. Acta XXV, 185 (1952).
13. I. Talmi, Phys. Rev. 89, 1065 (1953).
14. M. G. Redlich, Phys. Rev. 95, 448 (1954).
15. G. E. Tauber and T. Y. Wu, Phys. Rev. 93, 295 (1954).
16. J. P. Elliott and B. H. Flowers, Proc. Roy. Soc. A229, 536 (1955).

17. M. G. Redlich, "On the Agreement Between Nuclear Shell Theory and Experiment" (unpublished Ph.D. dissertation, Dept. of Physics, Princeton University, 1954).

18. E. U. Condon and G. H. Shortley, The Theory of Atomic Spectra (Cambridge University Press, 1953), p. 191.

19. I. Talmi (private communication).

20. C. R. Lubitz, University of Michigan (private communication).

21. G. Racah, Phys. Rev. 62, 248 (1942).
G. Racah, Phys. Rev. 63, 367 (1943).

22. K. W. Ford, Conference on Nuclear Structure (University of Michigan, 1955).

23. A. M. Lane, Conference on Nuclear Structure (University of Michigan, 1955).

24. S. Sueoka, Phys. Rev. 93, 302 (1954).

25. Condon and Shortley, op. cit., p. 268.

26. Ibid., p. 261.

27. Ibid., Ch. VII.

28. Ibid., p. 294.

29. R. G. Sachs, Nuclear Theory (Addison Wesley Publishing Co. Inc., 1953), p. 34 and p. 152.

30. W. Jarmie (private communication).

31. F. L. Ribe (private communication).

32. S. L. Miller, A. Javan, and C. H. Townes, Phys. Rev. 82, 454 (1951).

33. A. M. Lane and R. G. Thomas (private communication).

34. Atomic Instrument Company, Cambridge, Massachusetts.